KTH Energy and
Environmental Technology

Experimental Heat Transfer, Pressure Drop, and Flow Visualization of R-134a in Vertical Mini/Micro Tubes

Doctoral Thesis
By

Wahib Owhaib

Division of Applied Thermodynamics and Refrigeration
Department of Energy Technology
Royal Institute of Technology, KTH
Stockholm, Sweden 2007

TRITA REFER Report No 07/59
ISSN 1102-0245
ISRN KTH/REFR/07/59-SE
ISBN 978-91-7178-594-7

Abstract

Mini/Micro-channel type compact heat exchangers have attracted much attention during the last decade. The reason is mainly the possibilities of reducing the size, weight and cost of the heat exchangers compared to current designs. Also, new applications, where objects of small size need to be cooled, as electronics or micro-mechanical devices, require heat exchangers with miniature channels.

For the application of minichannel heat exchangers, it is necessary to have accurate design tools for predicting heat transfer and pressure drop. Until recently, this type of heat exchangers was not well studied, and in the scientific literature there were large discrepancies between results reported by different investigators. The present thesis aims to add to the knowledge of the fundamentals of single- and two-phase flow heat transfer and pressure drop in narrow channels, thereby aiding in the development of this new, interesting technology with the possibility of decreasing the size of electronics through better cooling, and of increasing the energy efficiency of thermal processes and thermodynamic cycles through enhanced heat transfer.

A comprehensive experimental single-phase flow and saturated flow boiling heat transfer and pressure drop study has been carried out on vertical stainless steel tubes with inner diameters of 1.700, 1.224 and 0.826 mm, using R-134a as the test fluid. The heat transfer and pressure drop results were compared both to conventional correlations developed for larger diameter channels and to correlations developed specifically for microscale geometries.

Contrary to many previous investigations, this study has shown that the test data agree well with single-phase heat transfer and friction factor correlations known to be accurate for larger channels, thus expanding their ranges to cover mini/microchannel geometries.

The main part of the study concerns saturated flow boiling heat transfer and pressure drop. Tests with the same stainless steel tubes showed that the heat transfer is strongly dependent on heat flux, but only weakly dependent on mass flux and vapor fraction (up to the location of dryout). This behavior is usually taken to indicate a dominant influence of nucleate boiling, and indicates that the boiling mechanism is strongly related to that in nucleate boiling.

The test data for boiling heat transfer was compared to several correlations from the literature, both for macro- and mini-channels. A new correlation for saturated flow boiling heat transfer of refrigerant R-134a correlation was obtained based on the present experimental data.

This correlation predicts the presented data with a mean absolute deviation of ±8%.

The frictional pressure drop results were compared to both macro- and mini channel correlations available from the literature. The correlation suggested by Qu and Mudawar (*2003*) gave the best prediction to the frictional two-phase pressure drop within the studied ranges.

A unique visualization study of saturated flow boiling characteristics in a vertical 1.332 mm inner diameter quartz tube, coated with a transparent heater has also been conducted. The complete evaporation process in a heated circular mini-channel has been studied visually in detail using high speed CCD camera. The study revealed the developments of the flow patterns and the behavior from bubble nucleation to the dry out of the liquid film. The bubble departure frequency, diameter, growth rate, and velocity were determined by analyzing the images. Finally, a flow pattern map for boiling flow in microchannels has been developed based on the test data.

Key words: *Minichannel, microchannel, heat transfer, pressure drop, single-phase, two-phase, flow boiling, flow visualization, dry out, bubble behavior, flow pattern.*

Acknowledgments

I would like to express my thanks to the following people for their support during my Ph.D. studies.

Foremost, my deepest thanks to my advisor Prof. Björn Palm for his support, initiating the project and accepting me as a Ph.D. student, ideas, discussions, and knowledge that I have learned so much from during the project.

Much appreciation and many thanks are expressed to Claudi Martín-Callizo, Peter Hill, Benny Sjöberg, Rahmatollah Khodabandeh, Joachim Claesson, Nabil Kassem, Prof. Per Lundqvist and Prof. Erik Granryd.

Thanks also to my colleagues at the division of applied thermodynamic and refrigeration, Richard Furberg, Primal Fernando, Oxana Samoteeva, Wimolsiri Pridasawas, Dimitra Sakellari,Yang Chen, Jaime Arias, Getachew Bekele, , Samer Sawalha, Raul Anton, Inga Du Rietz, Jan-Erik Nowacki, Erik Björk, Åke Melinder, Ali Rashid, Anders Johansson, Benny Andersson, Hans Jonsson, Marino Grozdek, Fridrek Lagergren, and Martin Forsén. Your time and discussions have been very valuable.

Special thanks to Prof. Ivo Martinac for accepting me as a graduate student, and Prof. Bal Raj Sehgal and Yyun Sun Park at nuclear power safety for helping me with my graduate thesis.

Finally, my great gratitude to you my wife Abir and our children Muhammad Nour and Yousef Ehsan, for their patience with me over the past few years, Thank also to my father and mother, brothers and sisters for your unlimited encouragement. I dedicate this thesis to you.

Publications

Journal papers

- Owhaib W. and Palm B., *2004*, Experimental investigation of single-phase convective heat transfer in circular microchannels. *Experimental Thermal and Fluid Science Journal,* Vol. 28, pp. 105-110.
- Owhaib W., Martín-Callizo C., and Palm B., *2004*, Evaporative heat transfer in vertical circular microchannels, *Applied Thermal Engineering Journal,* Vol. 24, pp. 1241-1253.
- Owhaib W., Palm B., and Martín-Callizo C., *2006*, Flow boiling visualization in a vertical circular minichannel at high vapor quality*, Experimental Thermal and Fluid Science Journal*, Vol. 30, pp. 755-763.
- Owhaib W., Palm B., and Martín-Callizo C., *2007*, A visualization study of bubble behavior in saturated flow boiling through a vertical mini-tube*, accepted for publication in Heat Transfer Engineering Journal.*
- Martín-Callizo C., Palm B., and Owhaib W., *2007*, Subcooled flow boiling of R-134a in a vertical channel of small diameter*, accepted for publication in Inter. Journal of Multiphase Flow Journal.*
- Owhaib W., Palm B., Martín-Callizo C., *2007*, Experimental investigation of single-phase pressure drop in circular minichannel, *submitted to Int. J. of Applied Thermal Engineering.*
- Owhaib W., Martín-Callizo C., Palm B., *2007*, Two-phase flow pressure drop of R-134a in a vertical circular microchannel, *submitted to Int. J. of Applied Thermal Engineering.*

Conference papers

- Owhaib W. and Palm B., *2002*, Experimental investigation of single-phase convective heat transfer in circular microchannels. *Proceeding of the Inter. Symposium on Compact Heat Exchangers, Grenoble, France,* August 24, pp. 101-105.
- Owhaib W. and Palm B., *2002*, Experimental investigation of convective single-phase heat transfer and pressure drop in circular minichannels. *IIR Inter. Conference, Zero Leakage Minimum Charge, Stockholm, Sweden,* August 26-28.
- Owhaib W. and Palm B., *2003*, Flow boiling heat transfer in a vertical circular microchannel tube. *Proceeding of Eurotherm Seminar No. 72, Valencia, Spain,* March 31-April 2, pp. 81-85.
- Owhaib W., Martín-Callizo C., and Palm B., *2003*, Evaporative heat transfer in a vertical circular microchannel, *the 8th UK national heat transfer, Oxford, UK,* September 9-10.

- Owhaib W., Martín-Callizo C., and Palm B., *2005*, Flow boiling visualization and heat transfer in a single vertical microchannel, *6th World Conference on Experimental Heat Transfer, Fluid Mechanics, and Thermodynamics, Matsushima, Miyagi, Japan,* April 17-21.
- Martín-Callizo C., Owhaib W., and Palm B., *2005*, Subcooled flow boiling of R134a in a vertical channel of small diameter*, 6th World Conference on Experimental Heat Transfer, Fluid Mechanics, and Thermodynamics, Matsushima, Miyagi, Japan,* April 17-21.
- Owhaib W., Martín-Callizo C., and Palm B., *2005*, Flow boiling visualization in a vertical circular minichannel at high quality, *ECI Inter. Conference on Heat Transfer and Fluid Flow in Microscale, Castelvecchio Pascoli, Italy,* 25-30 September.
- Martín-Callizo C., Owhaib W., and Palm B., *2005*, Subcooled Flow Boiling Heat Transfer and Visualization of R134a in a Vertical Transparent Heated Tube of Small Diameter, *IIR Inter. Conference, Thermophysical properties and Transfer processes of Refrigerants, Vicenza, Italy,*31 Aug. – 2 Sep..
- Celata G.P., Chmiel K., Kulenovic R., Martín-Callizo C., McPhail S., Mertz R., Owhaib W., Palm B., Sobierska E., Zummo G., *2006*, Frictional pressure drop in single-phase flow in narrow channels, *Inter. Conference Nano/Micro/MiniChannel, Limerick, Ireland,* June 19-21.
- Owhaib W., Palm B., and Martín-Callizo C., *2006*, A visualization study of bubble behavior in saturated flow boiling through a vertical mini-tube, *ECI Inter. Conference on Boiling Heat Transfer, Spoleto, Italy*, *May* 7-12.
- Martín-Callizo C., Palm B. and Owhaib W., Investigation on nucleate boiling incipience in subcooled flow of refrigerant R-134a through narrow channels, *Poster presentation at Micro and Nanoscale flows in Glasgow, UK, Dec. 2006*.
- Martín-Callizo C., Palm B., Owhaib W., and Ali Rashid, *2007*, Flow boiling visualization of R-134a in vertical channel of small diameter, *to be presented at HT2007, ASME-JSME Thermal Engineering Summer Heat Transfer Conference, July 8-12, Vancouver, British Columbia, Canada.*

Other publications

- Owhaib W., Microscale two-phase vapor-compression refrigerator for cooling of electronics to cryogenic temperatures, *internal report, May 2000.*
- Owhaib W., Martín-Callizo C., Palm B., Evaporative heat transfer and pressure drop in micro/minichannels: Correlations assessment and comparisons, *internal report, Feb 2007.*

Table of Contents

Papers

PAPER 1 Owhaib W. and Palm B., *2004*, Experimental Investigation of Single-Phase Convective Heat Transfer in Circular Microchannels. *Int. J. of Experimental Thermal and Fluid Science,* Vol. 28, pp. 105-110.

PAPER 2 Owhaib W., Palm B., Martín-Callizo C., *2007*, Experimental Investigation of Convective Single-Phase Pressure Drop in Circular Minichannel, *submitted to Int. J. of Applied Thermal Engineering.*

PAPER 3 Owhaib W., Martín-Callizo C., and Palm B., *2004*, Evaporative Heat Transfer in Vertical Circular Microchannels, *Int. J. of Applied Thermal Engineering*, Vol. 24, pp. 1241-1253.

PAPER 4 Owhaib W., Martín-Callizo C., Palm C., *2007,* Two-phase Flow Pressure Drop of R-134a in a Vertical Circular Mini/MicroChannel, *submitted to Int. J. of Applied Thermal Engineering.*

PAPER 5 Owhaib W., Palm B., and Claudi Martín-Callizo, *2006*, Flow Boiling Visualization in a Vertical Circular Minichannel at High Vapor Quality, *Int. J. of Experimental Thermal and Fluid Science,* Vol. 30, pp. 755-763.

PAPER 6 Owhaib W., Palm B. and Martín-Callizo C., *2007*, A Visualization Study of Bubble Behavior in Saturated Flow Boiling through a Vertical Mini-Tube, *accepted at the Int. J. of Heat Transfer Engineering.*

1 Introduction

Recently, there is worldwide interest in compact heat exchangers of the mini/microchannel types. Mini/microchannel evaporators present several advantages such as reduced size, higher efficiency and lower fluid inventory, which are beneficial for both cost and safety. These types of heat exchangers are already used, for instance, in heat pumps, air conditioners for automotive applications and for cooling of electronics. However, the understanding of the flow behavior on a microscale has not been on par with the fast development of such systems. A clear definition of microchannels and minichannels is still needed. In this thesis, the term microchannel will be used for the diameter range from a few micrometers to a few millimeters.

A fundamental requirement during heat exchanger design is the ability to predict heat transfer coefficients and pressure drop under the conditions of interest. In the last years, a number of experimental and theoretical investigations of two-phase flow and heat transfer in mini and microchannels have been conducted and their results published. Despite the large discrepancy existing among different authors, as a summary, it appears that boiling heat transfer, pressure drop and flow patterns in microchannels cannot be properly predicted by the existing macroscale correlations. The common explanation for this difference is that the physical mechanisms that are potentially dominant in microchannels are less important in macrochannels.

Studies in the literature reporting on single and two phase fluid flow and heat transfer in compact heat exchangers are relatively few. However, extensive applications in process industries exist where the heat is transferred utilizing flows via confined spaces and which can provide more compact design and better performance

In refrigeration and air conditioning industry, high performance and compact evaporators and condensers are always desirable. Therefore, a need for a fundamental understanding of multiphase flow and heat transfer involving boiling and condensing of refrigerants in mini and micro channels found in compact heat exchangers is necessary.

This study is focused on single-phase and two-phase flow heat transfer and pressure drop, dry out and visualization of the boiling process in mini- and micro channel.

Several features make compact heat exchangers attractive in industrial applications where the energy conservation, space and weight saving, and cost are important considerations. These features include high thermal effectiveness (ratio of actual heat transferred to the theoretical maximum heat which can be transferred), large heat transfer surface to volume ratio (surface area density), low weight per heat-

transfer duty, opportunity for true counter flow operation, close temperature approach (as a result of the ability to design for true counter flow), design flexibility, and reduced fluid inventory. Flow mal distribution and the design of headers to minimize mal distribution remain inherent problems in the application of such heat exchangers, especially in the case of phase-change heat transfer. The potential for fouling of small flow passages represents a major disadvantage in the use of compact heat exchangers. However, fouling should not be a problem in applications that involve clean fluids, such as refrigerants.

In the present study, smooth circular channels with diameters of 1.700, 1.224 and 0.826 mm were employed to simulate flow passages in typical compact heat exchangers.

1.1 Objectives for single-phase tests

The objective of this work is to gain a fundamental understanding of single-phase flow heat transfer and pressure drop in mini and micro channels with liquid R-134a as the test fluid. Particularly, an objective was to assess whether or not classical correlations for heat transfer and pressure drop are valid for mini-channels.

Another objective of the single phase tests was to validate the test rig for future boiling heat transfer tests.

1.2 Objectives for two-phase tests

Boiling and condensation can sustain large heat transfer rates with small temperatures differences. Processes associated with phase-change phenomena are among the most complex transport processes encountered in engineering applications. These processes include all the complexity of single-phase convective transport (non-linearity, transition to turbulence, instabilities) and additional elements resulting from the motion of the vapor-liquid interface, non-equilibrium effects and interactions between the phases. Two-phase flow of gases and liquids or vapors and liquids in pipes, channels, equipment, etc. is frequently encountered in industry and has been studied intensively for many years.

The objective of this part of the work was to develop the understanding of the fundamental processes in two-phase flow in mini-channels. The expected result of this increased understanding is the development of more accurate tools for prediction of heat transfer and pressure drop in this type of flow.

2 Review of Previous Work

2.1 Single-phase flow

2.1.1 Single-phase flow in macrochannels

This section presents briefly the methods for prediction of heat transfer and pressure drop of single-phase flow inside circular tubes.
A summary of well known correlations for single phase heat transfer and pressure drop for laminar and turbulent flow inside tubes is presented in the following section.

The most widely used correlation for prediction of fully developed turbulent flow heat transfer inside smooth tubes is the Dittus-Boelter (*1930*) correlation:

$$Nu = 0.023 \ \mathrm{Re}^{0.8} \ \mathrm{Pr}^{n} \tag{2.1}$$

The exponent n on the Pr is 0.3 for cooling, and 0.4 for heating of the fluid, which is the case in this thesis.
The Reynolds number inside tubes is defined as:

$$\mathrm{Re} = \frac{GD_i}{\mu} \tag{2.2}$$

where, G is the mass flux in kg/(m²s), determined by dividing the mass flow rate in kg/s by the cross sectional area of the tube in m². The Prandtl number Pr is obtained from the physical properties of the refrigerant as:

$$\mathrm{Pr} = \frac{C_p \mu}{k} \tag{2.3}$$

This correlation was developed for the following range of conditions: $Re \geq 10^4$, $0.7 \leq Pr \leq 160$, $L/D_i \geq 10$, where L is the total tube length. All the properties are evaluated at the bulk fluid temperature.

A more accurate correlation for fully developed turbulent flow was suggested by Petukhov *et al.* (*1973*). The correlation has a stated accuracy of ~ 10% for $4\times10^3 \leq Re \leq 10^6$, $0.5 \leq Pr \leq 10^6$.

Gnielinski (*1976*) suggested two correlations for the Nu number which is a modified version of Petukhov *et al.*, and for the friction factor, which gives higher accuracy and also can be used in the transition regime.

For the laminar regime, the temperature profile was not fully developed in many of the tests reported in this thesis, so the experimental data was compared to the average *Nu* number for laminar entrance regions according to Sieder and Tate (*1936*).

For fully developed laminar flows in circular channels, the product of the friction factor and Reynolds number is

$$f\,\mathrm{Re} = 64 \qquad (2.4)$$

$$Re < 2.3\times10^{3}$$

Blasius (*1913*) suggested the following relation for the turbulent flow regime in smooth circular pipes, at the recommended Re range:

$$f = 0.3164\,\mathrm{Re}^{-0.25} \qquad (2.5)$$

$$4\cdot10^{3} < Re < 10^{5}$$

Colebrook (*1939*) suggested a friction factor correlation which can be used for rough tubes.

2.1.2 Single phase flow in mini/microchannels

In the beginning of the 1980s, Tuckerman & Pease (*1981*) conducted one of the initial experiments on water flow pressure drop and heat transfer characteristics in microchannel heat sinks. This demonstrated that cooling of electronic components can be done effectively by use of forced convective flow of fluid through microchannels, and opened a wide door in the field of heat transfer in microscale geometries, and microchannel heat exchangers.

In the past years, many reports concerning the heat transfer and pressure drop behavior inside circular and noncircular microchannels have been published. Wu and Little (*1984, 1983*) measured the friction factors for trapezoidal geometry of gases flowing in silicon and glass channels with D_h= 55-76 μm, and they found it 3-5 times larger for glass channels than smooth tube predictions. They also reported higher heat transfer coefficients than predicted from the conventional correlations, and that the transition regime ranged from Re = 1000 to 3000. Wu and Little (*1984, 1983*) proposed a correlation for Nu in the turbulent regime and three friction factor correlations for the three regions, the laminar, transition and turbulent.

One of the first studies concerning circular microtube configurations instead of microchannels was reported by Choi *et al.* (*1991*). They

conducted experiments evaluating the heat transfer and pressure drop characteristics of circular silica microtubes with inside diameter D_i = 3, 7, 10, 53 and 81.2 μm, and length L = 24-52 mm using nitrogen gas as a working fluid. The conclusion was that the Reynolds analogy does not hold for microchannels. They also found that the Nusselt number in both laminar and turbulent flow depends on Re in a different manner compared to macroscale theory. Based on their measurements the critical Reynolds number is Re = 2000, which is concurrent with macrotubes. They did not observe any roughness dependence in the tubes tested.
Choi *et al.* (*1991*) suggested Nu correlations for both laminar and turbulent flow regimes. Their pressure drop data was correlated using separate expressions for the laminar and turbulent regions friction factors.

Yu *et al.* (*1995*) conducted experiments with liquid water flowing in circular microtubes having D_i = 19.2, 52.1 and 102 μm, measuring the heat transfer coefficients and the friction factor. They found that the heat transfer data at low Reynolds number agreed with those for macrotubes, while the values diverged as Re increased, in such a way that, with the microtubes the heat transfer coefficients were higher. Yu *et al.* (*1995*) found that in the laminar region, the friction factor constant C was less than the theoretical value of 64. The turbulent friction factor was also lower than the macroscale predictions. Yu *et al.* (*1995*) gave a correlation for microchannels in turbulent flow, and two friction factor correlations for his data.

Adams *et al.* (*1997, 1999*) investigated the heat transfer coefficient of turbulent water flowing in circular channels with D_i = 0.76 and 1.09 mm, they found that the Nusselt number for these channels were higher than those for macrochannels. Adams *et al.* (*1997, 1999*) modified Gnielinski correlation, which is a generalized correlation for the Nusselt number for turbulent flow.

Mala and Li (*1999*) experimentally tested water flow through microtubes with D_i from 50 to 254 μm. Their results on friction factor showed that the deviation from the macroscale theory increases as the Reynolds number increases, and as the microtube diameter decreases. They concluded also that there is an earlier transition from laminar to turbulent flow in microchannels.

Celata *et al.* (*2000*) experimentally investigated liquid R-114 flowing through six parallel tubes with D_i = 130 μm and the length 90 mm. The transition from laminar to turbulent flow was reported in the range $1881 < Re < 2479$, and the friction factor in laminar flow was found to be in good agreement with classical theory. Contrarily, they found a higher experimental heat transfer coefficients and friction factor in microchannels than those predicted by classical correlations at high Reynolds numbers.

Palm (*2000*) reviewed the literature regarding the heat transfer and pressure drop of single phase flow through microchannels, defined as channels having a hydraulic diameter of 1 mm or less. He concluded that the experimental difficulties are the probable reason for many of the deviating results.

Hrnjak and Tu (*2007*) investigated fully developed R-134a liquid and vapor flow through rectangular microchannels with D_i from 69.5 to 304.7 μm. Re ranged from 112 to 9180. They found a good agreement with classical correlations for the friction factor in the laminar region, the transition region and the turbulent region. Also the critical Re approached the conventional values.

Steinke and Kandlikar (*2006*) generated a database to evaluate the validity of the conventional friction factor theory. They found that, if one is carefully identifying the pressure drop components in the measurements data, the deviations become less.

The reasons for the deviations from the conventional theory reported by many investigators can be related to:

- Most of the early microchannel single phase investigations were done with silicon microchannels and with high pressure drop across the channel. It has been reported that the channel dimensions have been deformed in terms of geometry and shape, under the operation due to excessive pressure.

- Experimental uncertainties, which can be quite large for microchannels. Especially, the diameter measurement can have large uncertainties, as some investigators may have relied on the manufacturer's tolerance limits. This is known to be the reason for the significant deviation in some of the early papers in the literature. Also, diameters may change along the channel and it may not be enough measuring the hydraulic diameter at the ends of the channel. Better would be to measure the average channel geometry across the channel length.

- The Abrupt contraction and expansion pressure drop at the inlet and outlet ports have sometimes not been accounted for, and also, the fact that the flow is not fully developed might have a significant impact on the experimental results, thereby leading to deviations from macroscale theory.

The deviations from the classical theory has been show to be decreasing with time due to use of more accurate measurements equipment, and better understanding of the parameters that contribute to the total pressure drop across the channel.

2.2 Two-phase flow

Many researchers are still working extensively on boiling heat transfer. It has proven hard to find a common single model describing the boiling process. Each of these models is developed to serve a particular technology, application, branch, etc. This section will highlight some of the most commonly used models and correlations for flow boiling heat transfer inside tubes.

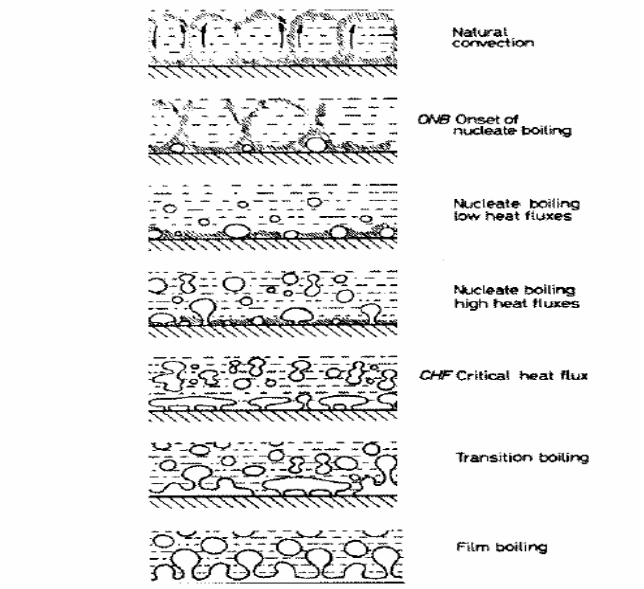

Figure 2.1: The various stages in the pool boiling curve, Collier and Thome (*1994*)

The first basic knowledge of the boiling process is obtained from pool boiling. Depending on the heat flux, several boiling mechanisms can be classified, as; convective boiling, nucleate boiling, transition boiling, and film boiling. From the boiling characteristics (the relation between the heat transfer coefficients, the heat flux and the mass flux), the boiling mechanisms in flow boiling inside confined spaces, is known to be similar to pool boiling, at least in flow regimes when the bubbles are squeezed by the tube wall, and become elongated.

In Pool boiling, vapor bubbles growing on the heated wall at active nucleation sites are formed by vaporization of superheated liquid surrounding the bubbles and by thin-film evaporation in the microlayer trapped beneath the bubbles. This thin-film evaporation in the microlayer we believe happens also in the thin film between the elongated bubbles and the heated wall. This could explain the similarity in behavior between pool boiling and boiling in mini/microchannels.

2.2.1 *Pool boiling*

According to Hsu and Graham (*1976*) three heat transfer mechanisms are controlling the nucleate pool boiling process, bubble agitation mechanism, vapor-liquid exchange mechanism and evaporation mechanism.

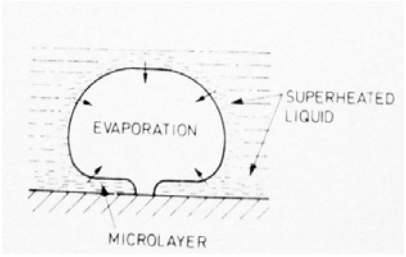

Figure 2.2: Plain surface nucleate pool boiling evaporation, Collier and Thome (*1994*).

In evaporation mechanism, vapor bubbles are growing in the superheated layer which is formed on the heated surface. The macro-evaporation takes place around the sides and top of the bubble which is surrounded by the thermal boundary layer. On the other hand, micro-evaporation is happening in the thin layer of liquid underneath the bubble which is trapped between a rapidly growing bubble and the surface (microlayer evaporation).

2.2.1.1. *Pool boiling correlations*

Nucleate boiling correlations express the heat transfer coefficient as a function of heat flux, fluid properties, and fluid pressure. Some nucleate pool boiling correlations are presented below. Rohsenow (*1962*) proposed one of the first nucleate pool boiling correlations, based on the bubble agitation mechanism.

Stefan and Abdelsalam (*1980*) analyzed a large number of data points mostly for horizontal tubes, and applying a statistical multiple regression technique. The data best fit if divided into four fluid correlations: water, organics, refrigerants and cryogens. The correlation proposed for refrigerants is given in appendix E.

Cooper (*1984*) based his correlation on an extensive study, where he used some 6000 pool boiling data points from published sources, related to over 100 experiments. He proposed a more accurate pool boiling correlation based on reduced pressure, which is in a sense simple to use. In the correlation, the heat transfer coefficient is a function of the heat flux, reduced pressure, surface roughness of the boiling surface, and molecular weight of the fluid:

$$h_{Pool} = 55 p_R^{0.12-0.2\log_{10}\varepsilon} \left(-\log_{10} p_R\right)^{-0.55} M^{-0.5} q''^{0.67} \qquad (2.6)$$

where ε is in μm, h in W/(m²K), and q'' in W/m².
Cooper's correlation is used and recommended by different authors, and beyond that it predicted the tendencies in our experimental heat transfer coefficient in microscale better than other pool boiling correlations.

2.2.2 *Macroscale flow boiling heat transfer*

In saturated flow boiling heat is usually considered to be transferred by two different mechanisms, convective evaporation and nucleate boiling. In convective evaporation where the heat is transferred by ordinary convective heat transfer in single-phase liquid, the heat transfer rate increases with increasing mass flux and/or vapor quality. The liquid temperature gradient close to the heated wall is high, since the main resistance to heat transfer is at the heated wall. This mechanism is often modeled using heat transfer correlations similar to single-phase heat transfer correlations including a fluid flow enhancement factor.

In nucleate boiling, heat is mainly transferred into the two-phase bulk flow by means of bubbles nucleating on the surface, growing and finally detaching from the surface. This heat transfer mechanism is similar to pool boiling and often modeled by a pool boiling correlation, where the heat transfer coefficient is increasing with increasing heat flux, and independent of vapor quality and mass flux.

Several correlations are calculating the heat transfer coefficient by combining the contribution of these two mechanisms. The combining process is treated differently in different correlations. Generally, a factor is introduced into the convective and nucleate boiling correlations. The enhancement factor, *E,* of the convective boiling contribution is motivated by the presence of bubbles. Also, the suppression factor, *S,* of the nucleate boiling contribution is due to the fact that the liquid flow might suppress bubble nucleation. The combined effect of these two boiling mechanisms is not fully understood.

There is no universal boiling heat transfer correlation that can be used for all types of boiling and all possible fluids. This section will point out some of the most commonly used correlations for flow boiling heat transfer inside tubes. The aim in the following chapters is to use the available correlations and try to apply these, if necessary after modification, to micro scale tube experimental data.

Cornwell and Kew (*1993*) reported the effect of confined space on the heat transfer. In a narrow channel, the growth of bubbles results in a thin liquid layer on the channel surface. A dimensional group, confinement number, N_{conf}, was defined as the ratio of a characteristic bubble departure size to the diameter of the flow channel as follows:

$$N_{conf} = \frac{\left[\frac{\sigma}{g(\rho_l - \rho_g)}\right]^{0.5}}{D} \tag{2.7}$$

2.2.2.1. Classification of different types of flow boiling heat transfer correlations

In forced convective boiling in tubes, two groups of correlations might be classified: *a)* Correlations giving an average heat transfer coefficient for the whole boiling process, and, *b)* correlations for the local heat transfer coefficient as a function of vapor quality. Further, models for local heat transfer coefficients can be according to Webb and Gupte (*1992*) divided into three different groups: enhancement, superposition and asymptotic models. These can be described as follows. The enhancement models calculated the two-phase heat transfer coefficient as an enhanced single-phase heat transfer coefficient.

$$h_{tp} = E \cdot h_{sp} \tag{2.8}$$

The single-phase heat transfer coefficient h_{sp} is normally calculated by the Dittus and Boelter (*1930*) equation or Gnielinski (*1976*) equation both presented above.
The superposition model assumes the two-phase heat transfer coefficient to be the sum of a nucleate boiling term and a convective evaporation term.

$$h_{tp} = h_{nb} + h_{cb} \tag{2.9}$$

The asymptomatic model is similar to the superposition model but a power function is added.

$$h_{tp}^{n} = h_{nb}^{n} + h_{cb}^{n} \qquad \text{where, } n > 1 \tag{2.10}$$

2.2.2.2. Flow boiling correlations

The Chen (*1966*) correlation was developed on the basis of 665 data points from six different data sources. This was the first generalized correlation. It was based on the assumptions that the heat transfer of flow boiling could be divided into two parts, namely the nucleate boiling contribution and the non-boiling forced convective contribution. For the convective contribution, the liquid heat transfer coefficient is calculated from the Dittus-Boelter single-phase equation with the liquid fraction flowing alone in the same tube. The factor, *E*, was introduced reflecting the fact that the velocities are much higher due to the presence of the vapor phase and hence forced convection heat transfer is higher in two-phase flow compared to the single-phase liquid only flow. E, often called the convective heat transfer enhancement factor or multiplier, was correlated against the Martinelli parameter. For the nucleate boiling contribution, the pool boiling heat transfer coefficient was calculated from Forster and Zuber`s pool boiling equation. The factor, *S*, or nucleate boiling suppression factor, reflects the fact that in flow boiling, due to the thinner thermal boundary layer, the mean effective superheat is lower than that in pool boiling. The suppression factor was correlated against Reynolds number.
The overall deviation for the data was 12%. But later on, many comprehensive comparisons showed that this correlation gives a rather poor fit to the data, at least for refrigerants.

Pierre (*1969*) proposed a correlation to calculate the average heat transfer coefficient in a long horizontal tube. His original work was based on the boiling of R-12 in copper tubes, heated by flowing water in a concentric tube. Later, the correlation was confirmed for R-22 and R-502 by his further experiments and for R-11 and methyl chloride by other investigators. He gave two correlations, one for incomplete and the other for complete evaporation. A correction factor was suggested by Palm (*1991*) to account for the changes in the accepted values for the thermodynamic and transport properties of the fluids used in the original tests since Pierre suggested his correlations.

Shah (*1976, 1982*) proposed a correlation in graphical form using the boiling number and the convective number. A total of 780 data points were used in developing the correlation. His correlation is in the form of a non-dimensional relation. Steiner and Taborek (*1992*) highlighted that the use of a convective heat transfer coefficient to give non dimensional nucleate boiling contribution to heat transfer is physically unreasonable. The heat transfer coefficient includes both mass flux and quality effects that are inappropriate in this regime.

Cooper (*1989*) used five sources for up or down flow of boiling water in tubes, for which he identified the nucleate boiling parts. He

concluded that the correlation in pool boiling can be used to give the trends of the heat transfer coefficient in nucleate flow boiling as well.

Wattelet (*1992*) reported experimental results of convective boiling of refrigerant R-134a and R-12 tested in smooth 10 to 21 mm diameter horizontal copper tube with a length of 2.43 m. The heat transfer coefficient of R-134a was on average 25% higher than that of R-12 at a similar test condition in the annular flow regime.

Gungor and Winterton (*1986*) presented a correlation based on a data bank consisting of over 4300 data points for water, refrigerants and ethylene glycol, for saturated boiling in vertical and horizontal tubes, and annuli. The mean deviation between the calculated and measured boiling heat transfer coefficient is 21.4%.

Klimenko (*1988, 1990*) suggested a correlation valid for vertical and horizontal channels with fully wetted perimeter, for two-phase forced flow heat transfer (nucleate and convective). Experimental data for 21 different liquids (water, organic liquids, refrigerants and cryogens), at the following main parameters : pressure, 0.61-196 bar, heat flux density, 10-8.10^3 kW/m^2, mass flow rate, 5.6-6240 kg/(m^{2}s), channel diameter, 0.47-74.7 mm. He found that both the nucleate boiling and the convective heat transfer coefficients depend on the thermal conductivity of the channel wall material. He demonstrated that nucleate boiling heat transfer is described by a single equation in dimensionless variables containing an individual constant for each of the four groups of fluids. The correlation represented the data with the mean absolute deviation of 14.4%. The data consisted of 3215 experimental points of which 511 points were for refrigerants.

The correlation of Kandlikar (*1991*) has separate terms representing nucleate-boiling and convection contributions to the heat transfer. These terms are of comparable magnitude at a high quality.

Liu and Winterton (*1991*) developed a flow boiling correlation for vertical and horizontal flow in tubes and annuli. The data used in developing their correlation are the same as those described in Gungor and Winterton (*1986*). They were collected from 29 different literature sources including nine different fluids. The data bank contains 4202 data points for saturated boiling. The presented correlation for predicting the heat transfer coefficient in saturated flow boiling contains an empirical boiling number correction. The boiling number correction was to allow for the enhancement of the forced convective heat transfer mechanisms arising from the generation of vapor in the boundary layer next to the wall.

They showed that the enhancement factor E should have a Prandtl number, vapor quality and liquid to vapor density ratio dependence. The Dittus-Boelter correlation was selected to evaluate the liquid single-phase heat transfer coefficient. The Cooper (*1984*) correlation was selected for the nucleate boiling term. If the tube is horizontal and the Froude

number less than 0.05, the authors included Froude number correction factors in their correlation.

Jung and Radermacher (*1991*) measured more than 3000 local heat transfer coefficients and 400 pressure drops of R-22, R-114, R-12, R-152a, and their mixtures at various concentrations during evaporation. The correlation of Jung and Radermacher (*1991*) is of the same type as Chen (*1966*) including two terms for convection and nucleate boiling, respectively. Based on their study of 13 different refrigerants/mixtures, they concluded that for a quality larger than 0.2, nucleate boiling is predicted to be fully suppressed for all refrigerants, indicated by the fact that the heat transfer coefficient increases with quality.

Wattelet *et al.* (*1994*) modified an empirical correlation developed for annular flow data using an asymptotic form to account for the decrease in heat transfer due to wavy-stratified flow pattern in horizontal flow for low mass fluxes. The Cooper (*1984*) correlation was selected for the nucleate boiling term, while for the convective boiling term, a modified form of the convective term in the Chen (*1966*) correlation was selected. The Dittus-Boelter correlation was selected to evaluate the single phase heat transfer coefficient $h_{D\text{-}B,\,f}$. For low mass fluxes, a Froude number correction was added to the convective boiling term to account for the decrease in available convective heat transfer area and a loss of turbulence. This correction offsets the over estimation of the single-phase liquid heat transfer coefficient through use of the Dittus-Boelter correlation for tests with Reynolds number below 10,000. This correlation is to predict both the annular and wavy-stratified flow data.

Note that in the correlations by Chen (*1966*), Gungor and Winterton (*1986*), Liu and Winterton (*1991*), Jung and Radermacher (*1991*), and Wattelet *et al.* (*1994*) correlations, the evaporative heat transfer coefficient consists of a compensated combination of the two mechanisms: Nucleate boiling, calculated using a pool boiling correlation corrected by a suppression factor S; and a convective boiling contribution, modeled by the Dittus–Boelter equation corrected by enhancement factor E.

It has been shown by Jung and Radermacher (*1991*), and Wattelet *et al.* (*1992*) that boiling heat transfer of refrigerants in large-diameter channels is dominated by the convection mechanism at a quality higher than 20-30%. In contrast, conclusions differ among various researchers as to the boiling heat transfer mechanisms in small channels over the entire quality range.

These correlations are not particularly suited for small tube flow boiling. However, since they were developed for refrigerants and are well known, they were used for comparison with the present experimental results.

2.2.3 *Microscale flow boiling heat transfer*

Applications of compact heat exchangers for both single- and two-phase flows have been increasing in recent years. To quantify the high surface-area-to-volume ratio characteristic of compact heat exchangers, Shah (*1986*) defined a compact heat exchanger as an exchanger with a surface area density > 700 m^2/m^3. This limit translates into a hydraulic diameter smaller than 6 mm. Relatively few studies have been reported in the open literature that focuses on boiling in small passages as compared to single-phase heat transfer in such microchannels.

Bergles (*1963*) conducted experiments to study the effect of system pressure, inlet subcooling, mass velocity, channel dimensions on stable burnout inside small tubes of boiling distilled water. The channels of hydraulic diameter 6.3 mm or less gave higher burnout compared to larger diameter tubes. He concluded that as the channel size goes down the data considerably deviates from that predicted based on larger channel dimension.

Lazarek and Black (*1982*), measured the local and average heat transfer coefficient, pressure drop, and critical heat flux of saturated boiling of R-113 flowing vertically upwards and downwards in single 3.17 mm tubes, L = 123 and 246 mm, G = 125–750 kg/(m^2s), p = 1.3–4.1 bar, q'' = 14–380 kW/m^2, and $\Delta T_{sub,in}$ = 3–73 K. The heat transfer coefficient was found to be independent of x for $x \geq 0$. They presented an empirical correlation for local saturated boiling heat transfer coefficients, where the Nusselt number is a function of the liquid Reynolds number and the boiling number.

$$h_{tp} = 30\left(\mathrm{Re}_{lo}\right)^{0.857}\left(Bo\right)^{0.714}\frac{k_l}{D_i} \tag{2.11}$$

They concluded that nucleate boiling was the dominant heat transfer mechanism in all tests, based on the observed strong dependence of heat transfer coefficient on heat flux and negligible influence of quality. They suggested that the occurrence of nucleate boiling dominated heat transfer all the way to CHF could be attributed to the high boiling number ($Bo > 5 \times 10^{-4}$) of their data. Predictions from the Chen (*1966*) and Shah (*1982*) correlations were compared with their experimental data, concluding that the Shah correlation showed reasonable agreement.

Wambsganss *et al.* (*1993*), investigated the nucleate flow boiling of R-113 through a single tube, 2.92 mm inside diameter, G = 50–300 kg/(m^2s), P = 1.24–1.6 bar, q'' = 8.8–90.7 kW/m^2, x = 0–0.9 and T_{in}= 20–50 °C. The heat transfer coefficient slightly decreased with increasing x for $x \geq 0$. Predictions from 10 empirical correlations were compared

with their experimental data. The Lazarek and Black correlation showed the best agreement.

Tran *et al.* (*1996, 1997*), measured the local heat transfer coefficients and overall two-phase pressure drop for three different refrigerants (R-113, R-12, R-134a) through both a single circular tube of 2.46 mm inner diameter and rectangular cross-sectioned channels of hydraulic diameter within 2.4 and 2.9 mm, and G = 44–832 kg/(m²s), P = 5.1 and 8.2 bar, q'' = 3.6–129 kW/m² and x = 0 – 0.94. Their results showed different behavior of the flow boiling in small channels from that of large hydraulic diameters. Nucleate boiling was dominant for wall superheats larger than 2.75 K, forced convective boiling for walls superheated less than 2.75 K, and the heat transfer coefficient was independent of x for $x \geq 0.2$. An empirical correlation was proposed, where the heat transfer coefficient was correlated with the boiling number, Weber number, and liquid to vapor density ratio. No significant geometry effect was found between circular and rectangular channels.

Misale and Bergles (*1997*) investigated the influence of channel width on subcooled and saturated boiling of FC-72 and HT-55, using the channel widths 3.3, 2, and 0.5 mm. q'' = 0-30 kW/m². In the convection dominated regime, the reduction of the channel width decreased the heat transfer coefficient, while in the nucleate boiling regime the heat transfer coefficient increased.

Kew and Cornwell (*1994*) found that simple nucleate boiling correlations predicted relatively well their results in single narrow tubes, in the confined bubbles flow region. They also underlined that pool boiling correlations often have no geometric components although the influence of surface angle and tube diameter for example have shown to be important. Nucleate boiling is enhanced in small channels at low wall superheats above that predicted by a pool boiling correlation.

Kew and Cornwell (*1997*) investigated nucleate boiling, confined bubble boiling, partial dry-out, and convective boiling of R-141b in single tubes with 1.39–3.69 mm inside diameter. For the larger tubes (2.87 and 3.69 mm), the heat transfer coefficient decreased slightly or remained constant with increasing x for $x \leq 0.2$, but increased for $x \geq 0.2$. For the smaller tube (1.39 mm inside diameter), the heat transfer increased with increasing x at low mass flux, G, for $x \geq 0$, but decreased rapidly at high G for $x \geq 0$.

Yan and Lin (*1998*), measured the heat transfer of R-134a evaporating in a horizontal bundle of 28 parallel tubes of 2 mm internal diameter, L = 20 mm, G = 50–200 kg/(m²s) and q'' = 14–380 kW/m². The heat transfer coefficient decreased with increasing x for $x \geq 0$. They concluded that the evaporation heat transfer in the small pipes is more effective than that in larger pipes, and their data fitting was made based

on a heat transfer correlation, where the non-dimensional convection number, boiling number, and liquid Froude number are included.

In Bao *et al.* (*2000*), the heat transfer coefficients of R-12, and R-123 flow boiling were measured for flow through a single horizontal tube of 1.95 mm inner diameter. The flow conditions were G = 50-1800 kg/(m²s), P = 2–5 bar, q'' = 5–200 kW/m², and x = 0–0.9. The heat transfer coefficient was independent of x for x ≥ 0, and their data showed a strong dependence of the heat transfer coefficient on the heat flux and the system saturation pressure, while it was independent of the mass flux and vapor quality.

Kennedy *et al.* (*2000*), investigated subcooled water flow instability and onset of nucleate boiling in 1.17 and 1.45 mm diameter horizontal uniformly heated circular channels, q'' = 0–4000 kW/m², and G= 800 to 4500 kg/(m²s). They used a correlation suggested by Bergles and Rohsenow to predict the onset of nucleate boiling.

Yu *et al.* (*2002*), studied the flow boiling heat transfer of water through a single horizontal tube of 2.98 mm inner diameter, L = 0.91 m, G = 50–200 kg/(m²s), P = 2 bar and T_{in} = ambient to 80 °C. They found nucleate boiling at wall superheats below 8 K, and transition boiling at wall superheats above 8 K. An empirical correlation was proposed for the nucleate boiling region of water flow boiling.

Warrier *et al.* (*2002*) investigated the heat transfer of convective single-phase, subcooled and saturated boiling of FC-84 through five parallel horizontal 0.75 mm hydraulic diameter microchannels, q'' = 0–59.9 kW/m². Based on their few experimental data points, they proposed a correlation for saturated flow boiling.

Khodabandeh (*2005*) investigated the flow boiling in advanced two-phase thermosyphon different evaporator consist of vertical circular minichannels with D_i= 1.1-3.5 mm, and L=14 mm, using isobutene. He concluded that the heat transfer behavior is indicating that nucleate boiling is the dominant mechanism. He also proposed a correlation to fit his experimental results.

2.2.4 Macroscale two-phase pressure drop

Steady flow of gas or vapor and liquid occurring in oil and gas lines, water and steam flow in boilers and evaporators, etc., are good examples of two-phase flow in many situations in the process industries. Because of the presence of the two-phase, there are considerable complications in describing and quantifying the nature of the flow compared to single-phase flow. Extensive work have been reported on two-phase flow in channels with hydraulic diameters greater than 6 mm, however,

considerably less work has been conducted with mini- and micro channels.

2.2.4.1. Homogeneous flow model

The simplest prediction of pressure drop in two-phase flow is done by assuming homogeneous flow. In this case the two-phase mixture is treated as a single-phase fluid characterized by mixture averaged properties. In the homogenous two-phase flow model, the liquid and vapor velocities are assumed to be the same, and the frictional pressure drop is estimated as if the flow is only liquid or gas single-phase flowing alone, with a correction to account for homogeneous density and viscosity.

A detailed description and derivation of equations applied to two-phase flow in channels can be found in Collier and Thome (*1994*). From the momentum equation, the total static pressure gradient can be separated into components of friction, acceleration and static head.

$$\left(\frac{dP}{dz}\right)_H = \left(\frac{dP}{dz}\right)_f + \left(\frac{dP}{dz}\right)_a + \left(\frac{dP}{dz}\right)_g \tag{2.12}$$

$$\left(\frac{dP}{dz}\right)_a = G^2 \frac{d}{dz}\left[\frac{x^2}{\rho_g \alpha} + \frac{(1-x)^2}{\rho_l (1-\alpha)}\right] \tag{2.13}$$

$$\left(\frac{dP}{dz}\right)_g = g \sin\theta\left[\alpha\rho_g + (1-\alpha)\rho_l\right] \tag{2.14}$$

$$\left(\frac{dP}{dz}\right)_f = \frac{f_{tp} P}{A}\left(\frac{\rho_H u_H^2}{2}\right) \tag{2.15}$$

Where, the homogenous density is given as:

$$\frac{1}{\rho_H} = \frac{x}{\rho_g} + \frac{1-x}{\rho_l} \tag{2.16}$$

and, the homogenous velocity of the two-phase fluid is: $u_l = u_g = u_H$

In case of a circular channel where $\phi / A = 4 / D_i$:

$$\left(\frac{dP}{dz}\right)_f = \frac{f_{tp} G^2}{2\rho_H D} = \frac{f_{tp} G^2}{2\rho_l D}\left[1 + x\frac{(\rho_l - \rho_g)}{\rho_g}\right] \tag{2.17}$$

Neglecting the compressibility of the liquid phase in the acceleration term, the homogenous model total pressure gradient is:

$$\left(\frac{dP}{dz}\right)=\frac{\dfrac{f_{lo}G^2}{2\rho_l D}\left[1+x\left(\dfrac{\rho_l-\rho_g}{\rho_g}\right)\right]+\dfrac{G^2}{\rho_l}\left(\dfrac{\rho_l-\rho_g}{\rho_g}\right)\dfrac{dx}{dz}+\dfrac{g\rho_l\sin\theta}{\left[1+x\left(\dfrac{\rho_l-\rho_g}{\rho_g}\right)\right]}}{1+G^2x\left(\dfrac{d}{dP}\dfrac{1}{\rho_g}\right)} \tag{2.18}$$

In case of saturation condition at the inlet (x=0) and a vapor-liquid mixture with mass quality x at the outlet, and a linear change of x over the tube length L, the total pressure drop will be.

$$\begin{aligned}\Delta P=&\frac{f_{lo}L_{tp}G^2}{2\rho_l D}\left[1+\frac{x}{2}\left(\frac{\rho_l-\rho_g}{\rho_g}\right)\right]+\frac{G^2}{\rho_l}\left(\frac{\rho_l-\rho_g}{\rho_g}\right)x\\&+\frac{gL\sin\theta}{x}\frac{\rho_l-\rho_g}{\rho_g\rho_l}\ln\left[1+x\left(\frac{\rho_l-\rho_g}{\rho_g}\right)\right]\end{aligned} \tag{2.19}$$

This model could be applied for the bubbly and wispy-annular flows (Collier and Thome, *1994*).

For determining the friction factor, a value for the viscosity is needed.

$$f_{tp}=\begin{cases}\dfrac{64}{\mathrm{Re}_{tp}} & for\ \ \mathrm{Re}_{tp}<2300\\[2ex] 0.316\,\mathrm{Re}_{tp}^{-0.25} & for\ \ \mathrm{Re}_{tp}>2300\end{cases}\text{, and}\qquad \mathrm{Re}_{tp}=\frac{GD_i}{\mu_{tp}} \tag{2.20}$$

Correlations have been presented in the literature to estimate the homogenous two-phase viscosity as:

McAdams *et al.* (*1942*): $\dfrac{1}{\mu_{tp,H}}=\dfrac{x}{\mu_g}+\dfrac{1-x}{\mu_l}$ (2.21)

Cicchitti *et al.* (*1960*): $\mu_{tp,H}=\left(x\mu_g+(1-x)\mu_l\right)$ (2.22)

Dukler *et al.* (*1964*): $\mu_{tp,H}=\rho_H\left(x\dfrac{\mu_g}{\rho_g}+(1-x)\dfrac{\mu_l}{\rho_l}\right)$ (2.23)

2.2.4.2. *Void fraction correlations*

The void fraction is defined as the cross sectional area occupied by gas over the total cross section area. Butterworth (*1975*) presented a general form of correlation valid for several void fraction correlations from the literature:

$$\alpha = \left[1 + A\left(\frac{1-x}{x}\right)^{B}\left(\frac{\rho_g}{\rho_l}\right)^{C}\left(\frac{\mu_l}{\mu_g}\right)^{D}\right]^{-1} \tag{2.24}$$

where the A, B, C, and D values are given in table 2.1 for different correlations:

Table 2.1 Butterworth constants for several void fraction correlations

Model or correlation	A	B	C	D
Homogenous Model	1	1	1	0
Lockhart-Martinelli correlation (*1949*)	0.28	0.64	0.36	0.07
Zivi Model (*1963*)	1	1	0.67	0
Baroczy correlation (*1963*)	1	0.74	0.65	0.13
Thome correlation (*1964*)	1	1	0.89	0.18
Turner-Wallis two-cylinder model (*1965*)	1	0.72	0.4	0.08

2.2.4.3. *Separated flow model*

In the separated flow model the phases are assumed to be separated into two streams, liquid and vapor, flowing at constant velocities, but not necessary the same velocity as in the homogenous model. The model uses empirical correlations or simplified concepts to relate the two-phase friction multiplier ϕ^2 and the void fraction α to the independent variables of the flow.

The total static pressure gradient as evaluated from the separated flow model is:

$$\left(\frac{dP}{dz}\right) = \frac{\dfrac{f_{lo}G^2}{2\rho_l D}\phi_{lo}^2 + G^2\dfrac{dx}{dz}\left[\left(\dfrac{2x}{\alpha\rho_g} - \dfrac{2(1-x)}{(1-\alpha)\rho_l}\right) + \left(\dfrac{\partial\alpha}{\partial x}\right)_p\left(\dfrac{(1-x)^2}{(1-\alpha)^2\rho_l} - \dfrac{x^2}{\alpha^2\rho_g}\right)\right] + g\sin\theta\left[\rho_g\alpha + \rho_l(1-\alpha)\right]}{1 + G^2\left[\dfrac{x^2}{\alpha}\left(\dfrac{d}{dp}\rho_g\right) + \left(\dfrac{\partial\alpha}{\partial p}\right)_x\left(\dfrac{(1-x)^2}{\rho_l(1-\alpha)^2} - \dfrac{x^2}{\rho_g\alpha^2}\right)\right]} \tag{2.25}$$

assuming that the compressibility of the gaseous phase may be neglected, and that for both phases the densities (ρ_l *and* ρ_g) and the friction factor f_{lo} remain constant over the length.

For saturated flow boiling with a linear change of x over the length *L*, the total pressure change is:

$$\Delta P = \frac{2 f_{lo} L_{tp} G^2}{\rho_l D}\left[\frac{1}{x}\int_0^x \phi_{lo}^2 dx\right] + \frac{G^2}{\rho_l}\left[\frac{x^2}{\alpha}\left(\frac{\rho_l}{\rho_g}\right) + \frac{(1-x)^2}{(1-\alpha)} - 1\right] + \frac{gL\sin\theta}{x}\int_0^x \left[\rho_g \alpha + \rho_l (1-\alpha)\right] dx \tag{2.26}$$

This model could be expected to be applicable for annular flow pattern (Collier and Thome, *1994*).

The Lockhart-Martinelli (*1949*) method is the basis for most of the recent methods to correlate two-phase frictional pressure drop. In the method, the two-phase multiplier is dependant upon the so-called Lockhart-Martinelli parameter (*X*), i.e. the ratio of pressure gradients between liquid and vapor phases. Chisholm (*1967*) presented an analytical form of the latter method that includes the Lockhart-Martinelli parameter and a constant, *C*, ranging from 5 to 20, based on the liquid and vapor flow regimes. Baroczy (*1965*) introduced a modification of the Lockart-Martinelli correlation, which includes the effect of mass flux and fluid properties on the two-phase multiplier. Friedel (*1979*) developed an empirical correlation for the two-phase multiplier, as a function of the Froude number, *Fr*, the Weber number, *We*, and the liquid and vapor properties.

To obtain two-phase fictional pressure drop in a way similar to single-phase frictional pressure drop, Lockhart and Martinelli (*1949*) expressed the two-phase flow frictional pressure drop in terms of a two-phase flow multiplier such that:

$$\left(\frac{dP}{dz}\right)_{f,tp} = \phi_{f,l}^2 \left(\frac{dP}{dz}\right)_{f,l} \tag{2.27}$$

and

$$\left(\frac{dP}{dz}\right)_{f,tp} = \phi_{f,g}^2 \left(\frac{dP}{dz}\right)_{f,g} \tag{2.28}$$

The terms $\left(\frac{dP}{dz}\right)_{f,l}$ and $\left(\frac{dP}{dz}\right)_{f,g}$ are the frictional pressure gradients that would result if the flow is liquid or vapor phase, flowing through the channel at the mass flow rate equal to *[(1-x)GA]* and *[xGA]*, respectively.

2.2.4.4. *Two-phase flow multiplier*

Lockhart and Martinelli (*1949*) proposed generalized correlation to determine the two-phase flow multipliers $\phi_{f,l}^2$ and $\phi_{f,g}^2$ for liquid and vapor, respectively.

The generalized correlations of $\phi_{f,l}^2$ and $\phi_{f,g}^2$ are expressed as:

$$\phi_{f,l}^2 = 1 + \frac{C}{X} + \frac{1}{X^2} \tag{2.29}$$

and

$$\phi_{f,g}^2 = 1 + CX + X^2 \tag{2.30}$$

The recommended value of the constant C depends on the flow regimes of gas and liquid flowing alone in the channel (i.e., either laminar or turbulent). The method of calculating two-phase flow frictional pressure drop using Equation 2.26 or Equation 2.27 is called C-coefficient method (Chisholm, *1973*).

The two-phase multiplier is a function of a variable C and the Lockhart-Martinelli parameter X^2, where X^2 is defined as:

$$X^2 = \frac{\left(\frac{dP}{dz}\right)_{fri,l}}{\left(\frac{dP}{dz}\right)_{fri,g}} \tag{2.31}$$

Chisholm and Sutherland (*1969*) used the "B-coefficient method" to calculate the two-phase flow pressure gradient due to friction in smooth tubes. They defined a "Physical property coefficient" to use in the calculation which is expressed as:

$$\Pi^2 = \frac{\left(\frac{dP}{dz}\right)_{fri,lo}}{\left(\frac{dP}{dz}\right)_{fri,go}} \tag{2. 32}$$

In Chisholm´s B-coefficient method, the liquid frictional multiplier has the following expression:

$$\phi_{f,lo}^2 = 1 + \left(\Pi^2 - 1\right)\left[Bx^{\left(\frac{2-n}{2}\right)}\left(1-x\right)^{\left(\frac{2-n}{2}\right)} + x^{(2-n)}\right] \tag{2.33}$$

where n=0.25 for flow inside a smooth tube and B values for smooth tubes is given in appendix F.

Friedel (*1979*) used a large data base of 25000 pressure drop data to develop an optimized correlation for predicting the two-phase flow multiplier $\phi^2_{fri,l,only}$ for vertical upward and horizontal flows in circular tubes.

Jung and Radermacher (*1989*) conducted experiments with refrigerants R-22, R-114, R-12, R-152, and mixtures in 9.1 mm inside diameter, 4 m long, and stainless steel horizontal tubes. They presented a correlation for two-phase flow multiplier of pure and mixed refrigerants as the following:

$$\phi^2_{f,lo} = 12.82 X_{tt} (1-x)^{0.18} \tag{2.34}$$

They refer to Cooper stating that the physical properties in the Martinelli parameter can be correlated by the reduced pressure P_R in case of pure fluids as:

$$\left(\frac{\rho_g}{\rho_l}\right)\left(\frac{\mu_l}{\mu_g}\right) = 0.551 P_R^{0.492} \tag{2.35}$$

The Martinelli parameter can then be rewritten as:

$$X_{tt} = 0.551 \left(\frac{1-x}{x}\right)^{0.9} P_r^{0.492} \tag{2.36}$$

2.2.4.5. Other correlations

Müller-Steinhagen and Heck (*1986*) suggested a correlation for the prediction of frictional pressure drop for two-phase flow in pipes which is simple and convenient, which was developed after evaluation 9300 measurements for a variety of fluids and flow conditions.

Pierre (*1969*) using the same arrangements as in the boiling heat transfer, he proposed a correlation to predict the frictional pressure drop.

2.2.5 Microscale two-phase pressure drop

Mishima and Hibiki (*1996*) investigated the flow regime, void fraction, rise velocity of slug bubbles, and frictional pressure drop of air-water flow in vertical tubes with D_i=1.05-3.9 mm, L=210-1000 mm. Their data was well correlated by Chisholm′s correlation with a new equation for Chisholm′s parameter C as a function of inner diameter.

$$C = 21\left(1 - e^{-0.319 D_h}\right) \tag{2.37}$$

where, D_h is the hydraulic diameter. The correlation could be used for rectangular horizontal or vertical channels.

Studies on refrigerant two-phase flow inside narrow tubes, such as those from Yang and Webb (*1995*) or Wang *et al.* (*1997*) have concluded that neither the Chisholm nor the Friedel correlation, can predict the experimental data. As a result, new correlations specifically developed for mini and microchannels have been suggested in the literature.

Tran et al (*1999*), measured horizontal two-phase flow pressure drop during evaporation of refrigerants R-134a, R-12 and R-113. Pressure drop measurements were carried out in two circular tubes of 2.46 and 2.92 mm inside diameter and one rectangular channel 4.06×1.7 mm, and at six system pressures ranging from 138 to 856 kPa, exit qualities were 0.2-0.95. The channels length ranged between 412 to 914mm, mass and heat fluxes were 33-832 kg/(m²s) and 2.2-129 kW/m², respectively. Five large-tube correlations were evaluated, but failed to predict the flow boiling pressure drop in small diameters for all test conditions. They presented a new correlation for two-phase frictional pressure drop on the basis of the *B*-coefficient method, taking into account the effect of surface tension and channel size.

Lee and Lee (*2000*) presented an experimental study on horizontal two-phase adiabatic pressure drop in small rectangular channels. Water (0.5-50 l/min) and air was forced through channel gap sizes of 0.4, 1, 2 and 4 mm and constant width of 20 mm in the experiments (D_h= 0.78-6.67 mm) with 640 mm in length. As expected, pressure drop increased with the increase of superficial velocities of liquid and gas, and with the decrease in the gap size. They presented a set of correlations, of the Lockhart-Martinelli type, redefined to take gap size and flow rate into account.

In Chen *et al.* (*2000, 2002*), measured two-phase pressure drop data for small horizontal tubes was compared with predictions of the empirical correlations of Chisholm (*1967*) and Friedel (*1979*), and with the homogeneous model. Measurements were conducted for air-water (G= 50-3000 kg/(m²s)) and R-410A (G=50-600 kg/(m²s)) in small horizontal tubes, with inner diameters of 1.02, 3.17, 5.05 and 7.02 mm and 150-995 mm in length for the air-water loop, and 3.17, 5.05, 7.02 and 9 mm and length of 700 mm for the refrigerant loop. The exit quality was 10^{-4}-0.9/ 0.1-0.9. The homogeneous model was modified with the inclusion of Bond number, *Bo*, and Weber number, *We*, to take account of the effects of surface tension, tube diameter and total mass flux in the pressure drop prediction. Also a slight modification to the Friedel correlation was given.

Zhang and Webb (*2001*) investigated horizontal single-phase and two-phase flow frictional pressure drop of R-134a, R-22 and R-404A in small diameter tubes having hydraulic diameters between 2.16 and 6.20 mm and 560-914 mm in length. As expected, the two-phase pressure drop was found to increase with both mass flux 200-1000 kg/(m²s) and vapor quality 0.2-0.89, and decrease with saturation temperature. They

found that the Friedel correlation over predicted the experimental data in the two-phase region. A new correlation, considering different property groups, was proposed for friction two-phase pressure drop in small diameter tubes.

Yu et al (*2002*) experimentally investigated the two-phase pressure drop, boiling water and Ethylene glycol heat transfer and critical heat flux in a small horizontal tube of 2.98 mm inside diameter and 910 mm heated length. Heat and mass flux ranged between 50-200 kg/(m²s) and 50-300 kW/m² respectably. The two-phase pressure drop data of the study were consistently lower than predicted by the Chisholm correlation, at the same mass fluxes. This difference was attributed to two-phase flow regime differences between the channel sizes. A modification to the Chisholm correlation was developed to better predict pressure drop in small-diameter channels.

Qu and Mudawar (*2002*) studied the hydrodynamic instability and pressure drop in a water-cooled two-phase (G=134.9-400.1 kg/(m²s)) heat sink containing 21 microchannels with hydraulic diameter of 0.349 mm and 44.8 mm in length. First, six widely used models and macro-channel correlations were examined in predicting pressure drop in the two-phase region. All these correlations over predicted the data by large margins. Better accuracy was achieved using correlations specifically developed for mini and microchannels. They suggested a new correlation for pressure drop prediction that incorporates the effects of mass flux and channel size.

Wen and Kenning (*2004*) investigated the two-phase pressure drop of boiling water in a vertical rectangular channel 2 × 1 mm at (q'' = 25-105 kW/m², G=57-211 kg/(m²s) and x_{exit}=0.09-0.3). They found that Lockhart-Martinelli correlation still applicable and gave best fit to their data, but they mentioned that none of the correlation from the literature were able to predict the boiling water pressure drop in a 50 × 70 μm channel.

Revellin and Thome (*2006*) measured the two-phase pressure drop of R-134a and R-245fa in 0.509 and 0.790 mm tubes. They classified three regions for the two-phase frictional pressure drop factor; laminar, transition and turbulent regime. Müller-Steinhagen and Heck correlation was best predicting their data in the turbulent region for two-phase Re ≥ 2000.

2.2.6 Dry out literature review

In 1948, Kutateladze (*1948*) introduced his critical heat flux (CHF) model based on the analysis of the hydrodynamic stability of the two-phase flow near the heated surface. For saturated pool boiling, Kutateladze proposed a correlation for the CHF as a function of density,

latent heat of evaporation, surface tension, gravity and a parameter, which is a function of the working fluid properties and evaporator geometry. Based upon Helmholtz instability of the vapor patch over the heater surface Zuber (*1959*) obtained an empirical equation similar to that of Kutateladze (*1948*).

For flow boiling, the way the heated surface reaches the condition at which the wall temperature rises and the heat transfer coefficient rapidly decreases due to a change of the heat transfer mechanism establishes whether it is termed *Critical Heat Flux (CHF)* or *Dryout* condition.

Critical Heat Flux*,* as in pool boiling*,* in heat flux controlled systems is the heat flux, at which there is a sudden and substantial increase in the wall temperature. In temperature controlled systems an increase of the surface temperature above this point results in a significant decrease of the heat flux. , i.e. it is the highest point of the boiling curve. Above this point, a vapor blanket covers the heated surface separating the wall from the liquid, hindering the heat transfer.

Dryout condition represents the breaking of the continuous liquid contact with the heated surface in a flow channel at moderate to high qualities. It follows the gradual decrease of liquid fraction due to evaporation or boiling of the liquid film. At this point, the liquid film at the heated surface dries up, while entrained droplets may still flow in the vapor core. These droplets occasionally hit the heated surface and evaporate. Dryout occurs, independently of the heat flux, at high vapor qualities. The flow pattern before the dryout condition is usually annular with the vapor phase occupying most of the channel core while the liquid flows as a thin film along the channel wall, (Collier and Thome, *1994*).

As indicated by the definitions above, both terms refer to a state where the heated surface loses contact with the liquid, but while the CHF is dependent on a high heat flux, dryout is caused mainly by a lack of liquid at the heated surface and therefore largely dependent on the vapor fraction. However, the two phenomena are closely related and it is sometimes difficult to decide which term to use.

Many CHF correlations are based on experimental results. The mechanisms involved with the CHF and dryout phenomena are discussed by many researchers and the fact that there are many alternative explanations indicates that the mechanisms are not fully understood.

For subcooled and low quality saturated CHF*,* a number of alternative mechanisms for CHF have been proposed and the following concepts appear to have been reasonably well established:

- The vapor generation at the heated wall hinders the near-wall liquid flow in the boundary layer. At CHF, this hindrance decreases the velocity gradient of the near-wall liquid resulting in a liquid stagnation at the

outside of the bubble layer. Kutateladze and Leont´ev (*1966*) presented the earliest subcooled CHF model based on boundary layer separation.

- When the boundary layer becomes too crowded with bubbles, vapor escape is impossible and the surface becomes dry. This mechanism is discussed, for instance by Tong *et al.* (*1972*), and Weisman and Pei (1983).
- Dryout of a trapped thin liquid sublayer underneath large vapor bubbles that move along the heated wall has been studied by a number of authors. Haramura and Katto (*1983*) improved the Katto and Yokoya (*1968*) pool boiling model by introducing the mechanism for macrolayer formation in both pool and flow boiling. Katto (*1990a, 1990b*) provided a detailed description of the model based on the macrolayer evaporation. Lee and Mudawar (*1989*) considered the effect of velocity in the subcooled flow in terms of stretching the large bubble in Haramura and Katto (*1983*) model to a vapor blanket of length equal to the critical Helmholtz wavelength. The Katto (*1990a, 1990b,* and *1992*) and Celata *et al.* (*1994*, *1999*) CHF models are all fairly similar to the Lee and Mudawar (*1989*) model.
- Galloway and Mudawar (*1993a, 1993b*) made flow visualization experiments of the wavy liquid vapor interface near the heated surface of short rectangular channels. They described the CHF to be the result of intense vapor production which lifted the upstream wetting front away from the heated surface, cutting the supply of liquid to the wall. Their interfacial lift-off model was expanded by Gersey and Mudawar (*1995a, 1995b*) to include a broader channel and longer heated lengths. Sturgis and Mudawar (*1999a, 1999b*) performed flow visualization on long rectangular channels for both near saturated and subcooled conditions.

For high quality saturated conditions*,* the flow pattern is usually annular flow and at some stage the liquid film dries out due to evaporation and due to the partial entrainment of liquid in the form of droplets into the vapor core. Hewitt and Hall Taylor (*1970*), Hewitt (*1978*), and many other workers demonstrated that the decrease of the heat transfer coefficient in annular flow at these conditions is a result of dryout of the liquid film on the wall. For the dryout in annular flow, two aspects are important: the thickness of the liquid film, and the exchange of liquid droplets between the core of the flow and the liquid. Surface parameters are usually of minor importance.

Shah (*1979, 1980*, and *1987*) proposed several CHF correlations of different situations for subcooled and saturated flow boiling in vertical uniformly heated tubes and annuli.

Lazarek *et al.* (*1982*) developed a CHF correlation for low reduced pressure conditions which predicts the refrigerant quality at dryout in terms of mass flux, inlet subcooling and heated length, for a 3.1 mm internal diameter vertical tube with R113. Yu *et al.* (*2002*) conducted

experimental studies on saturated CHF of water in horizontal single circular minichannel.
Qu and Mudawar (*2004*), performed experiments to measure CHF for water flow boiling in a heat sink consisting of several parallel rectangular microchannels. As the CHF was approached, flow instabilities induced vapor backflow into the heat sink's upstream plenum and nullified the advantage of inlet subcooling. Thus the CHF was virtually independent of inlet temperature but increased with increasing mass flux. Hall and Mudawar (*2000*), in an exhaustive literature search identified over 100 correlations for subcooled CHF applicable to water flow in a uniformly heated tube. Two new non-dimensional correlations for subcooled CHF of water flowing in uniformly heated channels were formulated.

2.2.7 Bubble behavior literature review

A summary of existing literature on bubble dynamics and video recordings of flow boiling is presented in this section. One of the first studies was conducted by Gunther (*1951*), who carried out high speed photography to examine the nucleate boiling process and the vapor bubble dynamics in forced convection subcooled up-flow boiling of water. Vapor bubble diameters were measured during the growth and collapse stages in subcooled flow, and the effects of flow velocity and subcooling were reported.

Plesset and Zwick (*1954*) and Forster and Zuber (*1954*) presented solutions for the radius of the vapor bubble as a function of time. Bubble growth in a superheated liquid was in the initial stage limited by the inertia force of the liquid, surface tension, and the vapor pressure. The bubble growth for the latter stage is controlled by thermal diffusion and their solutions indicated that bubble radius is proportional to the square root of time with the proportionality constant directly related to the Jakob number.

Bankoff (*1958*) observed that the incipience and continuance of bubble formation is repeatedly initiated from a small vapor presence, which was trapped by the surface roughness.
Hsu and Graham (*1963*) conducted a visual study with highly subcooled vertical up-flow boiling of water to investigate the hydrodynamic features of bubbly and slug flow regimes. Vapor bubble departure was observed for bubbly flow, while no measurements of bubble growth rate or departure diameter were made.

Hsu (*1965*) and Han and Griffith (*1965*) presented detailed observations and reasonable models, where they assumed that the vapor core would remain after the departure bubble which would completely remove the thermal boundary layer and the following bubble would start to grow after the thermodynamic equilibrium between the remained

vapor nucleus and the surrounding fluid temperature. They derived equations which predicted the maximum and minimum cavity size which could be active for a given heat flux at a given wall temperature based on their assumptions.

Chang (*1963*) developed an expression for flow boiling departure diameter by assuming the instant a vapor bubble departs from the heating surface is the point where the net forces acting on a vapor bubble (including forces acting parallel and normal to the heating surface) just balance each other. Sliding bubbles were not considered, and the expression was never experimentally verified.

Jiji and Clark (*1964*) photographed nucleation and measured the thickness of the layer with bubbles, called the "*bubble boundary layer*" and temperature profiles in the boundary layer for vertical up-flow boiling of water over a thin heated plate under varying pressure. They observed the presence and growth of a bubble boundary layer leading to a burnout condition at high heat flux values.

Darby (*1964*) conducted a photographic study of bubble growth and translational characteristics for two liquids of widely differing physical properties, water and R-113. He correlated the bubble radius and distance from the nucleation site as a function of time. He showed that the trajectory of the bubble after detachment from the surface can be accurately computed from a balance of buoyancy with inertial and viscous forces, at least for a distance of several diameters from the surface, if the bubble size at detachment is known.

Berenson and Stone (*1965*) obtained photographs of bubbles moving on walls of glass tube. R-113 was used as the test fluid. Heat was supplied by water flowing through the annular space between the test section and an outer glass tube.

Tolubinsky and Ostrovsky (*1966*) studied with the help of high speed photography the nucleate pool boiling mechanism for a number of pure liquids and mixtures boiling on wetted heating surfaces at various system pressures. They reported the diameter at departure, departure frequency and growth rate of vapor bubbles.

Cole *et al.* (*1966, 1967* and *1969*) experimentally investigated the bubble growth rates at high Jakob numbers, the bubble frequencies and the departure diameters. The boiling action was recorded using a high speed camera. Based on thermodynamic considerations, Cole (*1974*) theoretically proved the necessity of a vapor residue for a continuously active nucleation site.

Cooper (*1969*) presented a theory based on the experimental observation of a thin liquid layer (*microlayers*) on the wall beneath the growing vapor bubble to determine the rate of growth of such bubble growing from a heated wall in a saturated liquid. The evaporation of the *microlayers* contributed significantly to the growth of the bubbles. Cooper *et al.* (*1981*) measured vapor bubble growth and departure in saturated n-

hexane in forced up-flow over a flat wall. They reported that vapor bubbles roll along the heating surface and for this reason they claim that the point of departure is not well defined. Similar measurements were made for short duration microgravity flow.

Frost and Kippenhan (*1967*) measured growth rates and departure diameters of bubbles in subcooled up-flow of water both pure and containing various concentrations of a surface active agent added to reduce the surface tension. They found higher heat transfer, increased vapor bubble population and slower bubble growth rate when a surfactant was dissolved in water boiling during flow in a vertical annulus. They proposed a new model of flow boiling to explain their experimental results.

Levy (*1967*) developed a model to predict the volumetric vapor fraction during forced convection up-flow subcooled boiling of water. He obtained the vapor bubble departure diameter based on the considerations of buoyancy force, drag due to bulk flow, and surface tension.

Koumoutsos *et al.* (*1968*) measured vapor bubble lift-off radii from an artificial nucleation site with saturated water flowing horizontally. They observed that shortly after incipience vapor bubbles begin to slide away from the nucleation sites and continue to grow until they lift-off the surface. They obtained a correlation for lift-off diameter based on a vapor bubble net force balance (including forces acting both parallel and normal to the flow direction). The buoyancy force was found to be significantly influencing.

Mikic *et al.* (*1970*) derived a simple general relation for the bubble growth rates in a uniformly superheated liquid.

Dhir (*1991*) reviewed various aspects of boiling process including bubble dynamics such as bubble growth, bubble departure and bubble frequency of pool and external flow boiling of ordinary liquids.

Klausner *et al.* (*1993*) visually investigated and measured vapor bubble departure and lift-off diameters in forced convection boiling flow, and developed a criterion for the bubble departure from the heated surface in saturated horizontal flow boiling of R-113 in a square duct. They observed that the mean bubble departure diameter decreased with increasing mass flux and with decreasing heat flux. They also noted that before departure from its nucleation sites, the vapor bubbles typically slide a finite distance downstream along the heating surface before lift-off. They conducted a force balance acting on a bubble to predict its departure and lift-off diameter for horizontal flow boiling. This analysis was extended by Zeng *et al.* (*1993a, 1993b*) and developed into a model for pool boiling and for flow boiling. The model agrees well with a wide range of departure and lift-off diameter data reported in the literature.

The model by Zeng *et al.* (*1993b*) expresses calibration concerning a general extension to vertical flow boiling, for the following reasons: In

the vertical up-flow configuration, the sliding vapor bubble velocity is higher than that of the liquid, resulting in a shear lift force pushing the rising bubble against the heating surface, preventing lift-off from the surface.

For the vertical down-flow boiling configuration, sliding bubbles are slower than the liquid velocity due to the buoyancy force, resulting in an outward directed shear force which should be sufficient to lift vapor bubbles off the heating surface.

Helden *et al.* (*1995*) obtained bubble growth, detachment radius, and trajectory data from artificial cavities in a plane wall of a vertical rectangular channel during up-flow boiling of saturated and superheated water or injected nitrogen bubbles. Their experiments showed that steam bubbles take off into the liquid, while nitrogen bubbles more or les slide parallel to the wall.

Kandlikar and Stumm (*1995*) conducted theoretical and experimental work to measure the contact angle and bubble departure diameter of nucleating vapor bubbles in horizontal subcooled flow boiling of water at atmospheric pressure. Their model includes the reduction in the surface tension component in the flow direction caused by an increase in the contact angle, which would reduce the departure bubble diameters as compared to pool boiling.

Kandlikar *et al.* (*1992, 1996a*) visually analyzed the effect of flow rate, subcooling, and wall superheat on the nucleation behavior of cavities of different radii in subcooled horizontal flow boiling of water. Kandlikar *et al.* (*1996b*) examined the effect of flow velocity, wall superheat, subcooling, and cavity size on the vapor bubble growth rate, and compared growth rates in flow boiling to those for pool boiling.

Thorncroft *et al.* (*1998*) studied the vapor bubble growth and detachment in vertical rectangular channel up-flow and down-flow forced convection boiling of FC-87 using a visualization technique. They found that for upward flow, bubbles slide along the heater wall rather than lift-off from the wall when they depart from the nucleation cavities. Both the bubble growth and departure rates were noted to increase with the Jakob number, but the bubble departure diameter decreased with the mass flux.

Fournelle *et al.* (*1999*) investigated the effects of cavity spacing on bubble departure frequency, bubble diameter, and active site density in FC-72 on isolated cavities etched on a silicon surface. Observation from the high speed photography of boiling activity exposed that the bubble departure diameter increases with an increase in the wall superheat.

Sheng and Palm (*2000*) visualized the flow pattern and bubble shape for water in a single small glass tube (D_i = 1.0, 1.6, 2.0, 4.0 mm), in upward, downward and horizontal flow. The bubble departure diameter was noted to depend much on the mass flow rate.

The subcooled flow boiling and the associated bubble characteristics of R-134a in a horizontal annular channel were examined by Yin *et al.* (*2000*). Results from their flow visualization indicated that the bubble generation frequency is influenced by the heat flux but not the bubble size. The bubble generation was suppressed by mass flux and subcooling, and only the liquid subcooling showed a significant effect on the bubble size.

Warrier *et al.* (*2002*) measured the bubble diameter and bubble collapse process in the bulk subcooled liquid on a vertical flat heater using a high speed camera. They proposed two correlations, one for the bubble collapse history and the other for the corresponding condensation Nusselt number.

Chang *et al.* (*2002*) and Bang *et al.* (*2004*) investigated photographically the behavior of near-wall bubbles in subcooled flow boiling of water and R-134a in a vertical rectangular channel of conventional size. They described the coalescence behaviors of the bubbles during flow boiling. They observed that the near-wall bubble layer of nucleate boiling beneath vapor clots was quenched, and then the heated surface is locally covered by large vapor films, at CHF.

Lee *et al.* (*2004*) and Li *et al.* (*2004*) by using a high speed digital camera observed the bubble nucleation, growth, departure size, and frequency in a single trapezoid microchannel. Their results indicate that the bubble nucleation in the microchannel may be predicted from the classical model with micro sized cavities and the bubble typically grows with a constant rate. They found that the size at bubble departure from the microchannel wall was governed by surface tension and drag of bulk flow and fairly well correlated by a modified form of the Levy equation. The bubble frequency in the microchannel is comparable to that in an ordinary sized channel.

Situ *et al.* (*2004, 2005*) photographically studied the bubble behavior in forced convection subcooled vertical annular boiling of water. Detailed phenomena, such as bubble growth, condensation, coalescence and sliding, were clearly observed from the high speed digital video images. The bubble departure frequency, bubble lift-off diameters and bubble dynamics after lift-off were obtained by analyzing the images.

Lie and Lin (*2005*) experimentally investigated how the channel size affects the saturated flow boiling heat transfer and associated bubble characteristics of refrigerant R-134a in a horizontal narrow annular duct. Their results from the flow visualization showed that the mean bubble departure diameter slightly decreases with increasing the mass flux, and that the bubble departure frequency increases at reduced duct size. At a high imposed heat flux many bubbles generated from the cavities in the heating surface tend to merge together to form big bubbles.

2.2.8 *Two-phase flow pattern*

To explain the phenomena of the flow boiling heat transfer through microchannels, it is necessary first to understand the basic mechanisms of vertical flow boiling in macro scale. In vertical upflow the flow patterns are classified into different regimes as in Figure 2.4.

When an upward flowing saturated liquid is heated, bubbles start to form at the heated surface and they will be spread in the main liquid bulk. The regime is *bubble flow*. When the concentration of the bubbles becomes high, they will grow and collide forming a larger bubble diameter approaching the tube diameter, *slug flow*. In large tubes, these bubbles might break down and an unstable region called *churn flow* occurs. Liquid is moving upwards and downwards in an oscillatory motion. In narrow tubes, this churn flow may not occur. Increasing velocities will lead to *annular flow* where the vapor flows in the centre, while the liquid flows on the wall, forming a liquid film. At high vapor quality the liquid at the wall will dry out and the flow regime expands into *mist flow* or dispersed flow with the remaining liquid forming small droplets flowing in the vapor phase. Finally all droplets are vaporized and the gas phase is superheated.

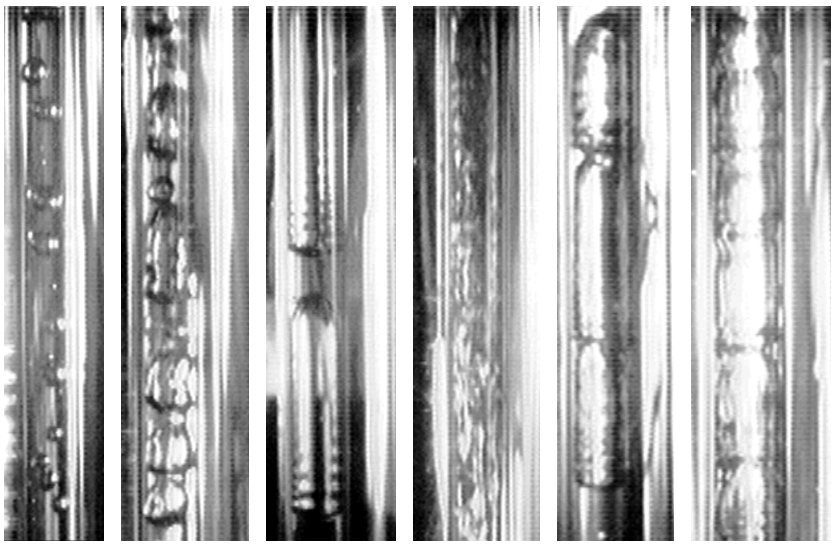

Figure 2.4 Flow patterns in vertical upflow

There are many flow patterns maps available in the literature. They can be divided into two groups: Co-current (adiabatic) flow pattern maps

that are developed for air-water two-phase flow, and heated channel (diabatic) flow pattern map developed for evaporating liquids. These flow patterns are essential to model the heat transfer and pressure drop.
Suo and Griffith (*1964*) The adiabatic two phase flow patterns of Heptane-N2, Water-N2, Heptane/He in microchannels tubes (D_i = 1.59 and 1.028 mm) was described, and was among the first studies. Three flow regimes presented; slug flow, churn flow, and annular flow, and from the slug flow characteristics, they concluded that in the flow, the surface tension forces were dominant over the gravity forces.

Kew and Cornwell (*1992, 1995, 1997*) carrying out tests with single and multi channels, in either vertical or horizontal configuration with R-113 using rectangular channels (D_h= 1.028 and 1.643 mm) and with R-141b using circular channels (D_i= 2.05, 3.69, 2.87, and 1.37 mm). The flow regimes they observed were isolated bubble, confined bubble, annular slug flow, and partial Dryout.

Mishima and Hibiki (*1996*) measured flow regime, void fraction of air-water in tubes (D_i= 1 to 4 mm), they observed new flow regimes connected to minichannels in additional to the commonly observed ones.

Tripplet *et al.* (*1999*) investigated using air-water the two-phase flow patterns in circular and triangular channels (D_i= 1.1 and 1.45 and D_h= 1.09 and 1.49 mm). The flow patterns and flow maps based on the gas and liquid superficial velocities as coordinates were similar for all the tested channels. They observed the following flow regimes: bubbly, churn, slug, slug-annular, and annular flow.

Coleman and Garimella (*1999, 2000*) conducted a visual study of the two-phase flow regimes of air-water and R-134a in horizontal circular channels (D_i=1.3, 1.75, 2.6, 4.91, and 5.5 mm) and rectangular channels (D_h=1, 2, 3, 4, and 4.67 mm). They obtained flow maps, identified the transition lines between different flow regimes (bubble, dispersed, elongated bubble, slug, stratified, wavy, wavy-annular, and annular). They also identified the effect of both the channel shape and hydraulic diameter on the flow map.

Sheng and Palm (*2000*) visualized water flow boiling in a single glass tubes (D_i= 1.0, 1.6, 2.0, 4.0 mm) at atmospheric pressure using high-speed video camera at different flow directions. They observed three flow regimes, isolated bubbles flow, slug bubble flow and annular flow.

Yang and Shieh (*2001*) generated a flow patterns map for air-water and R-134a two-phase flow in horizontal tubes (D_i= 1, 2, and 3 mm). They observed bubble, slug, plug, wavy stratified, dispersed and annular flow as flow patterns. They concluded that using of R-134a flow leads to shift in the slug to annular transition to lower value gas velocity. The location of bubble to plug and slug flow transition are also significantly affected by the working fluid properties. They added that the surface tension force is important parameter for flow pattern in small tubes.

Kattan *et al.* (*1998*) developed a flow pattern map for evaporation in horizontal tubes using five different refrigerants and wide range of mass flux and vapor quality which they stands as a coordinates. In their map different flow patterns as presented such as stratified, stratified wavy, intermittent, annular, and mist flow.

A flow map similar to Kattan *et al.* (*1998*) is developed in this thesis.

3 Experimental Approach

3.1 Experimental set-up

3.1.1 Single-phase and boiling flow

The experimental facility was designed and constructed as illustrated schematically in figure 3.1. In the apparatus, the system pressure, mass flux and subcooling can be adjusted independently.

A magnetic gear pump with microprocessor control, type MCP-Z standard, which was also used as flow meter, drives the circulation of the fluid. This pump allows a wide range of flow rates, from 1 ml/min to 552 ml/min. The circuit includes also an electrical pre-heater to control the inlet temperature, a 7 μm filter placed before the test section in order to prevent blocking of the flow from small particles, and a compact heat exchanger cooled by circulating cold water to control the pressure level and the subcooling of the fluid.

The system pressure was set and controlled within ± 0.2% by controlling the DC electrical power input to a heater on a tank connected to the main circulation loop. The heat added to the tank controls the level of fluid in the condenser, and therefore the pressure, all other conditions kept constant. The system works also as a fluctuations absorber, where PID regulator is connected to the DC power supply to the tank heater to fine control this added power, to ensure a stable system pressure from variations caused by processes beyond the test section.

The cooling water flow rate and temperature through the condenser, also influences the system pressure level, as well as the subcooling. Cooling water flow rate and the heat added to the tank thus together determines the pressure level and the subcooling. The working fluid is pumped from the condenser, and then passes through the pre-heater, where the inlet temperature to the test section is adjusted to just below the boiling point. The test section is heated using an electrical DC power supply (TTi, Thurlby Thandar Instruments, TSX) by applying a potential difference over the test tube itself (i.e. the test section tube is used as a heater). This direct heating ensures a homogeneous or uniform heat flux over the test section. The fluid absorbs heat when passing through the test section, causing, in the single phase tests, an increase in the temperature, and in the flow-boiling tests, an increase of the vapor fraction. At the condenser, the fluid is condensed and further subcooled in order to complete the loop back again to the pump.

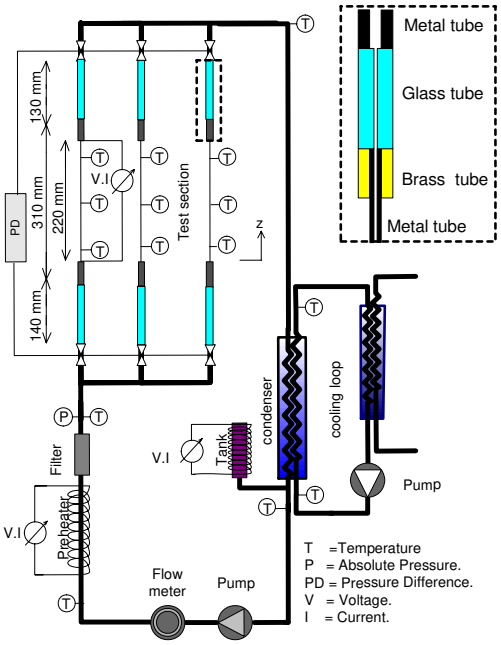

Figure 3.1 Micro scale test rig and test section

The experimental facility was instrumented with an absolute pressure transducer (Druck PDCR 4060, 25 bar absolute) to measure the system pressure (p). A differential pressure transducer (Druck PDCR 4160, 0-1 bar diff.) was used to measure the pressure drop (Δp) across the test section.

Six 0.1mm wire diameter T-type (copper-constantan) thermocouples were installed to measure the bulk liquid temperature at different locations and the water inlet and outlet temperatures as shown in figure 3.1. Due to the small size of the test section, the inside wall temperature was determined based on the measured outside wall temperature. Three thermocouples of the same type were also mounted to the outside surface of each test tube to measure the outer wall temperature.

The entire test rig, especially the test section, was surrounded with an insulation layer.

The test sections as shown in figure 3.1 consist of metal (AISI 316 stainless steel) tubes with inner diameters of 1.700, 1.224, and 0.826 mm, 310 mm in total length, and 220 mm in heated length. A glass tube with the same diameter as each test tube is placed in each end of the metal tube for visualization purposes, and also to insulate the test section, both electrically and thermally, from the rest of the system.

3.1.2 *Visualization of flow boiling and dryout*

The two-phase flow boiling and dryout visualization rig was designed and constructed as schematically illustrated in figure 3.2. Subcooled R-134a was pumped from the condenser, passed through the Corioli mass flow meter (Micromotion DS006) and the pre-heater where the inlet temperature to the test section was adjusted to just below the boiling point. The test section consisted of a vertical quartz glass tube with internal diameter of 1.33 mm coated at the outside by a transparent resistive coating of Indium Tin Oxide (ITO). The test section was heated by applying a potential difference over the coating using an electrical DC power supply (TTI EX752M) where the current through the test section is measured. The potential difference could be connected at four different locations along the tube allowing dividing the 354.5 mm test section into three different heated parts, thereby allowing the variation of the heated length. The experimental facility was instrumented with the necessary measuring equipment such as a pressure transducer (Druck PDCR 4060, 25 bar absolute) to measure the test section inlet pressure, and the corresponding saturation temperature, a pressure difference transducer (Druck PDCR 4160, 0-350 mbar diff.) to measure the pressure drop through the test section, and thermocouples type T at the locations indicated in figure 3.2.

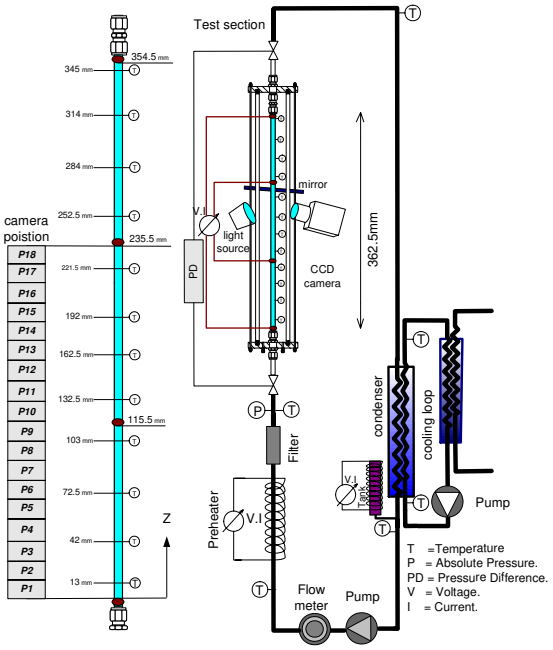

Figure 3.2: Visualization test facility. Transparent test section for flow boiling experiment.

The entire test rig was clad with a thermal insulation layer. The test section was placed inside a 40 mm diameter glass tube to which vacuum was supplied. The temperatures at locations indicated in figure 3.2, the system pressure and the test section DC voltage were recorded using a data logger (AGILENT 34970A) connected to a computer. The thermodynamic properties for R134a, including density, enthalpy, viscosity, saturation temperature and thermal conductivity, were calculated with the computer code REFPROP 6.01 (developed by the US National Institute of Standards and Technology, (NIST)).

A high speed CCD camera system (Redlake 8000S) with close up lens provided the high frame rate (1000 frames/second) and magnification needed to achieve temporal and spatial resolution of nucleate bubble growth and behavior in the channel. A light source and a mirror were placed on opposite sides of the test section for enlightening the heated flow channel. The use of a transparent heated tube enabled flow pattern visualization along the whole heated zone.
All tests were performed under steady-state conditions.

3.2 Data Acquisition and reduction

3.2.1 Data acquisition

Agilent data acquisition unit (34970A) and 34901A multiplexers were used for capturing the signals of temperature, pressure, and flow rate, as well as the DC voltage signal of the heat supplied to the test section. The DC current for the heat inputs to the test section were recorded manually for each data point measurements. First the test rig was allowed to run long enough at the desired data point to achieve steady state condition. When the steady state was reached, the temperatures, pressures, and mass flow rate were transmitted and recorded. Readings were performed every 2-3 seconds (administrated by the measurement program routines) and the logger continuously sent this data to a PC until about 100 separate measurements had been taken. The average of these values were then calculated and taken as a data point. The data was read by the PC with the aid of the program HP VEE, It is an interface software program which was used for monitoring of the experimental results and providing a link to a data file where the data was stored.

3.2.2 SEM micrograph

Figure 3.3 shows SEM images of the tested stainless steel tubes. These pictures were not used for measuring the tube diameters.

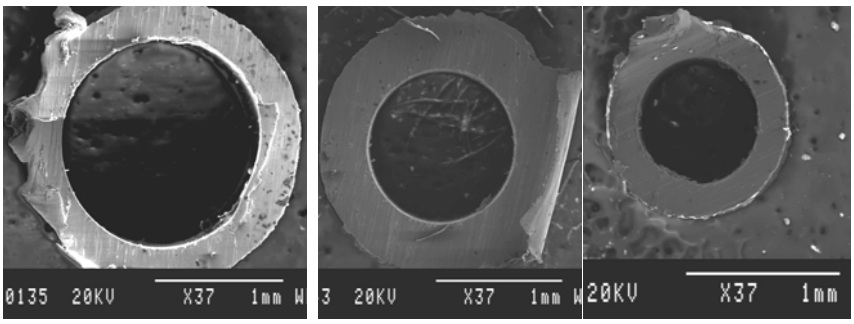

D_i= 1.700 mm D_i= 1.224 mm D_i= 0.826 mm

Figure 3.3: SEM image of stainless steel tubes

Figure 3.4 shows an SEM image of the inner surface of one of the tested metal tubes. Crevices, 1-3 μm in width, and cavities, 5-10 μm in diameter are seen to be distributed across the surface.

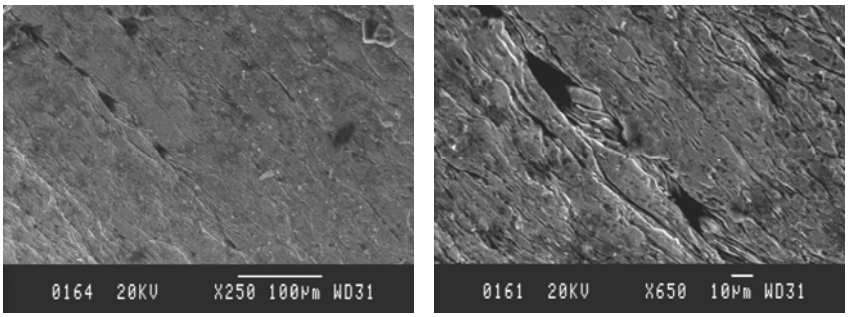

Figure 3.4: SEM image of inner wall of stainless steel tubes

3.2.3 Temperature measurements

In case of flow boiling, the fluid saturation temperature is obtained from the saturation pressure in the test section.

The inner tube wall temperature was calculated based on the measured outer tube wall temperature.

The following assumptions have been made; one dimensional conduction, steady state, and uniform heat generation in the tube wall.

The final equation from the derivation in Appendix B is:

$$T_{wall,in} = T_{wall,out} + \frac{Q}{4\pi K L_H}\left[\frac{\psi(1-\ln\psi)-1}{\psi-1}\right] \tag{3.1}$$

Where:

$$\psi = \left(\frac{r_{out}}{r_{in}}\right)^2 = \left(\frac{D_{out}}{D_{in}}\right)^2 \tag{3.2}$$

3.2.4 System pressure measurements

For the measurement of the system pressure, an electronic pressure transducer (Druck PDCR 4060, 25 bar absolute) was used. The pressure was measured just before the inlet of the test section.

The system pressure was set and controlled within ± 0.2% by controlling the electrical power input to a tank connected to the main circulation loop. The heat added to the tank controls the level of fluid in the condenser, and therefore the pressure can be controlled and set at any desired level.

3.2.5 Pressure drop measurement

For measuring single and two phase pressure drop across the test sections, differential pressure transducers (Druck PDCR- 4160, 1 bar diff. and Druck PDCR- 4160, 350 mbar diff.) were used.
In addition, the pressure difference transducers were connected to three pressure ports. The pressure ports were connected to 3 mm outside diameter and 2 mm inside diameter stainless steel tube. The tubes connecting the pressure transducers to the system were located inside a tube of larger diameter, where a water flow could be supplied. In most cases hot water was led in the annulus between the tubes to make sure that all the refrigerant in the pressure connection tubes was in a vapor phase. In case of tests with single phase liquid refrigerant, cold water was used. The temperature of the cooling or heating water was kept sufficiently much higher or lower than the system saturation temperature. This gave the possibility of controlling the phase of the fluid inside the connecting tube under operation.

3.2.6 Mass flow rate and heat input measurements

A gear pump with variable-speed drive (ISMATEC MCP-Z) was used to measure the volumetric flow in order to calculate the mass flow rate. And a Corioli mass flow meter (Micromotion DS006) also used to measure the mass flow rate in most of the tests.
The heat input was calculated by measuring the voltage and the current over the test section.

3.3 Data reduction process

3.3.1 Single-Phase Data Reduction

For a given test, the heat flux added to the test section, q'', was calculated from the change of enthalpy over the test section.

$$q'' = \frac{\dot{m}_{R-134a}\, C_p\,(T_{fluid,out} - T_{fluid,in})}{\pi D_i L} = \frac{I \cdot V}{A} \tag{3.3}$$

$T_{fluid,out}$, and $T_{fluid,in}$ are the temperatures of the liquid R-134a exiting and entering the test section.
Evenly distributed heat flux across the surface was assumed. Single-phase heat transfer coefficients were computed from measured wall and bulk fluid temperatures and the heat flux.

$$h = \frac{q''}{T_{wall} - T_{fluid}} \tag{3.4}$$

T_{wall} is the local inside wall temperature as determined from the outside wall temperatures, measured by thermocouples at three different locations, and equations 3.1 and 3.2. T_{fluid} is the local fluid temperature.
Assuming that the fluid temperature varies linearly within the heated test section, the local fluid temperature at any location z can be linearly interpolated and expressed as:

$$T_{fluid}(z) = T_{fluid,in} + \left[\frac{T_{fluid,out} - T_{fluid,in}}{L}\right] \times Z \tag{3.5}$$

Where Z is the length starting from the entrance of the heated test section, ΔZ in the test section length.
Using the average value of the local heat transfer coefficients at the locations of the thermocouples, the average Nusselt number for single-phase can be calculated by:

$$\overline{Nu} = \frac{\bar{h} D_i}{k} \tag{3.6}$$

the thermal conductivity k is calculated at the average fluid bulk temperature.

The friction factor f was calculated using the measured pressure drop across the test section,

$$f_l = \Delta P \frac{2}{\rho u_m^2} \frac{D_i}{L} \tag{3.7}$$

where L is the length between the locations at the inlet and the exit of the test section where the pressure transducer taps were connected, including the stainless steel test section and the two glass tubes.

3.3.2 Boiling Heat Transfer Data Reduction

For a given test, the heat flux added to the test section, q'', was calculated as:

$$q'' = \frac{I \cdot V}{A} \tag{3.8}$$

Evenly distributed heat flux across the surface was assumed. Boiling heat transfer coefficients were computed from the measured wall and bulk fluid temperatures and the heat flux as:

$$h(z) = \frac{q''}{T_{wall} - T_{fluid}} \tag{3.9}$$

where, T_{wall} is the calculated inside wall temperature based on the measured outside surface temperature, T_{fluid} is the local fluid bulk temperature calculated based on the temperatures before and after the test section, and q'' is the wall heat flux to the fluid. The average flow boiling heat transfer coefficient was determined by arithmetically averaging all local heat transfer coefficients.

The subcooled length Z_o can be calculated based on the energy balance for the liquid subcooled region, and the boiling is assumed to start at a position calculated as:

$$Z_o = \frac{\dot{m}_{R-134a} C_p (T_{sat,in} - T_{fluid,in})}{q'' \phi} \tag{3.10}$$

where ϕ is the perimeter, $T_{fluid,in}$ is the measured fluid temperature at the inlet of the test section, and T_{sat} is the saturation temperature at the entrance of boiling section.

The boiling length Z_B of the test section can be defined using the value of Z_o:

$$Z_B = Z_{TH} - Z_o \tag{3.11}$$

In this thesis, by assuming the fluid saturation temperature in the boiling section ($z > Z_o$) to vary linearly along the test section, the local fluid temperature is calculated as:

$$T_{fluid}(z) = T_{sat,in} - \left(\frac{T_{sat,in} - T_{fluid,out}}{Z_{TH} - Z_o} \right) \times (z - Z_o) \tag{3.12}$$

As the saturation temperature drop is usually less than 0.5 K this assumption introduces an error considerably smaller than the accuracy in the temperature measurement.
The vapor quality at any vertical location $x(z)$ was calculated from the heat transferred to the fluid. An energy balance over the boiling section gave:

$$x(z) = \frac{q'' \phi (z - Z_o)}{A_c G i_{fg}} \tag{3.13}$$

Similarly, the exit quality is expressed as:

$$x_{exit} = \frac{q'' \phi (Z_{TH} - Z_o)}{A_c G i_{fg}} \tag{3.14}$$

3.3.3 *Boiling Pressure Drop Data Reduction*

The differential pressure transducer is connected to the pressure taps placed before and after the heated section and the insulating glass tubes. The pressure drop measurements also include the tube contraction and expansion from the main loop tube diameter to that of the actual test section, and vice versa, as shown in figure 3.5.

The refrigerant is supplied into the test section in slightly subcooled state ($T_{in}<T_{sat}$). We assumed that the refrigerant remains in single-phase liquid state until zero thermodynamic vapor quality is reached, x=0. At this location boiling starts, and downstream from it, vapor is present in the flow in a two-phase mixture.

As illustrated in figure 3.5, the microchannel is divided into a single-phase region, Z_{sp}, and a two-phase region, $Z_{tp}=Z_T-Z_{sp}$.

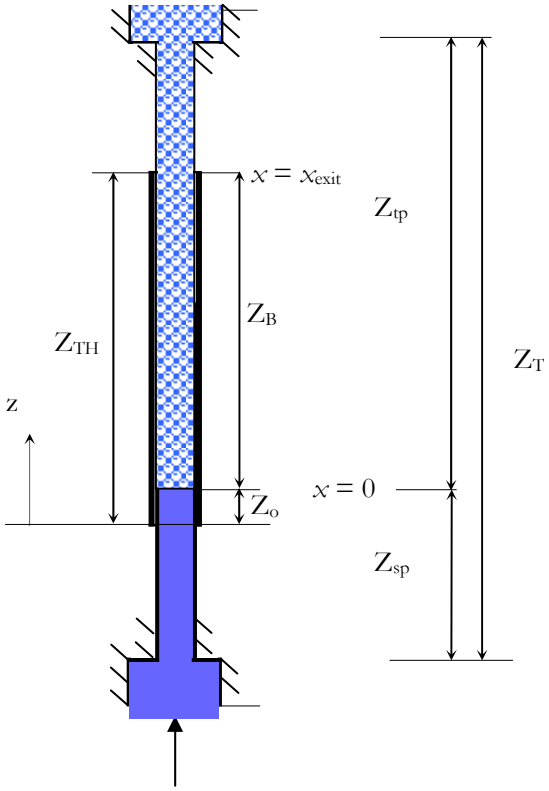

Figure 3.5. Flow regions in the microchannel

The measured pressure drop, $(\Delta P)_{meas}$, is the sum of the pressure drops corresponding to the flow across the single-phase length, $(\Delta P)_{sp}$, the flow across the two-phase length, $(\Delta P)_{tp}$, and the pressure drop due to the abrupt contraction near the inlet, $(\Delta P)_{ic}$, and abrupt expansion near the outlet, $(\Delta P)_{oe}$. , the total pressure drop can be expressed as:

$$(\Delta P)_{meas} = (\Delta P)_{ic} + (\Delta P)_{sp} + (\Delta P)_{tp} + (\Delta P)_{oe} \tag{3.15}$$

The pressure drop of the microchannel single-phase region can be expressed as the sum of a gravitational and a frictional component:

$$(\Delta P)_{sp} = \left|(\Delta P)_{sp}\right|_{frict} + \left|(\Delta P)_{sp}\right|_{grav} \tag{3.16}$$

Single-phase tests were conducted to validate the test rig reliability and data reduction method (Owhaib and Palm, *2002*). The experimental single-phase friction factor correlated well with the Blasius equation for

turbulent flow in smooth tubes, and for laminar flow the friction factor agreed with the classical correlation *f=64/Re*.

For the two-phase regions, a term representing the acceleration of the flow related to the phase-change phenomena, must also be considered:

$$\left(\Delta P\right)_{tp} = \left|\left(\Delta P\right)_{tp}\right|_{frict} + \left|\left(\Delta P\right)_{tp}\right|_{grav} + \left|\left(\Delta P\right)_{tp}\right|_{acc} \tag{3.17}$$

All components in equations (3.15) to (3.17), except $(\Delta P)_{tp,frict}$, can be quite easily determined with the expressions summarized in Table 3.1. Later in the text, experimental two-phase frictional pressure drop, $(\Delta P)_{tp,frict}$, is compared to predictions from correlations developed for both mini- and microchannels and larger scale tubes.

Table 3.1 Microchannel pressure drop components

Component	expression
Single-phase Abrupt contraction $(\Delta P)_{ic}$	$\left(\Delta P\right)_{ic} = \xi_{ic}\dfrac{\rho\left(u_2{}^2 - u_1{}^2\right)}{2}$; drag compression factor: $\xi_{ic} = f\left(lam/turb, {A_2}/{A_1}\right)$
Two-phase Abrupt expansion $(\Delta P)_{oe}$	$\left(\Delta P\right)_{oe} = \dfrac{G_1{}^2\sigma(1-\sigma)}{\rho_l}\left[\dfrac{x_{exit}^2}{\alpha_{exit}}\left(\dfrac{\rho_l}{\rho_g}\right) + \dfrac{(1-x_{exit})^2}{(1-\alpha_{exit})}\right]$, $\sigma = {A_1}/{A_2}$; collier and Thome (*1994*)
Single-phase, gravitational $\left\|\left(\Delta P\right)_{sp}\right\|_{grav}$	$\left\|\left(\Delta P\right)_{sp}\right\|_{grav} = L_{sp} g \rho_l$
Single-phase, frictional $\left\|\left(\Delta P\right)_{tp}\right\|_{frict}$	$\left\|\left(\Delta P\right)_{sp}\right\|_{frict} = f\dfrac{\rho_l u^2}{2}\dfrac{L_{sp}}{D_i}$; if Re<2300: $f_{lam} = {64}/{\mathrm{Re}}$ if Re>2300: $f_{turb} = {0.316}/{\mathrm{Re}^{0.25}}$ Blasius
Two-phase, gravitational $\left\|\left(\Delta P\right)_{tp}\right\|_{grav}$	$\left\|\left(\Delta P\right)_{tp}\right\|_{grav} = gL_{tp}\dfrac{1}{x_{exit}}\int_{x_{in}}^{x_{out}}\left[\alpha\rho_g + (1-\alpha)\rho_l\right]dx$ Zivi's void fraction: $\alpha = \left[1 + \left(\dfrac{1-x}{x}\right)\left(\dfrac{\rho_g}{\rho_l}\right)^{\frac{2}{3}}\right]^{-1}$
Two-phase, accelerational $\left\|\left(\Delta P\right)_{tp}\right\|_{acc}$	$\left\|\left(\Delta P\right)_{tp,i}\right\|_{acc} = \dfrac{G^2}{\rho_l}\left[\dfrac{x_{exit}{}^2}{\alpha_{exit}}\left(\dfrac{\rho_l}{\rho_g}\right) + \dfrac{(1-x_{exit})^2}{(1-\alpha_{exit})} - 1\right]$ Zivi's void fraction: $\alpha_{exit} = \left[1 + \left(\dfrac{1-x_{exit}}{x_{exit}}\right)\left(\dfrac{\rho_g}{\rho_l}\right)^{\frac{2}{3}}\right]^{-1}$

4 Uncertainty Analysis

In the experiential data, the true values of measured quantities are always unknown. The estimation of the error in these data is called an uncertainty, *u*. usually, the estimated uncertainty, u_x, in a given measurement of a physical quantity, *x,* is made at a 95% confidence level (20:1). The statistical suggestions to estimate the uncertainty in single- and multi-sample experiments was described by Kline and McClintock (*1953*) and Moffat (*1988*) and these publications still form the basis for this branch of the art.
The uncertainty of the experimental data was estimated by performing an uncertainty analysis based on the method of sequential perturbations, described by Moffat, (*1988*). This method provides a process to estimate an overall uncertainty of a set of data by integrating the uncertainty of each source of error into the data base independently and then using a root sum square method to calculate the overall uncertainty.

4.1 Measurement systems and error sources

Measurement systems consist of the instrumentation, the procedures for data acquisition and reduction, and the operational environment. Measurements are made of individual variables, x_i, to obtain a result, *y* which is calculated by combining the data for various individual variables through data reduction equations

$$y = f(x_1,...,x_i,...,x_n) \tag{4.1}$$

Each of the measurement systems used to measure the value of an individual variable, x_i, is influenced by various elemental error sources. The effects of these elemental errors are shown as bias errors (estimated by W_{x_i}) and precision errors (estimated by S_{x_i}) in the measured values of the variable, x_i. These errors in the measured values then propagate through the data reduction equation, thereby generating the bias, W_y, and precision, S_y, errors in the experimental result, *y*.
The *root-sum-square* (*RSS*), combination is the basic form used for combining uncertainty contributions in both single-sample and multiple-sample analyses of the individual uncertainties.

4.1.1 Bias Limits (i.e., Systematic Uncertainties)

The bias limit, *W*. The bias limit is an estimate of the magnitude of the systematic inaccuracy (i.e. fixed and constant error). It is assigned with the understanding that the experimenter is 95% confident that the true value lies within the limits of the bias error. We can adjust measurements to account for bias errors.
If we assume that all x_i are independent variables, then the bias limit of the result is given by the following expression:

$$W_y^2 = \sum_{i=1}^{m} \left(\left(\frac{\partial f}{\partial x_i} \right)^2 W_{x_i}^2 \right) \tag{4.2}$$

where, $\frac{\partial f}{\partial x_i}$ are the sensitivity coefficients, and W_{x_i} is the bias limits in x_i.

The bias limit W_{x_i} for each variable is an estimate of elemental bias errors from different types: calibration errors; data acquisition errors; data reduction errors; and theoretical bias. Within each type, there may be several elemental sources of bias. For instance, if for the i_{th} variable x_i there are J elemental bias errors identified as major, and whose bias limits are estimated as: $(W_{x_i})_1, (W_{x_i})_2, \ldots, (W_{x_i})_J$,then the bias limit for the measurement of x_i is calculated as the *RSS* combination of the elemental limits.

$$W_{x_i}^2 = \sum_{k=1}^{J} \left(W_{x_i} \right)_k^2 \tag{4.3}$$

The bias limits for each element $(W_{x_i})_k$ must be estimated for each variable x_i using the best information available.
Bias limits contribution are identified (calibration accuracy, data acquisition, data reduction, or conceptual bias) and combined.

4.1.2 Precision Limits (i.e., Random Uncertainties)

To determine the random errors, the measured data must be obtained from a process in a statistically controlled condition. Limits of random errors are stated by means of an estimate of the standard deviation of the mean value ($\bar{x}$) of a series of measurements. In this, the number of measurements (n) is sufficiently large (>20).
The standard deviation (S), which can be calculated from n measured values x_i (i=1, 2, ……., n) as:

$$\left[S_{\bar{x}} = \frac{1}{n \cdot (n-1)} \sum_{i=1}^{n} (x_i - \bar{x})^2 \right]^{1/2} \tag{4.4}$$

where, the mean value is given by: $\bar{x} = \frac{1}{n} \sum_{1}^{n} x_i$.

In case the measured data is performed only once, the standard deviation has to be determined from experience, or if the bias error interval in the measured data is known, then the standard deviation can be calculated by:

$$S_{x_i} = \left(\frac{W_{x_i}}{3} \right)^{1/2} \tag{4.5}$$

The precision limits, *S*. The $\pm S$ interval about a nominal value is the 95% confidence range within which the mean of many such results would fall, if the experiment were repeated many times under the same conditions using the same equipment. Thus, the limit on the precision of a measurement is an estimate of the non-repeatable inaccuracy caused by an unknown or an uncontrollable influence.
S_y can be estimated by the *RSS* of the precision limits for the measurements of the individual variables.

$$S_y = \sqrt{\sum_{i=1}^{n} \left(\left(\frac{\partial f}{\partial x_i} \right)^2 S_{x_i}^2 \right)} \tag{4.6}$$

The value of S_x is determined from n readings over an appropriate and sufficient time interval that includes all factors causing variability in the result.

4.1.3 Overall combined uncertainties

The 95% (20:1) confidence overall combined uncertainty (i.e., the total uncertainty in the result, *y*,) is calculated from the *RSS* of the bias and precision limits.

$$U_y = \sqrt{S_y^2 + W_y^2} \tag{4.7}$$

The $\pm U_y$ interval about the nominal result is the range within which the experimenter is 95% confident that the true value of the result lies.

4.2 Computing uncertainty of measurement

Two methods are available to calculate the measurement data uncertainties. Analytical method, and sequential perturbation, both methods are based on the errors *RSS* estimation.
The analytical method requires deriving a single formula for the measurement uncertainty, which is easy to compute, but the derivations become more difficult as the data reduction procedures become more and more complex.

Applying the sequential perturbation procedure is easy to when the data reduction procedure is conducted using a computer program. The sequential perturbation method gives an approximate of the uncertainty estimation of the measured data, not exact as in the analytical method, but it is simple to apply, and gives the ability to identify the component that consist a major uncertainty in the *model* of the data reduction.

In this thesis the uncertainty analysis is computed using the sequential perturbation method.
As a result of the basic theory of calculus

$$\frac{\partial f}{\partial x_i} = \lim_{\Delta x_i \to 0}\left[\frac{f(x_i + \Delta x_i) - f(x_i)}{\Delta x_i}\right] \approx \frac{f(x_i + \delta x_i) - f(x_i)}{\delta x_i} \tag{4.8}$$

where δx_i is a finite perturbation in the measured value of x_i.
If we use $\delta x_i \approx u_i \approx W_{x_i}$ or S_{x_i}, then

$$\left[\frac{\partial f}{\partial x_i}\delta x_i\right]^2 \approx \left[\frac{f(x_i + \delta x_i) - f(x_i)}{\delta x_i}u_i\right]^2 \approx \left[f(x_i + u_i) - f(x_i)\right]^2 \tag{4.9}$$

The uncertainty in f due to the uncertainty in component x_i can be predicted by perturbing the data reduction formula by u_i, and equation (4.9) becomes:

$$u_y = \left[\sum_{i=1}^{n}\left[f(x_i + u_i) - f(x_i)\right]^2\right]^{1/2} \tag{4.10}$$

The uncertainty in y is estimated by sequentially perturbing the input values x_i by their respective uncertainty.

Equation (4.10) is valid for small perturbations, u_i. If $f(x_i)$ is strongly nonlinear, or if any of the u_i are large, then the u_y computed from Equation (4.10) may not be a good approximation to the U_y computed from equation (4.7).

The following procedure according to (Moffat, *1988*) was used in an excel sheet in order to implement the uncertainty analysis by the sequentially perturbing the inputs:

1. Calculate the results y for the recorder data.
2. For $i = 1$ to n, where n is the number of parameters that have uncertainty and are related to the calculation of f, increase the value of the i-th parameter x_i by its uncertainty u_i for both bias and precision errors, and calculate the result f using x_i+u_i with all other parameters unchanged. The difference $f(x_i+u_i)-f(x_i)$ is stored as the contribution to the uncertainty u_y caused by the i-th parameter.
3. The uncertainty in the results u_y is the *RSS* of $f(x_i+u_i)-f(x_i)$.

4.3 Uncertainties in measured parameters

4.3.1 Uncertainty in temperature measurement

The T-type thermocouple (Thermocouple wire-Magnesium Oxide Insulation with Metal Sheath, 304SS-T-MO-0.5 mm) measurements were captured using an Agilent 34970A data acquisition and switch unit.

The thermocouple specifications:

Copper-Constantan, Thermocouple 304SS-T-MO-0.5 mm from Omega has:

- Sheath material is 304 stainless steel.
- Sheath diameter is 0.5 mm.
- Wall thickness is 0.076 mm.
- Wire diameter is 0.089 mm. The thin wire thermocouple implies a faster response time.
- Temperature range is: -40 to 125 ^{O}C.
- Tolerance according to specifications is ±0.5 ^{O}C, at 0 ^{O}C reference junction.

The DC voltage measurements accuracy at 100 mV range signal is 0.007 mV, the temperature coefficient is 0.03 ^{O}C, and the conversion accuracy (the error in the function which converts the voltage to an equivalent temperature inside the instrument) was less than 0.05 ^{O}C, which is claimed by the data acquisition logger manufacturer.

In order to improve the accuracy of the temperature measurements, a special system has been developed. The system is described in detail by Palm (*1991*), and involves a multiplex unit (Agilent 34901A multiplexer), an isothermal block (Aluminum Block), and connecting wiring (copper wires). All measured temperatures were measured by the same multiplex unit. The reference junctions of the thermocouples were put in an isothermal block. The block consists of a homogenous aluminum block with a narrow hole for each thermocouple, insulated on all sides. The tip of each junction was electrically insulated by a small tube of Teflon, *PTFE*. The temperature of this isothermal block was measured by a *Pt100* (Platinum Resistance sensor) *RTD* Probe. This method has been proven to give very high accuracy in the temperature measurements by Palm (*1991*). The concept with such system arrangements is to eliminate the error due to the error in the reference junction temperature. This is achieved by making sure that all thermocouples have the same reference junction temperature, thereby eliminating the offset in all temperature difference measurements. Since most of the measurements of temperature are used to estimate temperature differences, this error is eliminated and the accuracy is improved. A further improvement in accuracy in temperature measurement is made by manufacturing all the thermocouples from the same wire.

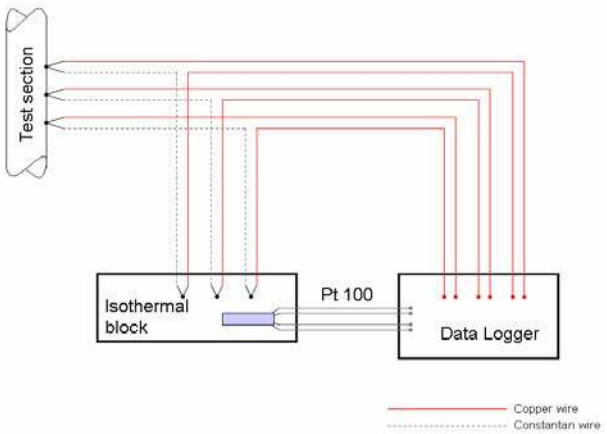

Figure 4.1: A schematic drawing of the temperature measurement system (Palm, *1991*)

The thermocouples were calibrated against an ice bath, and at steady condition all the measured temperature readings fluctuated between ± 0.1 ^{O}C (20:1 odds), which is also the temperature difference among these thermocouples. From this we can estimate the bias limit of the temperature measurement. Before the start of each experiment, the temperature readings of all thermocouples were compared. The readings were in most cases at stable conditions.

The temperature difference between the test section tube outer wall, measured by thermocouples, and the refrigerant temperature, determined from the measured saturation pressure, was examined at the condition where no power was added to the test section. These measurements conclude that this temperature difference lay in the range of ± 0.2 ^{O}C, which was then taken as the bias limits in the temperature difference in the experimental runs.

4.3.2 Uncertainty in the pressure drop measurement

Two different pressure difference transducers were used to record the pressure drop across the test section, depending on the pressure difference range of the specific test.

- Druck PDCR 4160 (1 bar d), Sensitivity 100.17 mV, Non linearity & hysteresis max ±0.04% BSL (Best Straight Line), Temperature error band max ± 1.0 %.
- Druck PDCR 2160 (350 mbar d), Sensitivity 50 mV, Non linearity & hysteresis max ±0.1% BSL (Best Strait Line), Temperature error band max ±0.5%, Temperature Compensated range 0 ^{O}C to +50 ^{O}C.

As already explained, the tubes connecting the pressure drop sensors were cooled down or heated up using water flowing through an outer tube to ensure that the connecting tubes were filled with liquid or vapor only.

The pressure difference and absolute pressure transducers were calibrated against a certified test gauge (Druck DPI 603 Pressure calibrator). The calibration points and linear calibration equations obtained are shown in the figures below.

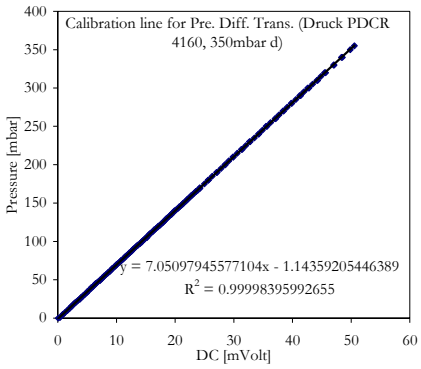

Figure 4.2 Pressure difference transducer calibration

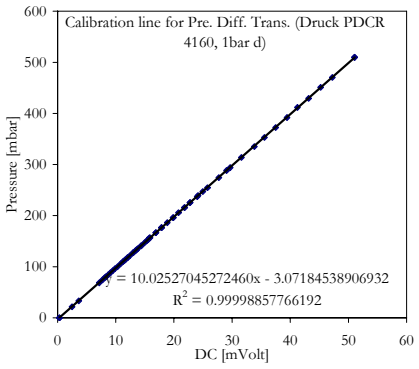

Figure 4.3: Pressure difference transducer calibration

4.3.3 Uncertainty in system pressure measurement

The system pressure was measured by the following pressure transducer:

- Druck PDCR 4060 (0-20 bar). The Non linearity and hysteresis is max ±0.04 % BSL (Best Straight Line), and the temperature error band is max ± 0.3 %. FRO (Full Range Output), Compensated temperature range 0 ^{O}C to +50 ^{O}C.

The bias interval uncertainty in these pressure measurements was thus estimated to be less than ± 10 mbar.

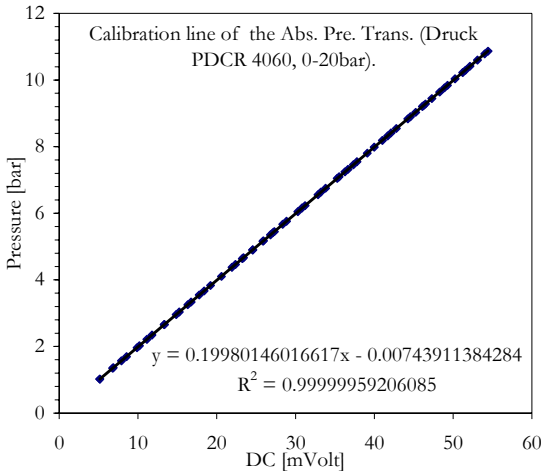

Figure 4.3: Absolute pressure transducer calibration

The system pressure measurements were used to calculate the refrigerant saturation temperature by REFPROP computer program, which is estimated for pure fluids with high accuracy. The bias uncertainty interval of the refrigerant saturation temperature was estimated based on the earlier argument to be ± 0.2 ^{O}C.

Two methods were used to check this estimation. First, at the start of each test, and at stable conditions (usually over the night), the difference between the thermocouple measurement before and after the test section, and the saturation temperature calculated from the pressure measurements at the test section inlet were compared.

Second, during the measurements, the exit temperature measured at the outlet of the test section was compared to the saturation temperature at the same location calculated from the pressure measurement.

4.3.4 Uncertainty in mass flow meter

4.3.4.1. Micropump

In the first single phase and boiling measurements, the gear pump (ISMATEC MCP-Z) was calibrated and used for metering the flow. It was later found that with high pressure drop in the system, this method was not accurate enough, and a Corioli mass flow meter was installed.

4.3.4.2. Mass flow meter

The mass flow rate in most tests was measured by a Micromotion DS006 Corioli mass flow meter. According to the manufacturer, the flow rate sensor has the following specifications:

- Nominal Flow range is 0-7.5 g/s
- Maximum Flow rate is 15.278 g/s
- Zero stability is 0.001667 g/s
- Sensor Accuracy is ±0.15% ± ((zero stability/flow rate) × 100) % of rate.
- Sensor combined repeatability, linearity, and hysteresis is ±0.05% ± (1/2 (zero stability/flow rate) × 100) % of rate.
- Temperature effect on flow accuracy (the worst case zero offset due to changes in the process fluid temperature from the zeroing temperature) is ± 0.01 % of nominal flow rate/^{O}C.

Table 4.1 The sensor accuracy and pressure drop over the nominal flow range

Nominal Flow rate (%)	1%	5%	10%	100%
Accuracy (± %)	2.29	0.58	0.36	0.17
Pressure Drop, [bar]	~0	0.01	0.02	1.1

The refrigerant mass flow sensor was connected to a transducer, calibrated together with the sensor by the manufacturer and adjusted to the working conditions before the delivery. The output signal from the transducer was measured by the logger.
The mass flow rate (kg/s) Bias uncertainty interval, which includes all the above uncertainties, the sensor signal, and the calibration linear equation curve fittings error, is estimated to be ± 0.5%.

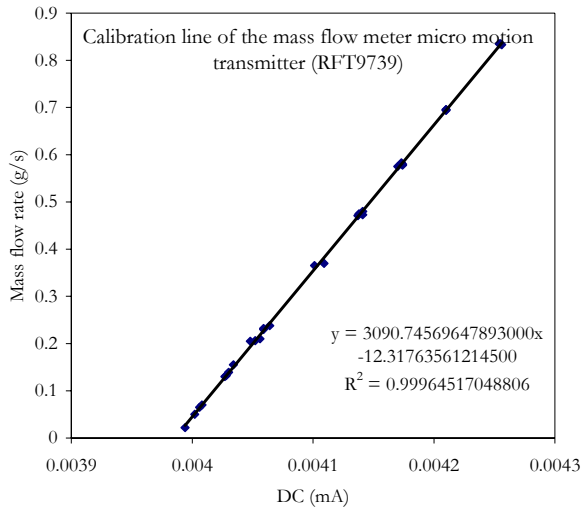

Figure 4.5: Calibration line of the Corioli mass flow meter

4.3.5 Uncertainty in the channel dimension measurement

The channel dimensions were carefully measured, with a special attention to the tube diameter. Since it is hard to measure the average tube diameter using a metric instrument, the average tube diameters were measured using a very accurate balance, (Mettler Toledo AX) with maximum error less than ± 1 mg. The idea is to measure the tube weight, fill it with distillate water, and weight it again. The mass difference was used to calculate the tube volume and average inside diameter.
Each channel dimension was estimated to have an error as:

Table 4.2 channel dimension uncertainties

Tube diameter, [mm]	Uncertainty, [mm]
D_i= 1.700	± 0.0035
D_i=1.224	± 0.0047
D_i=0.826	± 0.0070
D_i=1.332	± 0.0024

4.3.6 Uncertainty in the heat input

The heat input was determined from the product of the DC voltage across the test section and the current. Measurements were done with a FLUKE 85 III Digital Multimeter, having the following specifications:
DC Voltage, 0.1mV to 1000V, and the accuracy is ±0.08 %+1.

DC Current, up to 10A, accuracy: ±0.2 %+2, and the maximum resolution 0.1 μA

Resistance, 0.1Ω to 40 MΩ, and accuracy: ±0.2 %+1

In some tests the power was determined from the digital readings of voltage and current from the power supplies (TTi EX752M multi-mode PSU 75V/150V 300W, and TTi Thurlby Thandar Instruments TSX1820P).

The error of the heat input based on the multimeter-readings and the power supply-reading was estimated to be ±1%.

The error due to heat loss to the surroundings through a thick insulation on the test section and associated piping was estimated to be about ±2% of the heat input.

4.4 Summary of uncertainties

The accuracy of the data was assumed by performing an uncertainty analysis based on the method of sequential perturbation (Moffat, 1988). This method provides a means to estimate an overall uncertainty of data by integrating the uncertainties of individual sources of error into the data base independently, then using a root-sum-square method to calculate the overall uncertainty.

Table 4.3 Summary of uncertainties

Uncertainty variable	Uncertainty interval
Temperature, [°C]	±0.2
System pressure transducer, P_{in} [bar]	±0.1%
Differential pressure transducer, ΔP [mbar]	±0.2%
Mass flow rate (Corioli), $\dot{m}$ [kg/s]	±0.5%
Mass flow rate (Micropump), $\dot{m}$ [kg/s]	±2%
DC voltage measurement, [V]	±0.1%
DC current measurement, [A]	±0.5%
Measured channel diameter, [mm]	±0.007

Error analysis was performed for every test run of each data set and the maximum uncertainty of, the single-phase heat transfer coefficient h_{sp} was found to be ±14%. The measured single-phase pressure drop uncertainty was estimated to be ±2 mbar.

The maximum uncertainty of the boiling heat transfer coefficient h_{tp} was ± 17%. Uncertainty estimation of the measured two-phase frictional pressure drop was found to be ± 5 mbar.

5 Single-Phase Fluid Flow Tests

5.1 Objective

The objective of the single phase tests was to determine if classical correlations for heat transfer and pressure drop in circular tubes are applicable for tube diameters around 1 mm.

Also, the ability to calculate single phase heat transfer and pressure drop was necessary for the evaluation of the following two-phase tests.

5.2 Single-phase heat transfer results

Before conducting flow boiling heat transfer experiments, adiabatic liquid single-phase test and single-phase heat transfer test were performed to ensure appropriate instrumentation calibration and overall system performance. The single-phase heat transfer results were then compared with existing correlations. The single-phase heat transfer data was also used to evaluate the system heat loss.

5.2.1 Experimental Results and comparison (Paper #1)

Heat transfer experiments for single-phase flow were conducted for three different diameters tubes, 0.826, 1.224 and 1.700 mm, covering a wide range of Reynolds numbers from less than 1000 up to 18,000. These tubes were heated by applying a DC across the test section allowing a constant heat flux condition. At steady-state conditions, about 100 readings were captured and an average was calculated and used for the following evaluation.

From figure 5.1, where the variation of the experimental heat transfer coefficients with the Reynolds number of three different tube diameters are shown, it is clear that the heat transfer coefficient increases with decreasing tube diameter in the turbulent region. Note also the high heat transfer coefficient values. The slopes of the curves are different in the turbulent regime. With the smallest tube diameter the transition from laminar to turbulent flow is smoother than for the larger diameter tube.

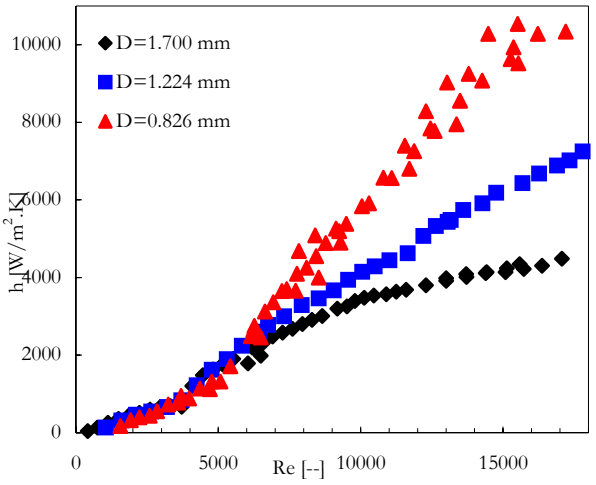

Figure 5.1: Experimental results of heat transfer coefficients for different tube diameters

The measured single-phase liquid R134a heat transfer data was compared to well known correlations such as Dittus-Boelter (*1930*) for fully developed turbulent flow in smooth channels, Gnielinski (*1976*) correlation, which can be used in the transition regime from laminar to turbulent that suggested by Petukhov *et al.* (*1973*).
For the laminar regime, the temperature profile was not fully developed so the experimental data was compared to the average Nu number for laminar entrance according to Sieder and Tate (*1936*). Comparisons were also done with the following correlations suggested recently based on microscale experiments: Wu and Little (*1984*) correlation for Nu in the turbulent regime, Choi *et al.* (*1991*) correlations for both laminar and turbulent flow regimes, Yu (*1995*) correlation for microchannels in turbulent flow, and Adams *et al.* (*1998*, *1999*) modification of the Gnielinski correlation, which is a generalized correlation for the Nusselt number for turbulent flow.
Figures 5.2, shows the comparison of the experimentally obtained Nusselts numbers with both the conventional correlations developed for macroscale channels (Dittus-Boelter, Gnielinski, and Petukhov), and with some of the correlations that have been suggested for microscale channels. The figure indicates the applicability of the classical correlations at fully developed turbulent flow. Of the suggested microscale correlations, the observations from Figure 5.2 show that none is in agreement with the obtained experimental data.

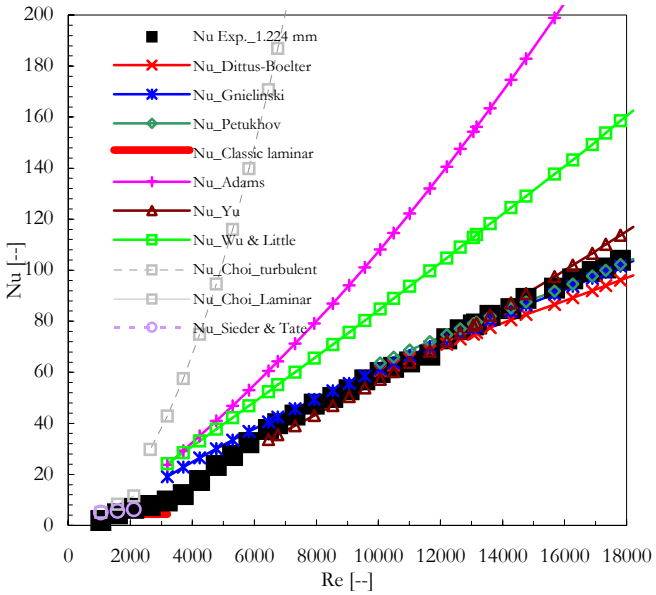

Figure 5.2: Comparison of the experimental Nu for D_i=1.224 mm with the macroscale, and the suggested microscale correlations

5.2.2 *Pressure drop experimental results and comparison (Paper #2)*

The experimental pressure drop results were obtained, for both laminar and turbulent flow regimes, and are shown in Figure 5.3. The figure indicates the high influence of the tube inner diameter on the pressure drop.

The friction factors were calculated from the experimental results and compared with the correlations for macroscale channels, such as Blasius (*1913*) for the turbulent flow regime in smooth circular pipes, and, Colebrook (*1939*) for rough tubes. For fully developed laminar flow (Re < 2300) through macroscale smooth pipes, the product of the friction factor and Reynolds number is $f\,\mathrm{Re} = 64$. The experimental friction factor was also compared with suggested microscale correlations from the literature such as Wu and Little (*1984*) correlations for the three regions, the laminar, transition and turbulent, Choi *et al.* (*1991*) correlation for the laminar and turbulent regions and Yu *et al.* (*1995*) two friction factor correlations.

The friction factor correlations for micro, and macro scale mentioned above are given in the table in appendix D.

Comparisons of the experimentally obtained friction factors with the predicted curves for the macroscale correlations and some correlations suggested for microchannels are shown in figure 5.4.

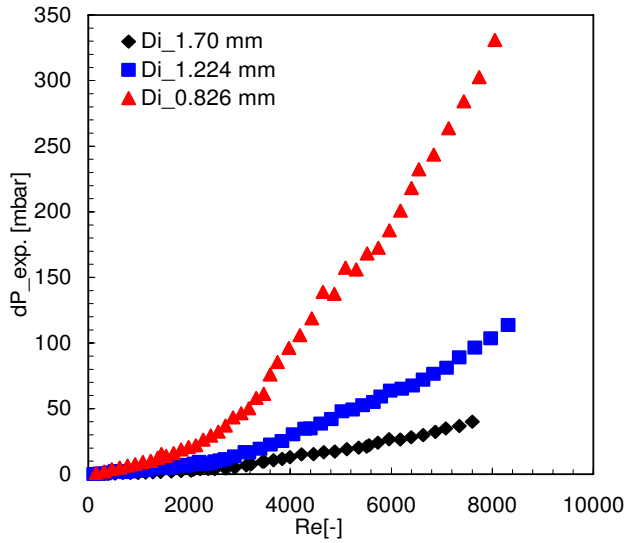

Figure 5.3: The experimental pressure drop for different tube diameters

As seen in figure 5.4, the experimentally obtained friction factors are in good agreement with the conventional macroscale correlations, but not with any of the microscale correlations. No early transition from laminar to turbulent flow was observed, which has been reported in the literature.

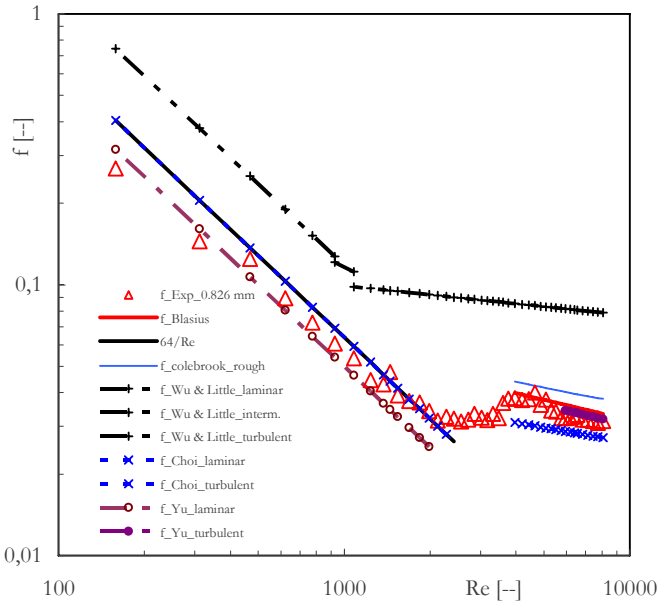

Figure 5.4: Comparison of the experimental *f* for D_i=0.826 mm with the classical, and the suggested microscale correlations

6 Flow Boiling in Vertical Tubes

6.1 Objective

The objective if this work is to gain a fundamental understanding of the flow boiling heat transfer process in mini and micro channels (< 2mm). Refrigerant R-134a was selected as a test fluid because of its wide application. An important purpose is to enable a close examination of the flow boiling heat transfer characteristics of R-134a in a minichannel.

The present results will serve as a tool for designing new R-134a refrigeration systems.

The following topics related to flow boiling heat transfer were investigated in the study:

1. Heat transfer mechanism that dominates the flow boiling in mini- microchannels.
2. Effects of pressure on the two-phase flow heat transfer performance in small channels.
3. Effects of mass flux and heat flux on two-phase flow heat transfer performance in small channels.
4. Comparison of the present heat transfer data with existing correlations which are both for small and large channels.

In addition, the knowledge of flow boiling heat transfer mechanism in small channels will be used to discuss the difference between large channel and small channel flow boiling.

6.2 Flow boiling heat transfer results (Paper #3)

Saturated vertical upflow boiling heat transfer tests were conducted at the operating conditions shown in table 6.1.

Table 6.1: Measurement operating conditions

Parameter	Operating range:
D_i [mm]	1.700, 1.224, 0.826
G [kg/(m^{2}s)]	50-400
q'' [kW/m^2]	3-34
T_{sat} [^{o}C]	24, 34
x_{exit}[--]	0-0.6
Z_{TH} [mm]	220

6.2.1 *Boiling curves*

Figure 6.1 shows the typical boiling curve for tube diameter 1.700 mm, T_{in} = 34 ºC and G = 50–400 kg/(m²s). In these curves the heat flux, q'', is plotted versus the temperature difference between tube wall and bulk fluid, $\Delta T_{sat} = T_{wall} - T_{saturation}$.

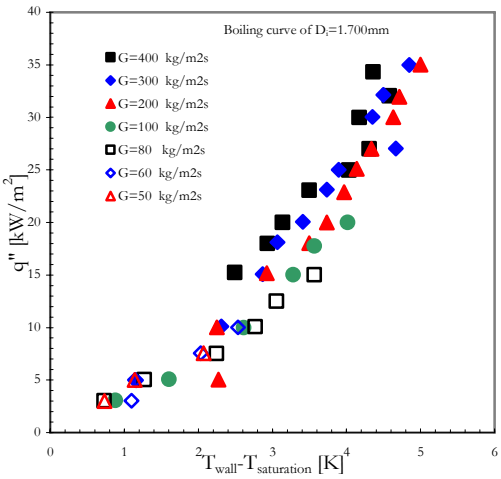

Figure 6.1: Heat flux vs. temperature difference for R-134a boiling in a 1.700 mm tube at various values of mass flux at T_{sat}=34 ºC.

Nucleate boiling is generally associated with bubbly, slug or low velocity annular flow patterns, while forced convection boiling is associated with annular flow pattern. In general, in nucleate boiling, bubbles are formed by nucleation in the superheated liquid near the walls. The heat transfer coefficient in this type of boiling is a function of the heat flux, but almost independent upon vapor quality or mass flux. In the convective boiling dominant region, heat is transferred by single-phase conduction and convection through the thin liquid film and evaporation takes place at the liquid-vapor interface. The heat transfer coefficient when forced convection boiling is dominant is fairly independent of the heat flux, but dependent upon vapor quality and mass flux. Even though some authors have assumed that only one of the boiling types occurs at any one situation, it is generally suggested that both mechanisms can coexist, one being dominant.

For flow in narrow tubes, the bubbles will grow to a diameter close to the diameter of the channel, thereby forming a vapor plug surrounded by a thin liquid film in between the wall and the bubble. At the two ends of the bubble, a liquid meniscus will form, similar to that underneath a growing bubble in pool boiling. It is well known that this meniscus is extremely important for the vapor formation in the case of pool boiling.

The similarity between the menisci at the ends of plug bubbles and those underneath a growing stationary bubble may explain the similarity in terms of the heat transfer dependence on the heat flux between the two different processes.

Figure 6.1 may be interpreted as indicating that convective boiling is dominant for q'' <5–10 kW/m² and ΔT_{sat}<2.5 K, and that nucleate boiling, or a similar mechanism, is dominant for higher values of heat flux and wall superheat. For the smaller diameters, the heat flux dependence occurs at even lower heat flux.

6.2.2 *The effect of mass flux*

The effects of the imposed mass flux on the heat transfer coefficient are examined first. Figure 6.2 presents the variation of the measured average heat transfer coefficient along the tube with the mass flux, *G*, for the 1.700 mm tube diameter.

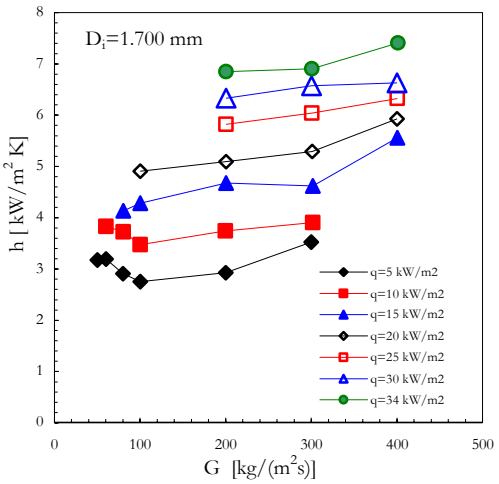

Figure 6.2: Average heat transfer coefficient as a function of mass flux for different heat fluxes. D_i=1.700 mm and T_{sat}=34 °C.

The results show that the heat transfer coefficient is very weakly dependent on the mass flux, with all other conditions fixed. This, again, indicates that the contribution of forced convection heat transfer to the overall transfer rate is small, and that heat transfer by a mechanism similar to that in nucleate boiling is dominant. From the same figure, one can see that the heat transfer coefficient is dependent on the heat flux, which corroborates the dominance of a mechanism related to nucleate boiling.

6.2.3 *The effect of heat flux*

Figure 6.3 shows the measured local heat transfer coefficient as a function of the local vapor quality for imposed wall heat fluxes 10 and 34 kW/m², different mass fluxes and for tube diameters of 1.224 mm, at a constant pressure.

The results indicate, first, that for vapor qualities below 0.6 the heat transfer coefficient is higher for a higher heat flux. The data also show that there is no evident influence of the vapor quality on the heat transfer coefficient below this threshold value. The explanation to the sudden decrease in the heat transfer coefficient for values of vapor quality above 0.6 (as indicated by the single measurement point in this range) is not quite clear, but may be caused by dry-out of part of the tube surface; in microchannels, dry–out or partial dry–out is more likely to happen at lower vapor quality compared to larger tubes.

The dependency of the heat transfer coefficient on the imposed wall heat flux and its independence upon the vapor quality suggest, again, that heat transfer is dominated by a mechanism related to that in nucleate boiling, with forced convection heat transfer being very weak.

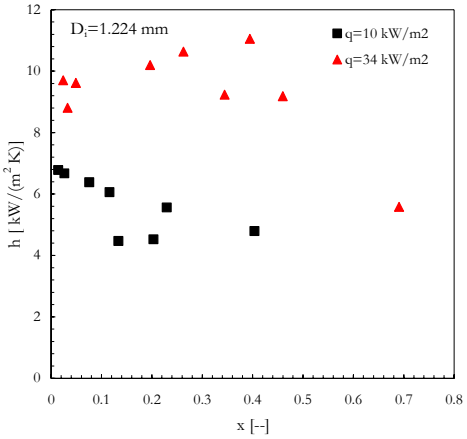

Figure 6.3: Local heat transfer coefficients as function of local vapor quality for two different heat fluxes. D_i=1.224 mm, T_{sat}=34 °C and G=100-300 kg/(m²s).

6.2.4 *The effect of system pressure*

The experimental measurements were conducted at two different pressures: 6.458 and 8.626 bars, corresponding to saturation temperatures of 24 °C and 34 °C, respectively. Figure 6.4 shows experimental data for R134a for constant mass and heat fluxes at the two

different pressures. These results indicate that an increase in the system pressure improves the heat transfer performance.

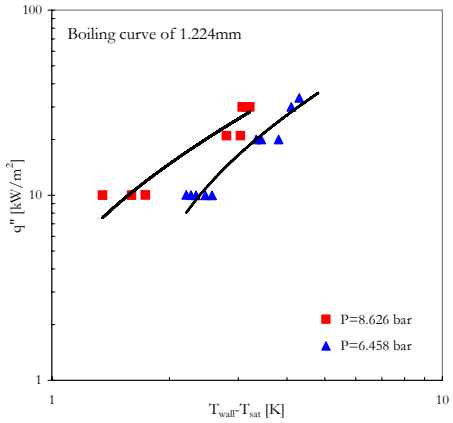

Figure 6.4: System pressure effect on flow boiling heat transfer of R-134a through a 1.224 mm diameter tube.

The trend coincides with that found in nucleate boiling, where it may be related to the activation of additional, smaller nucleation sites. From the present tests it is not possible to determine if this is also the cause of the increase in this case.

6.2.5 The effect of channel size

The experiments were conducted at three different tube diameters 1.700, 1.224, and 0.826 mm to examine the influence of this characteristic length on the heat transfer. Figure 6.5 shows that the heat transfer coefficient increases as the tube diameter decreases. The increasing importance of some parameters when the tube diameter is reduced may explain this improvement of the heat transfer coefficient. In small tubes, capillary effects gain importance, so, due to the surface tension, the thickness of the liquid film on the tube wall may become smaller as the tube diameter is reduced. Thinner liquid film results in lower thermal resistance and therefore, better heat transfer coefficients.

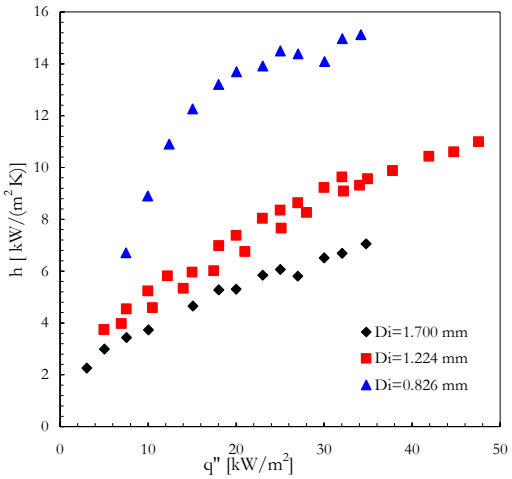

Figure 6.5: Average heat transfer coefficient as a function of heat flux for three different tube diameters, T_{sat}=34 °C.

6.3 Heat transfer results comparison

The experimental data from Owhaib *et al.* (2004) are compared with predictions of correlations from the literature for flow boiling heat transfer, using the conditions from the tests, i.e. R-134a flow boiling in a single circular tube at 24 °C and 34 °C.

There are a large number of saturated flow boiling correlations available in the literature. These correlations may be classified into two categories. The first category contains those developed by experimental investigators to fit their own data. Of course this kind of correlation may work well with the investigator´s own data or with other data with the same fluid. But generally they give rather poor results for other fluids or other data with a different parameter range. In the second category, the correlations were developed on the basis of a large body of data involving a number of fluids from different experimental investigators. These correlations usually are valid over a relatively wide range of parameters and different conditions and therefore they are more valuable.

It is now known that boiling heat transfer for flow inside channels is governed by two mechanisms: nucleate boiling and convective boiling. Nucleate boiling is characterized by the formation of vapor bubbles at a heated wall when nucleation conditions, i.e., a thin liquid layer near the surface superheated enough to allow nucleation, are reached. Convective boiling is characterized by heat transferred by conduction and convection through the liquid film and vaporization at the liquid-vapor interface.

In appendix E, different models to predict the heat transfer coefficient are tabulated.

1) Macroscale correlations

For all the operating conditions of this study, the experimental data were compared with the following correlations from the literature for macroscale boiling heat transfer: Wattelet (*1994*), Jung and Radermacher (*1991*), Liu and Winterton (*1991*), Kandlikar (*1990*), Klimenko (*1990*), Cooper (*1989*), Cooper (*1984*), Gungor and Winterton (*1986*), Shah (1976), Chaddock and Brunemann (*1967*), and Chen (*1966*).
Some of the correlations are in good agreement with the experimental heat transfer coefficients for the tube with internal diameter of 1.700 mm, but under predict the measurements for the tubes of 1.224 and 0.826 mm of diameter. This is true for the correlations by Cooper (*1984*) (for pool boiling), Shah (*1982*), and Chaddock and Brunemann (*1967*).
Some other correlations, such as Wattelet (*1994*), Liu and Winterton (*1991*), and Cooper (*1989*) under predict all experimental data and some, such as Pierre (1969) over predict these results.
Predictions from the Kandlikar (*1990*), Jung and Radermacher (*1991*), Gungor and Winterton (*1986*), and Klimenko (*1990*) correlations are in agreement with the experimental data for 1.224 mm, but under predict the measurements for 0.826 mm and over predict those for 1.700 mm.
The Chen correlation properly predicts the heat transfer coefficient for 1.700 and 1.224, but again under predicts the data for 0.826 mm.

2) Microscale correlations

Comparisons were made between the experimental data and published microchannel correlations for refrigerant flow boiling. Comparisons with the correlations by Lazarek and Black (*1982*), Tran (*1996*, *2000*), Kew and Cornwell (*1997*), and Warrier *et al.* (*2002*) are shown in appendix E. Comparisons were made between the experimental data and published microchannel correlations for refrigerant flow boiling. Comparisons with the correlations by Lazarek and Black (*1982*), Tran (*1996*), Kew and Cornwell (*1997*), and Warrier et al. (*2002*) are shown in Appendix E.

In Lazarek and Black (*1982*) and the modified Lazarek and Black (Kew & Cornwell, *1997*) correlations, the heat transfer coefficient is a function of the Reynolds number, *Re*, and the Boiling number, *Bo*. Figures in Appendix E, show that the agreement is good for flow boiling in the 1.7 and 1.2 mm tubes, but for the 0.8 mm tube the experimental data is underestimated. Wambsganss (*1993*) and Bao (*2000*) have

reported that the Lazarek and Black (*1982*) correlation predicted their data in agreement, but not over the whole examined range.

The Tran (*1996*) correlation under predicts the heat transfer coefficient for 1.2 and 0.8 mm tubes, and the Warrier (*2002*) correlation is not following the trend of experimental heat transfer coefficients at all.

Only one correlation seems to catch the influence of the tube diameter in the correct way, the Pierre (*1969*) correlation, which was based on flow boiling in large diameter tubes over predicts most data by up to 150%. None of the other correlations studied predict the trend of the heat transfer coefficients for all three tested diameters.

6.4 Experimental results correlation

From the discussion above, it is clear that none of the correlations can predict well the convective boiling heat transfer of R-134a in the studied smooth mini-tubes. Therefore a new correlation (equation 6.1) is developed to predict the flow boiling heat transfer of refrigerant through minichannels.

Based on the fact that the saturated flow boiling heat transfer coefficient is strongly dependent on the heat flux which indicates a nucleate boiling mechanism is dominant, the correlation has a heat flux influence, which could be interpreted in the boiling number.

The correlation also shows the small effect of the vapor quality (*power* to 0.1) and the independence on mass flux.

The Correlation includes the confinement number to account for the heat transfer enhancement in mini channels due to the confinement effect. It also includes the surface tension, which is an important fluid property in minichannel flow boiling.

$$h_{tp} = C.\left(\mathrm{Re}_{lo}\, Bo\right)^{0.5}\left(1-x_{exit}\right)^{0.1} N_{conf}^{0.55} P_R^{1.341}\left(\frac{\rho_l}{\rho_g}\right)^{0.37} \frac{k_l}{D_i} \qquad (6.1)$$

where, C=400, correlates the present experimental data.

This correlation predicts the experimental data with a mean absolute deviation of less than 8%.

7 Two-Phase Pressure Drop

7.1 Objective

The objective of this work is to gain a fundamental understanding of pressure drop of two-phase flow in mini- and microchannels (D_i < 2mm) using R-134a as a refrigerant. The following topics will be investigated:

1. Two-phase flow pressure drop characteristics of R-134a in circular tubes (D_i = 1.700, 1.224, 0.826 mm).
2. Effects of the channel size, and pressure on two-phase flow pressure drop.
3. comparison of the data with existing both large tube and mini or micro channel tube correlations in the literature

7.2 Two-phase pressure drop results (Paper #4)

Tests of pressure drop were preformed with R-134a, at the operation conditions presented in table 7.1.
The flow entered the test section slightly subcooled or at saturated liquid condition, i.e. the onset of nucleate boiling at a position close to Z=0.

Table 7.1: Measurements operating conditions

Parameter	Operating range
D_i [mm]	1.700, 1.224, 0.826
G [kg/(m²s)]	100, 200, 300, 400
q'' [kW/m²]	10, 15, 20, 25, 30
p_{sat} [bar]	8.625
x_{exit}[--]	0-0.9
Z_{tp} [mm]	220 (heated)+185 (adiabatic)

Figure 7.1 illustrates that the friction pressure drop is the most important component in the measured pressure drop.

The experimental frictional pressure drop data, ΔP, including both the heated section and the adiabatic section downstream, was calculated from the measured pressure drop between the pressure taps (figure 3.1) according to the data reduction started in section 3.3.3. The results are shown in the following diagrams. First, ΔP was plotted versus the exit quality at the system saturation pressure 8.625 bar, for several mass flux,

from 100 to 400 kg/(m²s). From figure 7.2, it is clear that the two-phase frictional pressure drop increased with increasing mass flux, as expected.

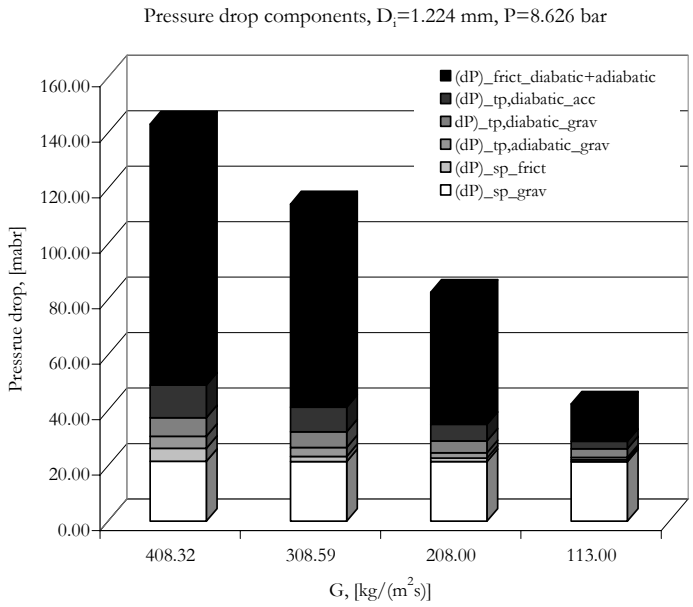

Figure 7.1: Measured pressure drop components at 30 kw/m2 for different mass fluxes in 1.224 mm tube, at P=8.625 bar

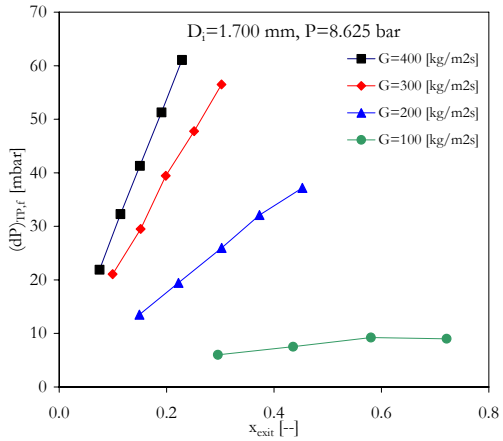

Figure 7.2: Frictional pressure drop as a function of quality through D_i=1.700 mm tube at various values of mass flux at P=8.625 bar

It also increased more or less linearly as the outlet quality increased. At high mass fluxes, this influence of quality was the strongest. The values should be compared to those for single phase flow, which according to classical correlations should be between 1.3 and 6.5 mbar

for the 1.700 mm tube. The analysis of the result is complicated by the fact that the pressure drops are the sums of the diabatic and the adiabatic sections' pressure drops. It should also be noted that some liquid may be present inside the differential pressure sensor, thereby adding an additional gravitational term to the equation 3.15. In fact, the data in figure 7.3 seems to indicate a certain offset in the data, especially, the data at the lowest mass flux is not increasing with vapor fraction as expected.

Figure 7.3 presents the variation of the measured two-phase frictional pressure drop with the mass flux, G, for different imposed wall heat fluxes, 10 to 30 kW/m^2 for 1.700 mm tube diameter. Increasing the mass flux at a constant heat flux results a decreased in outlet vapor fraction, and since the pressure drop expected to increase with the mass flux, therefore, this acts to decrease the slope of increasing in the pressure drop. As shown in figure 7.2, the pressure drops for the lowest mass flux were almost constant. Keeping in mind that the pressure drop must be zero at zero mass flux, some of the results indicate a remarkably linear behavior. The data for the smallest tube, however, does not follow this simple trend.

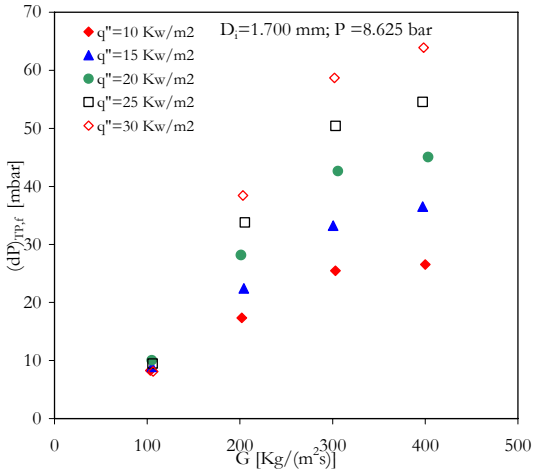

Figure 7.3: Frictional pressure drop through D$_i$=1.700 mm tube versus mass flux at various values of heat flux at *P*=8.625 bar

7.2.1 The effect of channel size

Figure 7.4 show the frictional pressure drop versus the exit quality for the three tube diameters at the same mass flux, 300 kg/(m^{2}s). As shown, the pressure drops in this representation seem more or less independent of the tube diameter. Similar plots could be draw for other mass fluxes.

The result is quite contrary to what would be expected. It should be noted that the tests have been repeated, with similar results. The flow pattern is an important key factor for the pressure drop, which might explain the unexpected influence of the tube diameter.

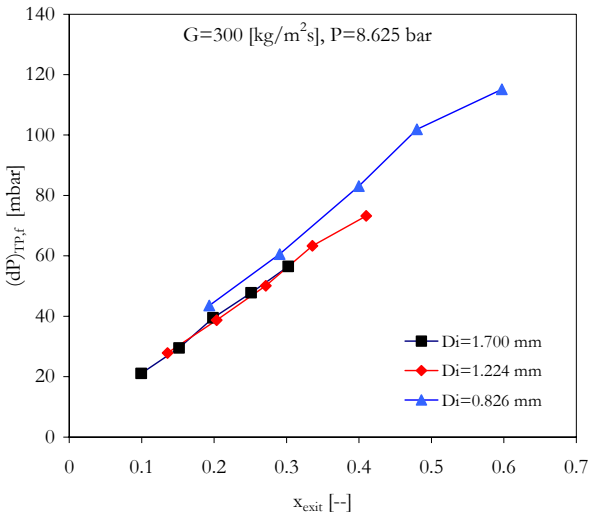

Figure 7.4: Tube diameter effect on frictional two-phase flow pressure drop of x=0.25 kg/m²s, at P=8.625 bar

7.3 Pressure drop results comparison

Since the frictional pressure drop is the major component of the total two phase pressure drop, the experimental data of frictional pressure drop of R-134a flow boiling, through a single circular tested tube with three different diameters of 1.700, 1.224, and 0.826 mm, at p=8.625 bar were compared with correlations from the literature for predicting the two-phase flow frictional pressure drop in both large tubes (macro-scale), and small tubes (micro-scale).

1) Macroscale correlations

The experimental data was compared with four correlations for large tubes: The homogenous model, Lockhart-Martinelli method (*1949*), Chisholm (*1973*), Pierre (*1964*), Friedel correlation (*1979*), Müller-Steinhagen & Heck (*1986*), and Jung & Radermacher (*1989*). Figures in Appendix F show the comparison plots of these four large tube models with the experimental friction pressure drop. It is clear that the pressure drop of the 1.700 mm tube is better correlated than the 1.224 mm, and 0.826 mm tubes. The possible reason for the larger scatter as the tube

diameter decreases is that these correlations were developed specifically for large tubes where the flow is mostly turbulent, but with smaller tube diameter and low refrigerant flow rate the flow becomes laminar. The correlation by Müller-Steinhagen & Heck (*1986*) predicted the studied data by MAD=30.4%.

2) Microscale correlations

Figures in Appendix F, give the comparison with Mishima and Hibiki correlation (*1996*), Tran correlation (*2000*), Lee and Lee correlation (*2001*), Zhang and Webb correlation (*2001*)Yu correlation (*2002*), Chen correlation corrected to Homogenous model, Chen corrected to Friedel correlation (*2002*), and Qu and Mudawar correlation (*2003*). Mishima and Hibiki correlation (*1996*) predicted quite well the results with MAD= 22.45%. A better prediction was by a modified correlation to Mishima and Hibiki correlation suggested by Qu and Mudawar correlation (*2003*) with MAD 20.45%.

8 Two-Phase Dryout and Flow Visualization

In this chapter a summary of two papers results will shown.

8.1 Dry out experiments and visualization (Paper #5)

In this study, the transparent glass test section described in section 3.1.2 was used, and the heated length Z_{TH} was 235.5 mm. Eight thermocouples were mounted along this length. The flow direction was vertical upflow, the refrigerant was R-134a, and the operating conditions as listed in Table 8.1.

Table 8.1: Operating conditions

Parameter	Operating range, case:				
	(1)	(2)	(3)	(4)	(5)
D_i [mm]	1.332				
G [kg/(m²s)]	47.7	124.4	166.5	99.5	164.7
q'' [kW/m²]	8.31	25,95	41.79	21.82	41.7
T_{sat} [°C]	24	24	24	34	34
x_{exit} [m/s]	0.58	0.73	0.91	0.80	0.91
Z_{TH} [mm]	235.5				

Figure 8.1 shows the dryout heat flux and vapor fraction at different mass fluxes at two system pressures. As seen from this figure, the heat flux at the position of dryout increases with increasing mass flux. The two data points taken at higher pressure indicate that the dryout heat flux increases with decreasing pressure. For lower mass flux, the dryout is reached at lower quality.

Further increase in the heat flux resulted in post dryout conditions, and transition to mist flow was observed. This flow type was particularly obvious by the "smoky" character of the flow in the non-heated section following the test section.

Even though the wall temperature increase was quite obvious at a certain heat flux, it was still possible to reach steady-state conditions with moderate wall temperatures, without burnout of the heater. In Figure 8.2 the wall temperatures at the last four thermocouple positions are shown as a function of time. All the measurement data shows that the dryout always first occurred at the end of the heated test channel, as expected.

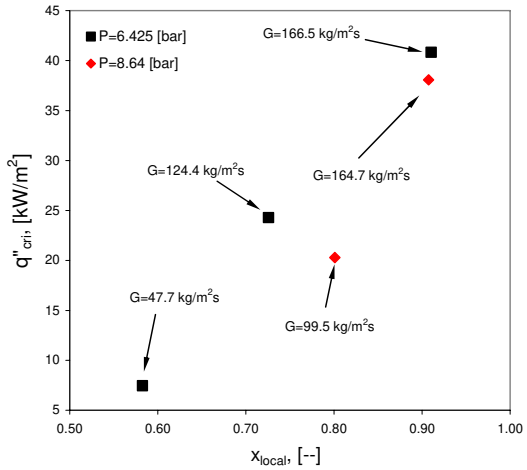

Figure 8.1: Dryout heat flux at different mass fluxes and system pressures.

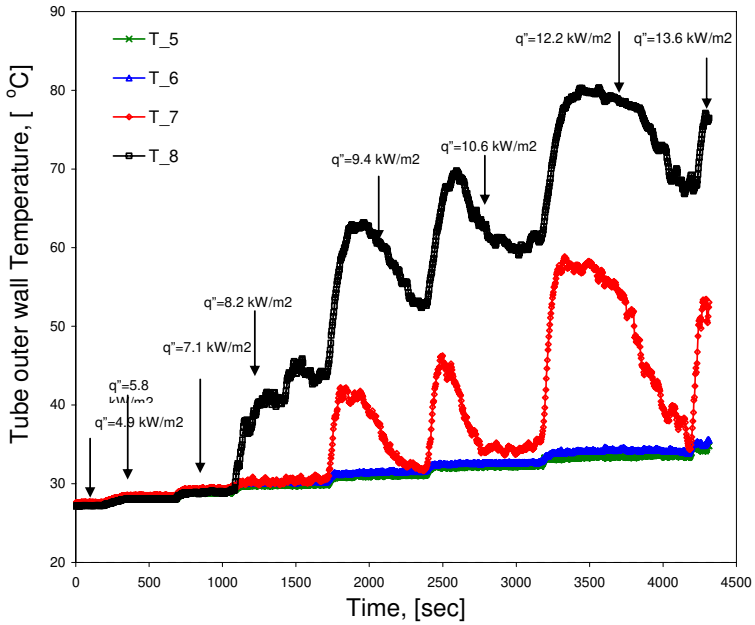

Figure 8.2: Outer wall temperature behavior for varied heat flux at G=47.7 kg/(m²s), and P=6.425 bar.

The short time scale oscillation in the temperature reading is higher at the higher mass flux. For the low mass flux conditions, the wall temperature decreased during a relatively long period of time after each increase in the heat flux. This behavior is not quite understood but may be an effect of redistribution of the flow regimes along the tube.

8.1.1 Visualization results

The glass test section was studied using high speed camera and close up lens. Saturated flow boiling characteristics were captured just before and after dryout at the last thermocouple position of the heated tube. For the visualization tests, the pressure was kept at 6.425 bar and the R-134a mass flux was 47.7 and 124.4 kg/(m²s).

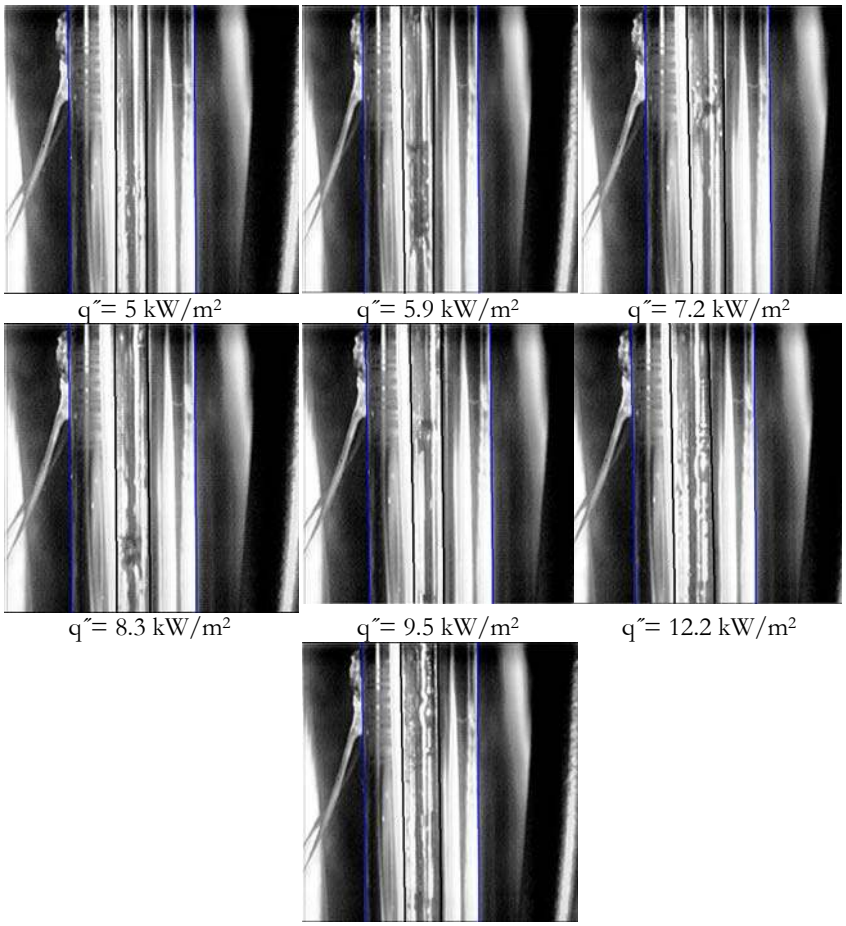

Figure 8.3: Images at camera position P17 at *G*=47.7 kg/(m²s) at different heat fluxes

Figure 8.3 shows images of the flow pattern for mass flux of 47.7 kg/(m²s) at different heat fluxes. The original video recordings can be viewed at the web address:

http://www.energy.kth.se/index.asp?pnr=10&ID=288&lang=1.

From these video recordings, from which the images in figure 8.3 are taken, it is found that the flow pattern is generally annular. Flow characteristics which are observed from the videos are:

1. The liquid flow in the film on the walls.
2. The vapor flow in the core
3. The liquid entrained in the core flow.
4. The liquid drop deposition on the wall.

Based on the visual inspection of the videos shown in the link the dominating mechanisms at dryout are found to be different depending on the mass flux:
At low mass flux (47.7 kg/(m²s)) the liquid front is fluctuating with waves regularly passing the position where the wall temperature starts to increase. In between these waves the surface is temporarily dry.
At high mass flux (124.4 kg/(m²s)) there are less fluctuations of the liquid front and the liquid film breaks up into drops and rivulets which evaporate while sliding along the tube wall.

8.1.1.1. Low mass flux annular flow

Figure 8.3 presents the visualization of the dryout at low mass flux, (and low heat flux), where the small waves are not significant, because of the low velocity difference between the liquid film and the vapor core. After a large wave, resulting from the merging of bubbles, flows over a certain cross section in the heated tube, a thin but stable liquid film is formed. Further up the tube the wave height seems to decrease, allowing the vapor in the core to pass. The remainder of the wave then frequently tends to change direction and flow downward, contrary to the main flow direction.
At the location where the wall temperature started to increase, the wall surface was temporarily dry and temporarily flushed by a passing wave. Even though the surfaces are temporarily dry, the vapor quality, calculated as an average over time, is as low as 0.58 due to the liquid waves periodically passing the location.
In between the waves, a thin liquid film was seen at the surface. This film gradually dried up without breaking up.
After the location in the heated channel where increased wall temperature was seen, the intermittent wave front gradually evaporated leaving small droplets deposited at the heated wall. By increasing the heat flux, the onset of the dryout occurred closer to the heated channel entrance. Also, the frequency of waves passing a certain downstream location decreased resulting in longer dry periods and higher surface temperature. The difference in wave frequency was found to be caused by the process at the onset of nucleate boiling: At high heat flux the

small bubbles tend to merge before forming Taylor bubbles while at low heat flux each bubble created its own Taylor bubble. For this reason the Taylor bubble frequency was smaller at high heat flux, resulting in lower frequency of the large waves.

8.1.1.2. High mass flux annular flow

From the images capturing the dryout at high mass flux, (high heat flux), the small waves have higher amplitude because of the higher velocity difference between vapor and liquid. The large waves including trapped vapor bubbles are sliding along the heated tube wall.
At the location where the wall temperature starts to increase, the film breaks down, and the liquid tends to collect and flow as liquid streams on the heated wall, while the remaining areas are exposed to the vapor. As these liquid streams flow on the heated wall, they evaporate and finally small size liquid droplets are formed, before evaporating completely. The break-up of the film is believed to be a result of the high heat flux which causes local dryout of the film. Once a dry patch is formed, the surface tension forces tend to collect the liquid into streams and droplets. Drops from the liquid film and the liquid streams are also entrained into the vapor core where large size entrained liquid drops are observed.

8.2 Observation analysis of bubble behavior (Paper #6)

In this study, the same glass test section described previously was used. As before, the flow direction was vertical up-flow, the test fluid was R-134a, and the operating conditions as listed in table 8.2. All the results correspond to vapor qualities between 0 and 2 %.

Table 8.2: Operating conditions

Parameter	Operating range, case:				
	(1)	(2)	(3)	(4)	(5)
D_i [mm]	1.33				
G [kg/(m²s)]	202	202	91	90	29
q'' [kW/m²]	20	5	20	5	5
T_{sat} [°C]	24				
U_f [m/s]	0.167	0.167	0.075	0.074	0.024
Z_{TH} [mm]	235.5				

8.2.1 *Visualization results*

High speed digital images of saturated flow boiling were obtained and used to measure nucleation site density, bubble growth rate, departure diameter, lift-off diameter, and sliding or flowing velocity.
Saturated flow boiling and bubble characteristics were captured at the position of onset of nucleate boiling in the heated tube. Figure 8.4 shows images of the flow characteristics and bubble behavior at the first camera position P1 in figure 3.2. The original video recordings can be viewed at the web address:

http://www.energy.kth.se/index.asp?pnr=10&ID=288&lang=1.

The visible light and dark regions surrounding the flow channel change with the image capture rate. The ambient light and exposure time may also have some effect on the appearance of the channel and its surroundings.

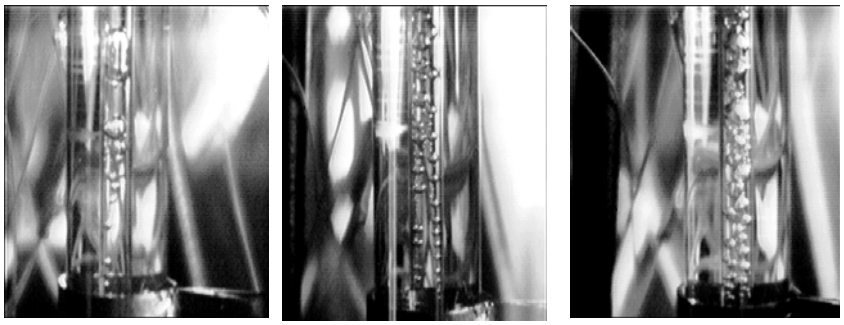

G = 29kg/m²s, and q″ = 5kW/m², P1 | G = 90kg/m²s, and q″ = 5kW/m², P1 | G = 91kg/m²s, and q″ = 20kW/m², P1

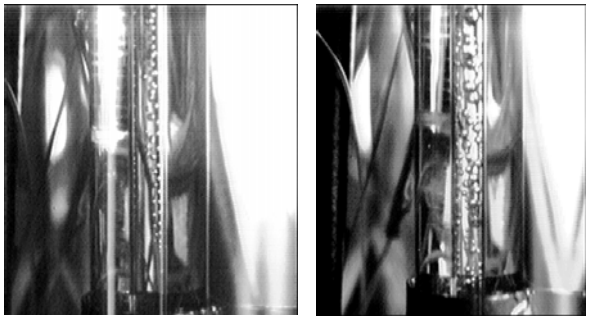

G = 202kg/m²s, and q″ = 5kW/m², P1 | G = 202kg/m²s, and q″ = 20kW/m², P1

Figure 8.4: Images illustrating bubble nucleation, departure, and growth. P1 and P2 refer to the camera positions in figure 3.2.

8.2.2 *Image analysis results*

The effect of the heat and mass flux on the number of activated nucleation sites, the bubble frequency, the bubble departure diameter, the bubble lift-off diameter, bubble growth rate and the bubble velocity for the saturated flow boiling of R-134a in the tube are shown in figures 8.5-8.9. The frequency of vapor bubble departure was defined for each active nucleation site by counting the number of successive departing bubbles during a given number of frames. The departure is taken to be the instant the bubble leaves the nucleation site, while the instant the bubble moves away from the heating surface is the lift-off.

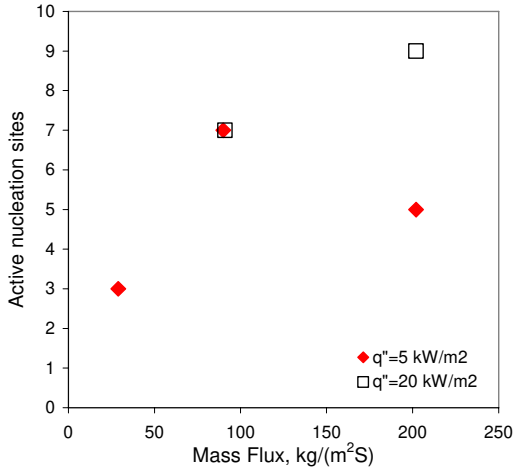

Figure 8.5: The number of active nucleation sites as a function of mass flux and heat flux.

Figure 8.5 shows the number of active nucleation sites in the view of the camera as a function of the mass flux for the two different heat fluxes. As shown, the results are not conclusive, most probably due to the small statistical base. As higher heat flux results in higher surface temperature and activation of a wider size range of nucleation sites, the number of active nucleation sites would be expected to increase with increasing heat flux. An increase in the mass flux, on the other hand could be expected to hamper the activation of nucleation sites.

Figure 8.6 shows the bubble frequency as a function of the mass flux for the two tested heat fluxes. Clearly, the bubble frequency increases with increasing mass flux. This could be understood as a result of the stronger force acting on the bubble at increased flow velocity, which forces the bubble to depart at a smaller size. For a given vapor production rate the bubble frequency thus has to increase with the mass flux. It was also noted that the bubble departure frequency is higher for

positions further up in the tube, i.e. toward the downstream end where the vapor fraction and the flow velocity are higher. The differences in bubble frequency between the different nucleation sites at given conditions are probably also caused by differences in the microstructure of the surface (pore size) at the nucleation site. From figure 8.6 there is also an indication that the frequency increases with increasing heat flux, which could be expected.

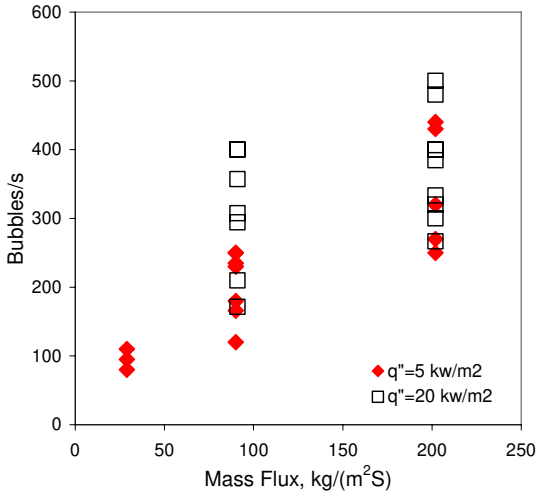

Figure 8.6: The bubble departure frequency of each nucleation site in figure 3

Figure 8.6 shows the bubble frequency as a function of the mass flux for the two tested heat fluxes. Clearly, the bubble frequency increases with increasing mass flux. This could be understood as a result of the stronger force acting on the bubble at increased flow velocity, which forces the bubble to depart at a smaller size. For a given vapor production rate the bubble frequency thus has to increase with the mass flux. It was also noted that the bubble departure frequency is higher for positions further up in the tube, i.e. toward the downstream end where the vapor fraction and the flow velocity are higher. The differences in bubble frequency between the different nucleation sites at given conditions are probably also caused by differences in the microstructure of the surface (pore size) at the nucleation site. From figure 8.6 there is also an indication that the frequency increases with increasing heat flux, which could be expected.

The variations of the bubble departure diameter with the mass flux and heat flux are shown in figure 8.7. It can be seen that the departure bubble diameter decreases with increasing mass flux, as a result of the increasing drag forces. Also, the departure diameter increases slightly with increasing heat flux.

It has been observed that the vapor bubble which departs from a nucleation site, first slides along the heating surface and continues to grow until it lifts off from the surface at some distance downstream of the nucleation site, at which time the velocity of the bubble will increase.

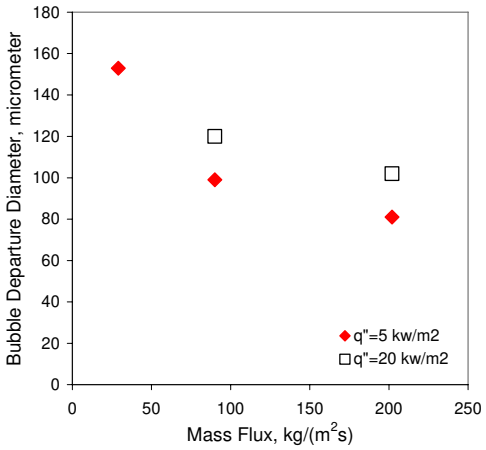

Figure 8.7: The bubble departure diameter as a function of mass flux, and heat flux.

Figure 8.8 shows the bubble growth rate for the five combinations of heat flux and mass flux tested. The sharp increase in size towards the right in the diagram is the result of the bubble coalescing with another bubble. The starting diameter at time zero is ≠0 because the first phase of the growth is extremely quick and difficult to follow in the video recordings.

As seen, the growth rate is highest at the two high heat flux conditions. At the low heat flux, the growth rate seems to decrease with increasing mass flux. As expected, the growth rate decreases with time.

At high heat flux, a large number of bubbles generated from the nucleation site tend to merge together to form a bigger bubble. As the bubbles get larger, they become distorted and elongated. As the heat flux is increased, the bubble departure density and the growth rate increases and bubbles are observed to coalesce a shorter time from departure. The bubble size at coalescence seems to be about the same for the two heat fluxes. At the lower heat flux, it decreases somewhat with increasing mass flux.

The larger size bubbles resulting from bubble growth or coalescence was seen to be rising faster than the tiny bubbles due to the relative difference in the drag force.

After the bubble lift-off, the bubble velocity increases as the bubble moves away from the tube wall into the core of the flow where the liquid velocity is higher. This is shown in figure 8.9. It would be expected that the velocity is mainly dependent on the mass flux in the tube. For the

high heat flux case this is clearly shown. For the low heat flux case, the dependence is not as clear as in the other studied cases.
The uncertainty in the measured distances (i.e. the bubble diameter measurement) is within 25 μm.

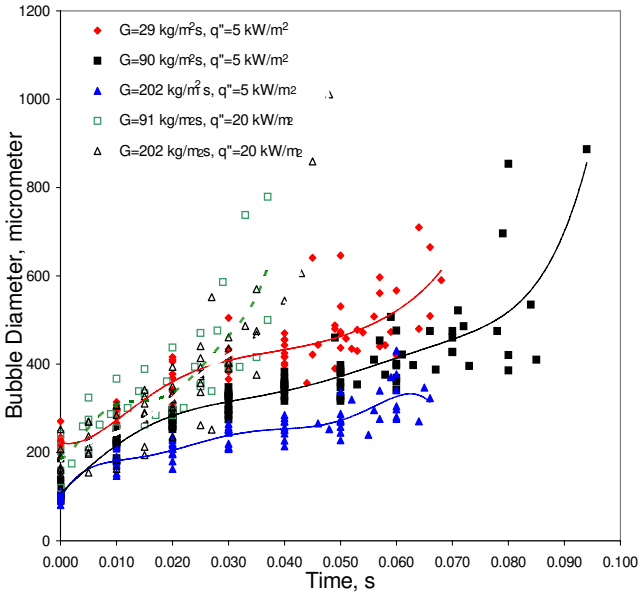

Figure 8.8: Bubble growth rate after detachment at different mass and heat fluxes

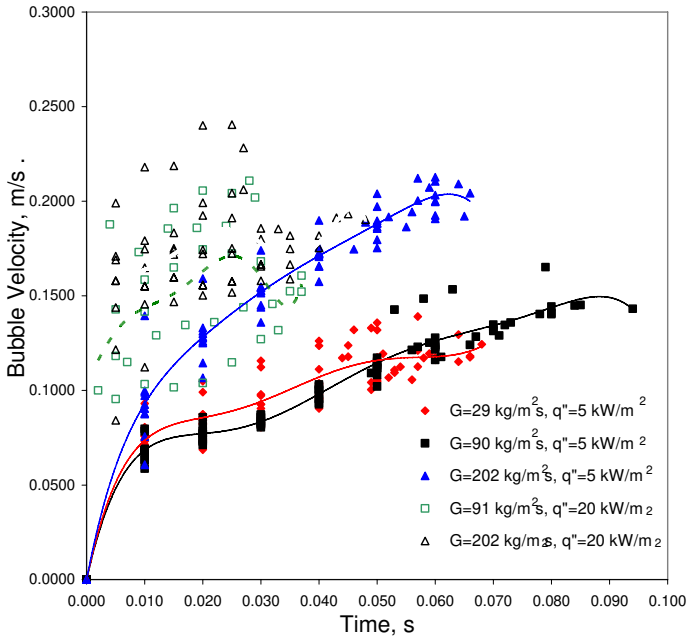

Figure 8.9: Bubble velocity after detachment at different mass and heat fluxes

8.3 Flow pattern map

The tests on a vertical quartz glass tube with inner diameter 1.33 mm which was coated by transparent resistive coating of indium tin oxide (ITO) are performed using high speed camera and close up lens. The bulk flow direction in the tube is vertical upward. The test tube was divided into 18 sections. For each section, sequences of 100 to 200 frames were captured at camera speed of 1000 frame per second. A movie from these frames was created to observe the behavior and characteristics of the boiling process and the two-phase flow pattern. Appendix A shows images of flow boiling of five tested points.
The nucleation sites on the wall generate micro bubbles, which at low heat flux, slide before their departure, forming bubbly flow. The bubbles gradually increase in size and subsequently develop into a slug. The bubble grow rate is depending on the heat flux applied. At higher mass flow rates the bubbles coalesce and form bigger bubbles, which further expand and develop into a slug. Appendix A shows the movement of the slug in the direction of bulk flow. This process of bubble growth, slug formation and slug movement are shown clearly at low heat and mass flux, Appendix A, e. With increasing the vapor quality churn flow and annular annular/wavy and wavy flow pattern can be identified.

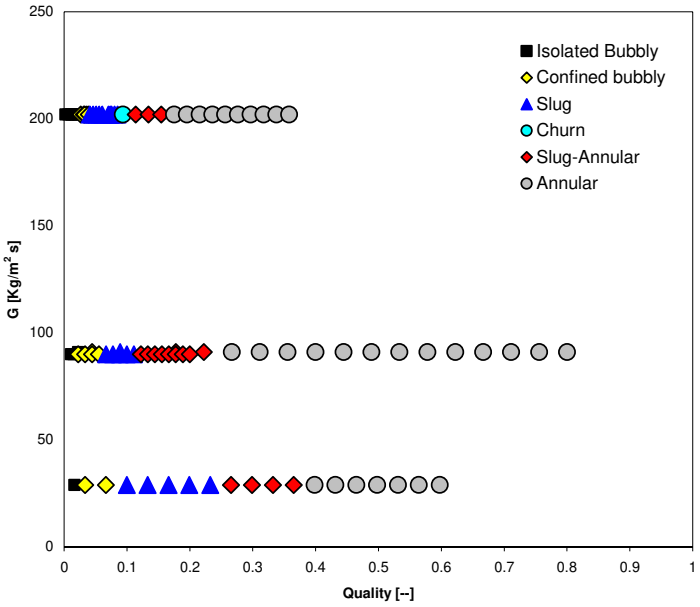

Figure 8.10: Flow pattern map

9 Summary and Conclusions

Micro/minichannel compact heat exchangers provide high performance within a small space, which is desirable for all types of transportable systems, cryogenic and integrated two-phase applications. These minichannels provide high heat transfer coefficients, high surface area/volume ratio and high heat transfer per unit volume.

In order to design and optimize heat exchangers based on mini/microchannels, design tools are needed. These tools should be able to correctly predict the heat transfer, pressure drop, and, for evaporators, flow pattern and critical heat flux inside these micro/minichannels.

This thesis will give some of these design tools in order to help the designer to understand the nature of the flow inside these compact mini/microchannels heat exchanges,

The following studies were conducted, and the following conclusions were drawn:

- An experimental investigation of heat transfer and pressure drop in forced convective single-phase flow of R-134a through single circular microchannels having inner diameters of 1.700, 1.224, and 0.826 mm and 220 mm heated length was conducted. The results were compared to suggested microscale and macroscale correlations from the literature. The comparison shows that the classical correlations were in good agreement with the experimental data. On the contrary, none of the microscale correlations were in agreement with the experimentally obtained data. It has thus been shown that the classical correlations for single phase heat transfer and pressure drop are applicable within the range of conditions of the tests.
- The boiling heat transfer characteristics have been experimentally studied. The saturated flow boiling heat transfer coefficient was found weakly dependent of vapor quality and mass flux, but strongly dependant on heat flux for $x < 0.6$. Also, an increase in the system pressure improves the heat transfer performance. This indicates that the contribution of forced convection heat transfer to the overall transfer rate is small, and that heat transfer is dominated by a mechanism similar to nucleate boiling. The flow boiling heat transfer coefficient was found to be higher for smaller diameter tubes.
- The experimental data was compared to predictions by correlations available in the literature. None of the compared correlations predicts the heat transfer coefficient for all three tested diameters. A new correlation anticipated the present measured data is presented. This correlation predicts the results within ±8%.

- The two-phase pressure drop has been measured in the three tubes at mass fluxes from 100 to 400 kg/(m^2 s) with saturated liquid at the inlet and outlet vapor fractions ranging from 15 to 85%. The frictional pressure drop was found to change with mass flux and outlet quality in a systematic way. The frictional pressure drop was the same for the three tested channels at the same mass flux and outlet vapor quality, which is surprising.
  The experimental data was compared to predictions by correlations available in the literature. None of the correlations tested could predict the trend of the pressure drop for all three tested diameters.
- A unique visualization technique has been used to study the effect of mass flow, heat flux and system pressure on the annular upward flow in the dryout region of a single circular vertical quartz tube with the diameter 1.332 mm. High-speed visualization technique was employed to study the two-phase flow behavior, the liquid film dryout and the resulting transition to mist flow.
  The dryout heat flux was found to increase with increasing mass flux and decreasing pressure. The results point to a difficulty in utilizing minichannel heat exchangers as evaporators as the heat transfer at vapor qualities above about 0.6 is fairly low due to the early dryout.
- Experimental high speed visualization has been performed to study the effect of the mass flux and heat flux on the bubble nucleation and departure in upward flow at the position of onset of nucleate boiling. It was found that as the mass flux increases, the bubble departure diameter decreases and the bubble frequency increases. The bubble frequency was somewhat higher at high heat flux. The bubble growth rate was found to be slightly higher at high heat flux. At high heat flux the bubbles tended to merge a shorter time after departure, but at a similar size as for the low heat flux case.
- The study provides visual information on bubble characteristics for flow boiling in narrow channels available on the web address http://www.energy.kth.se/index.asp?pnr=10&ID=288&lang=1.

Nomenclature

A	Heat transfer area, [m^2]
A_c	Cross sectional area, [m^2]
B	Coefficient in Chisholm correlation, [--]
bd	Bubble diameter, [m]
C	Fiction constant, [f/Re]
C	Constant in Chisholm correlation, [--]
C_a	Acoustic velocity, [m/s]
C_p	Specific heat of R-134a, [J/kg K]
CHF	Critical heat flux, [--]
DC	Direct current, [--]
D_h	Channel hydraulic diameter, [m]
D_i	Channel inner diameter, [m]
E	Enhancement factor, [--]
f	Friction factor, [--]
G	Mass flux, [kg/m^{2}s]
g	Acceleration due to gravity, [m/s^2]
h	Heat transfer coefficient, [W/m^{2}K]
i	Specific enthalpy, [J/kg]
I	Current through the test section, [A]
i_{lg}	Latent heat of evaporation, [J/kg]
k	Liquid thermal conductivity, [W/mK]
L	Test section length, [m]
M	Molecular weight, [g/mol]
MAD	Mean absolute deviation, [%]
$\dot{m}_{R-134a}$	R-134a mass flow rate, [kg/s]
P	Camera position, [--]
q''	Heat flux, [W/m^2]
r	Tube radius, [mm]
S	Suppression factor, [--]
T	Temperature, [^{o}C]
u	Velocity, [m/s]
U	Velocity, [m/s]
u_m	R134a liquid average velocity, [m/s]
V	Voltage supply to the test section, [volt]
x	Vapor fraction, quality, [--]
Z_o	Position where the boiling starts, [m]
Z_{TH}	Total heating length, [m]
ε	Absolute roughness height, [m]

ρ	Density, [kg/m^3]
μ	Dynamic viscosity, [kg /m s]
ν	Kinematics viscosity, [m^2/s]
σ	Surface tension, [N/m]
ϕ	Test section perimeter, [m]
α	Thermal diffusivity, in modified Peclet number, [m^2/s],
ϕ^2	Two-phase multiplier, [--]
α	Void fraction, [--]
Δi	Enthalpy difference, [kJ/kg K]
ΔP	Pressure drop, [mbar]
ΔT	Temperature difference, [K]

Parameters and definitions

b	Laplace constant, $\sqrt{\frac{\sigma}{g(\rho_l-\rho_g)}}$
Bo	Boiling number, $\frac{q''}{i_{lg}G}$
BO	Bond number, $\frac{g(\rho_l-\rho_g)D_i^{\,2}}{\sigma}$
Co	Convective number, $\left(\frac{1-x}{x}\right)^{0.8}\left(\frac{\rho_l}{\rho_g}\right)^{-0.5}$
Fr	Froude number, $\frac{G^2}{\rho^2 g D_i}$
Fr_l	Liquid Froude number, $\frac{G^2}{\rho_l^2 g D_i}$
Fr_{tp}	Two-phase Froude number, $\frac{G^2}{gD_i\rho_{tp}^2}$
$\left(\frac{dP}{dz}\right)_{f,l}$	Liquid-phase frictional pressure gradient, $\frac{f_l G^2}{2D_i\rho_l}(1-x)^2$
$\left(\frac{dP}{dz}\right)_{f,g}$	Gas-phase frictional pressure gradient, $\frac{f_g G^2}{2D_i\rho_g}x^2$
$\left(\frac{dP}{dz}\right)_{f,lo}$	Liquid-phase alone frictional pressure gradient, $\frac{f_{lo}G^2}{2D_i\rho_l}$
$\left(\frac{dP}{dz}\right)_{f,go}$	Gas-phase alone frictional pressure gradient, $\frac{f_{go}G^2}{2D_i\rho_g}$

f_l Liquid-phase friction factor, $\begin{cases} \frac{64}{\mathrm{Re}_l} & for \quad \mathrm{Re}_l < 2300 \\ 0.316\mathrm{Re}_l^{-0.25} & for \quad \mathrm{Re}_l > 2300 \end{cases}$

f_g Gas-phase friction factor, $\begin{cases} \frac{64}{\mathrm{Re}_g} & for \quad \mathrm{Re}_g < 2300 \\ 0.316\mathrm{Re}_g^{-0.25} & for \quad \mathrm{Re}_g > 2300 \end{cases}$

f_{lo} Liquid-phase alone friction factor, $\begin{cases} \frac{64}{\mathrm{Re}_{lo}} & for \quad \mathrm{Re}_{lo} < 2300 \\ 0.316\mathrm{Re}_{lo}^{-0.25} & for \quad \mathrm{Re}_{lo} > 2300 \end{cases}$

f_{go} Gas-phase alone friction factor, $\begin{cases} \frac{64}{\mathrm{Re}_{go}} & for \quad \mathrm{Re}_{go} < 2300 \\ 0.316\mathrm{Re}_{go}^{-0.25} & for \quad \mathrm{Re}_{go} > 2300 \end{cases}$

f_{tp} Two-phase friction factor, $\begin{cases} \frac{64}{\mathrm{Re}_{tp}} & for \quad \mathrm{Re}_{tp} < 2300 \\ 0.316\mathrm{Re}_{tp}^{-0.25} & for \quad \mathrm{Re}_{tp} > 2300 \end{cases}$

Gz Graetz number, $\frac{\mathrm{Re}\,\mathrm{Pr}\,D_i}{L}$

$h_{D\text{-}B,\,l}$ $0.023(\mathrm{Re}_l)^{0.8}(\mathrm{Pr}_l)^{0.4}\frac{k_l}{D_i}$

$h_{D\text{-}B,\,lo}$ $0.023(\mathrm{Re}_{lo})^{0.8}(\mathrm{Pr}_l)^{0.4}\frac{k_l}{D_i}$

K_f Pierre's boiling number, $\frac{\Delta i}{L_{tp}.g}$

K_k Relative thermal conductivity, $\frac{k_{wall}}{k_{fluid}}$, in Klimenko.

K_p Dimensionless parameter for Klimenko, $\frac{\mathrm{pb}}{\sigma}$

MAD $\frac{1}{n}\sum_{1}^{n}\frac{\left|V_{Exp}-V_{pred}\right|}{V_{Exp}}\times 100$

N_{CB} Convective boiling number, in Klimenko.
$\left(\frac{1}{Bo}\right)\left(1+x\left(\frac{\rho_l}{\rho_g}-1\right)\right)\left(\frac{\rho_l}{\rho_g}\right)^{-1/3}$

N_{conf} Confinement number, $\frac{\left[\frac{\sigma}{g(\rho_l - \rho_g)}\right]^{0.5}}{D_i}$

Nu Nusselt number, $\frac{hD_i}{k}$

Pe_m Modified Peclet number, $\frac{q''b}{i_{lg}\rho_g\alpha_l}$ in Klimenko's correlation.

Pr Prandtl number, $\frac{\mu\ C_p}{k}$

P_R Reduced pressure, $\frac{p}{p_{crtical}}$

Re Reynolds number, $\frac{GD_i}{\mu}$

Re_{tp} Two-phase Reynolds number, $\frac{GD_i}{\mu_{tp}}$

Re_g Gas-phase Reynolds number, $\frac{GxD_i}{\mu_g}$

Re_{go} Two-phase gas only Reynolds number, $\frac{GD_i}{\mu_g}$

Re_l Liquid-phase Reynolds number, $\frac{G(1-x\ )D_i}{\mu_l}$

Re_{lo} Two-phase liquid only Reynolds number, $\frac{GD_i}{\mu_l}$

Re_m Reynolds number of the mixture, $\frac{w_m\rho_l b}{\mu_l}$ in Klimenko's correlation.

We Weber number, $\frac{G^2 D_i}{\rho\sigma}$

We_l Liquid Weber number, $\frac{G^2 D_i}{\rho_l\sigma}$

We_{tp} Two-phase Weber number, $\frac{G^2 D_i}{\rho_{TP}\sigma}$

w_m Mixture velocity, $\frac{G}{\rho_l\left(1+x\left(\rho_l/\rho_g-1\right)\right)}$

X_{tt}	Lokhart-Martinelli Parameter (turbulent-turbulent), $\left(\frac{\rho_l}{\rho_g}\right)^{-0.5}\left(\frac{\mu_l}{\mu_g}\right)^{0.1}\left(\frac{1-x}{x}\right)^{0.9}$
ρ_{tp}	Two-phase homogenous density, $\left[\frac{x}{\rho_g}+\frac{1-x}{\rho_l}\right]^{-1}$
μ_{tp}	Two-phase McAdams et al. (1942): $\left[\frac{x}{\mu_g}+\frac{1-x}{\mu_l}\right]^{-1}$

Subscripts

acc	Acceleration
conv	Convection boiling
D-B	Dittus-Boelter
e	Exit
Exp.	Experimental
g	Gas (vapor phase)
grv	Gravitation
hs	Heated section
Hom	Homogenous
ic	Abrupt contraction
in	Inlet
l	Liquid phase
lg	Liquid-gas
lo	Liquid phase alone
local	Local
mod	Modified
nuc	Nucleate boiling
oe	Abrupt expansion
pool	Pool boiling
pred	Predicted
sat	Saturated
sp	Single-phase
sub	Subcooled
tp	Two-phase
w	Wall

References

- Adams T.M., Dowling M.F., Abdel-Khalik S.I., Jeter S.M., *1999*, Applicability of traditional turbulent single-phase forced convection correlations to non-circular microchannels, *Int. J. Heat and Mass Transfer,* Vol. 42, pp. 4411-4415.
- Adams T.M., Abdel-Khalik S.I., Jeter S.M. and Qureshi Z.H., *1997*, An experimental investigation of single-phase forced convection in microchannels, *Int. J. Heat and Mass Transfer,* Vol. 41, No. 6-7, pp. 851-857.
- Bang C., Chang S. H., and Baek W. P., *2004*, Visualization of the subcooled flow boiling of R-134a in a vertical rectangular channel with an electrically heated wall, *Int. J. Heat Mass Transfer,* Vol. 4, pp. 4349-4363.
- Bankoff S.G., *1958*, Entrapment of gas in the spreading of a liquid over a rough surface, *AIChE J.*, Vol. 4, pp. 24–26.
- Bao Z.Y., Fletcher D.F., Haynes B.S., *2000*, Flow boiling heat transfer of R11 and HCFC123 in narrow passages, *Int. J. Heat Mass Transfer.* Vol. 43, pp. 3347-3358.
- Beattie D.R.H., Whalley P.B., *1981*, A simple two-phase frictional pressure drop calculation method, *Int. J. Multiphase flow*, Vol. 8, pp. 83-87.
- Berenson P.J., and Stone R.A., *1965*, A Photographic Study of the Mechanism of Forced Convection Vaporization, *Chemical Engineering Progress, Symposium Series*, Vol. 61, no. 57, pp. 213-219.
- Bergles A.E., *1963*, Subcooled burnout in tubes of small diameter, *ASME*, paper No. 63-WA-182.
- Blasius H., *1913,* Das Ähnlichkeitsgesetz bei Reibungsvorgängen in Flüssigkeiten, *Forchg. Arb. Ing.-Wes.*, No. 131, Berlin.
- Butterworth D., A comparison of some void fraction relationship for co-current gas liquid flow, *Int. J. Multiphase Flow,* Vol. 1, pp. 845-850, 1975.
- Carey V.P., *1987*. Liquid-vapor phase-change phenomena. An introduction to the Thermophysics of vaporization and condensation processes in heat transfer. *Hemisphere Publishing Corporation.*
- Celata G.P., Cumo M., Katto Y., Mariani A., *1999*, Prediction of the critical heat flux in water subcooled flow boiling using a new mechanistic approach, *Int. J. Heat Mass Transfer,* Vol. 42, pp. 1457–1466.
- Celata G.P., Cumo M., Mariani A., Simoncini M., Zummo G., *1994*, Rationalization of existing mechanistic models for the prediction of water subcooled flow boiling critical heat flux, Int. J. Heat Mass Transfer, Vol. 37, pp. 347–360.

- Celata G.P., Cumo M., Gugleilmi M., and Zummo G., October *2000*, Experimental investigation of hydraulic and single phase heat transfer in 0,130 mm capillary tube, *International Conference on Heat transfer and Transport Phenomena in Microscale, Banff, Canada*, pp. 108-113.
- Chaddock J.B., and Brunemann H., Forced convection of refrigerants in horizontal tubes, school of engineering, Duke University, HL-113 *1967*.
- Chang S.H., Bang C., and Baek W.P., *2002*, A photographic study on the near-wall bubble behavior in subcooled flow boiling, *Int. J. Thermal Sciences,* Vol. 41, No. 7, pp. 609-618.
- Chang Y.P., *1963*, Some possible critical conditions in nucleate boiling, *ASME J. Heat Transfer,* Vol. 85, pp. 89-100.
- Chen I.Y, Yang K.S., Chang Y.J., Wang C.C., *2001*, Two-phase pressure drop of air-water and R-410A in small horizontal tubes, *Int. J. of Multiphase Flow*, Vol. 27, pp. 1293-1299.
- Chen I.Y., Yang K.S., Wang C.C., *2002*, An empirical correlation for two-phase frictional performance in small diameter tubes. *Int. J. of Heat and Mass Transfer*, Vol. 45, pp. 3667-3671.
- Chen J.C., *1966*, Correlation for boiling heat transfer to saturated fluids in convective flow, *I&EC Process Design Develop,* Vol. 5, pp. 322-329.
- Chisholm D.A., *1967*, Theoretical basis for the Lockhart-Martinelli correlation for the two-phase flow, *Int. J. of Heat and Mass transfer,* Vol. 10, pp. 1767-1778.
- Chisholm D., *1973*, Pressure gradients due to frication during the flow evaporating two-phase mixtures in smooth tubes and channels, *Int. J. of Heat and Mass Transfer*, Vol. 16, pp. 347-358.
- Choi S.B., Barron R.F. and Warrington R.O., *1991*, Fluid flow and heat transfer in microtubes, *In Micromechanical Sensors, Actuators and Systems, ASME DSC-Vol. 32 (edited by D. Choi et al.)* pp. 123-128.
- Cicchitti A., Lombardi C., silvestri M., soldaini G., Zavalluilli R., *1960*, Two-phase cooling experiments pressure drop, heat transfer and burnout measurements, *Energia Nucleare,* Vol. 7, pp. 407-425.
- Cole R., and Rohsenow W. M., *1969*, Correlation of bubble departure diameters for boiling of saturated liquids, *Chem. Engng Prog. Symp.* Ser. 65, pp. 211-213.
- Cole R., and Shulman H.L., *1974*, Bubble growth rates at high Jakob numbers. *Int. J. Heat Mass Transfer*, Vol. 9, pp. 1377–1390, 1966.
- Cole R., Boiling nucleation, *in Advances in heat transfer. NewYork: Academic*, Vol. 10, pp. 103–110.
- Cole R., *1967*, Bubble frequencies and departure volumes at subatmospheric pressures, *AIChE J.*, Vol. 13, pp. 779-783.
- Colebrook F., *1939*, Turbulent flow in pipes with particular reference to the transition region between the smooth and rough pipe laws, *J. Inst. Civ. Eng.,* Vol. 11, pp. 133-156.

- Coleman J.W. and Garimella S., *1999*, Characterization of two-phase flow patterns in small diameter round and rectangular tubes. *Int. J. Heat Mass Transfer,* Vol. 42, pp. 2869-2881.
- Coleman J.W. and Garimella S., *2000*, Two-phase flow regimes transtions in microchannel tubes: the effect of hydraulic diameter. *Proceeding of the ASME Heat Transfer Division,* Vol. 4, pp. 71-83.
- Collier J.G., Thome J.R., *1994*. Convective boiling and condensation, 3rd Edition. *Oxford University Press*.
- Cooper M.G., and Stone, C. R., *1981*, Boiling of binary mixtures-study of individual bubbles, *Int. J. Heat Mass Transfer*, Vol. 24, pp. 1937-1950.
- Cooper M.G., *1969*, The microlayer and bubble growth in nucleate pool boiling, *Int. J. Heat Mass Transfer*, Vol. 12, pp. 915-933.
- Cooper M.G., Saturated nucleate pool boiling- a simple correlation, *1st UK National Heat Transfer Conference, IchemE Symposium Series 86*, No. 2 , *1984*, pp. 785-793.
- Cornwell K. and Kew P.A., Evaporation in microchannel heat exchangers, *Proceedings of 4th UK National Conference on Heat Transfer, Manchester, UK, 1995.*
- Darby R., *1964*, The dynamics of vapor bubbles in nucleate boiling, *Chemical Engineering Science,* Vol. 19, pp. 39-49.
- Dhir V.K., *1991*, Nucleate and transition boiling heat transfer under pool and external flow conditions *Int. J. Heat and fluid flow,* Vol. 12, pp. 290-314.
- Dukler A. E., Wicks M. III, Cleveland R.G., *1964*, Frictional pressure drop in two-phase flow: (a) A comparison of existing correlation for pressure loss and holdup, (b) An approach through similarity analysis, *AIChE J*., Vol. 10, pp. 38-51.
- Dittus F. W., and Boelter L.M.K., *1930*, Heat transfer in automobile radiators of tubular type, *University of California, Berkeley, Publications on Engineering,* Vol. 2, No.13, pp. 443-461.
- Forster H.K., and Zuber N., *1954*, Growth of a vapor bubbles in superheated liquid, *Appl. Phys.*, Vol. 25, pp. 474–478.
- Fournelle G., Bhavnani S.H., and Jaeger R.C., *1999*, Optical study of enhanced heat transfer from a heat sink for microelectronics applications, *in Proc. Pacific Rim/ASME Int. Intersoc. Electron. Packag. Conf*., Lahaina, HI.
- Friedel L., *1979*, Improved friction pressure drop correlations for horizontal and vertical two-phase pipe flow, *presented at the European two-phase group meeting, Ispra, Italy,* paper E2.
- Frost W., and Kippenhan C.J., *1967*, Bubble growth and heat-transfer mechanisms in the forced convection boiling of water containing a surface active agent, *Int. J. Heat Mass Transfer,* Vol. 10, pp. 931-949.

- Galloway J.E., Mudawar I., *1993a*, CHF mechanism in flow boiling from a short heated wall—I. Examination of near wall conditions with the aid of photomicrography and high-speed video imaging, *Int. J. Heat Mass Transfer,* Vol. 36, pp. 2511–2526.
- Galloway J.E., Mudawar I., *1993b*, CHF mechanism in flow boiling from a short heated wall—II. Theoretical CHF model, *Int. J. Heat Mass Transfer,* Vol. 36, pp. 2527–2540.
- Gersey C.O., Mudawar I., *1995a*, Effects of heater length and orientation on the trigger mechanism for near-saturated flow boiling critical heat flux—I. Photographic study and statistical characterization of the near-wall interfacial features, *Int. J. Heat Mass Transfer* Vol. 38 ,pp. 629–641.
- Gersey C.O., Mudawar I., *1995b*, Effects of heater length and orientation on the trigger mechanism for near-saturated flow boiling critical heat flux—II. Critical heat flux model, *Int. J. Heat Mass Transfer,* Vol. 38, pp. 643–654.
- Gungor K. E. and R. Winterton H. S., *1986*, A general correlation for flow boiling in tubes and annuli, *Int. J. of Heat and Mass Transfer,* Vol. 29, No. 3, pp. 351-358.
- Gunther F.C., *1951*, Photographic Study of Surface-Boiling Heat Transfer to Water With Forced Convection, *Transactions of ASME, Series C, Journal of Heat Transfer*, Vol. 73, pp. 115-123.
- Hall D.D., Mudawar I., *2000*, Critical heat flux (CHF) for water flow in tubes II. Subcooled CHF correlation, *International Journal of Heat and Mass Transfer,* Vol. 43, pp. 2605-2640.
- Han C.H., and Griffith P., *1965*, The mechanism of heat transfer in nucleate pool boiling- Part I Bubble initiation, growth and departure, *Int. J. Heat Mass Transfer*, Vol. 8, pp. 887–904.
- Haramura Y., Katto Y., *1983*, New hydrodynamic model of critical heat flux applicable widely to both pool and forced convective boiling on submerged bodies in saturated liquids, *International Journal of Heat and Mass Transfer*, Vol. 26, pp. 379-399.
- Helden W., Geld C., and Boot P., *1995*, Forces on bubbles growing and detaching in flow along a vertical wall. *Int. J. Heat Mass Transfer*, vol. 38 (11), pp. 2075–2088.
- Hewitt G.F., Critical Heat Flux in flow boiling, *proc. 6th Int. Heat Transfer conf.*, *1978*, 143.
- Hewitt G.F., Hal Taylor N.S., Annular two-phase flow, *Pergamon Press, Oxford,1970*.
- Hrnjak P., Tu X., *2007*, Single phase pressure drop in microchannels, *Int. J. Heat and Fluid Flow,* Vol. 28, pp. 2-14.
- Hsu Y.Y., and Graham, R. W., *1963*, A visual study of two-phase flow in a vertical tube with heat addition, *NASA Technical Note* D-1564.

- Hsu Y.Y., *1962*, On the size range of active nucleation cavities on a heating surface *ASME J. Heat Transfer,* Vol. 84, pp. 207-216.
- Jiji L.M., and Clark J.A., *1964*, Bubble Boundary Layer and Temperature Profiles for Forced Convection Boiling in Channel Flow, *Journal of Heat Transfer*, Vol. 86, pp. 50-58.
- Jung D.S. and Radermacher R., *1989*, Prediction of pressure drop during horizontal annular flow boiling of pure and mixed refrigerants, *Int. J. of Heat and Mass Transfer*, Vol. 32, No. 12, pp. 2435-2446.
- Jung D., Radermacher R., *1993*, Prediction of evaporation heat transfer coefficient and pressure drop of refrigerant mixtures, *Int. J. of Refrigeration,* Vol. 16, No. 5, pp. 330-338.
- Kandlikar S.G., *1990*, A general correlation for saturated two-phase flow boiling heat transfer inside horizontal and vertical tubes, *ASME J. Heat Transfer*, Vol. 112, pp. 219-228.
- Kandlikar S.G., *1992*, bubble behavior and departure bubble diameter of bubbles generated over nucleating cavities in flow boiling. Pool and External Flow Boiling, *Proceedings of the Engineering Foundation Conference, Santa Barbara, CA, March 22-27*, pp. 447–451.
- Kandlikar S.G., Cartwright M.D., and Mizo V.R., *1996a*, A photographic study on nucleation characteristics of cavities in flow boiling. *In: Chen JC, editor. Convective flow boiling conf. Washington D.C.: Taylor and Francis*, pp. 73–78.
- Kandlikar S.G., Mizo V.R., and Cartwright M.D., *1996b* Investigation of bubble departure mechanism in subcooled flow boiling of water using high speed photography, *In: Chen JC editor. Convective flow boiling conf. Washington D.C.: Taylor and Francis*, pp. 161–166.
- Kandlikar S.G., Stumm B.J., *1995*, A Control Volume Approach for Investigating Forces on a Departing Bubble Under Subcooled Flow Boiling, *J. Heat Transfer*, Vol. 117, pp. 990-997.
- Katan N., Thome J.R. and Favrat D., *1998*, Flow boiling in horizontal tubes: Part I – development of a diabatic two-phase flow pattern map. *J. Heat Transfer,* Vol. 120, pp. 140-147.
- Katto Y., *1990a*, A physical approach to critical heat flux of subcooled flow boiling in round tubes, *Int. J. Heat Mass Transfer*, Vol. 33, pp. 611–620.
- Katto Y., *1992*, A prediction model of subcooled water flow boiling CHF for pressure in the range 0.1–20 Mpa, *Int. J. Heat Mass Transfer* , Vol. 35, pp. 1115–1123.
- Katto Y., *1990b*, Prediction of critical heat flux of subcooled flow boiling in round tubes, *Int. J. Heat Mass Transfer*, Vol. 33, pp. 1921–1928.
- Katto Y., Yokoya S., *1968*, Principal mechanism of boiling crisis in pool boiling, *International Journal of Heat and Mass Transfer,* Vol. 11, pp. 993-1002.

- Kennedy J.E., Roach Jr G.M., Dowling M. F., Abdel-Khalik S. I., Ghiaasiaan S. M., Jeter S.M., Quershi Z.H., *2000*, The onset of flow instability in uniformly heated horizontal microchannels, *Transaction of ASME, Journal of Heat Transfer,* Vol. 122, pp. 118-125.
- Kenning D.B. R. and Cooper M.G., *1989*, Saturated flow boiling of water in vertical tubes, *Int. J. of Heat and Mass Transfer*, Vol. 32, No.3, pp. 445-458.
- Kew P.A. and Cornwell K., *1997*, Correlations for the prediction of boiling heat transfer in small-diameter channels, *Applied Thermal Engineering*. Vol. 17, pp. 705-715.
- Kew P.A. and Cornwell K., *1994*, Confined bubble flow and boiling in narrow spaces, *Proc. Of 10th International Heat Transfer Conference, UK*, pp. 473-478.
- Kew P.A. and Cornwell K., *1997*, Correlations for the prediction of boiling heat transfer in small-diameter channels, *Applied Thermal Engineering* , Vol. 17, pp. 705-715.
- Khodabandeh R., *2005*, Heat transfer in evaporator of an advanced two-phase thermosyphon loop, *Int. J. of Refrigeration*, Vol. 28, pp. 190-202.
- Klausner J.F., Mei R., Bernhard D.M., and Zeng L.Z., *1993*, Vapor bubble departure in forced convection boiling, *Int. J. Heat Mass Transfer*, Vol. 36, pp. 651–662.
- Klimenko V.V., *1988*, A generalized correlation for two-phase forced flow heat transfer, *Int. J. of Heat and Mass Transfer* , Vol. 31, No. 3, pp. 541-552.
- Klimenko V.V., *1990*, A generalized correlation for two-phase forced flow heat transfer-second assessment, *Int. J. of Heat and Mass Transfer,* Vol. 33, No. 10, pp. 2073-2088.
- Koumoutsos N., Moissis R., and Spyridonos A., *1968*, A Study of Bubble Departure in Forced-Convection Boiling, *ASME J. Heat Transfer*, Vol. 90, pp. 223-230.
- Kutateladze S.S., Leont'ev A.I., *1966*, Some applications of the asymptotic theory of the turbulent boundary layer, in: *Proceedings of the Third International Heat Transfer Conference, New York, AIChE J.* Vol. 3, pp. 1–6.
- Kutateladze S.S., *1984*, On the transition to film boiling under natural convection, *Kotloturbostroenie*, Vol. 3, pp. 10-12.
- Lazarek G.M., Black S.H., *1982*, Evaporative heat transfer, pressure drop and critical heat flux in a small vertical tube with R-113, *Int. J. Heat Mass Transfer* , Vol. 25, No. 7, pp. 945-960.
- Lee C.H., Mudawar I., *1989*, A mechanistic critical heat flux model for subcooled flow boiling based on local bulk flow conditions, *Int. J. Multiphase Flow*, Vol. 14, pp. 711– 728.

- Lee H.J., Lee S.Y., *2001*, Pressure drop correlations for the two-phase flow within horizontal rectangular channels with small heights, *Int. J. of Multiphase Flow,* Vol. 27, pp. 783-796.
- Lee H.J., Lee S.Y., *2001*, Heat transfer correlation for boiling flows in small rectangular horizontal channels with low aspect ratios. *Int. J. of Multiphase Flow,* Vol. 27, pp. 2043-2062.
- Lee P.C., Tseng F.G. and Pan C., *2004*, Bubble dynamics in microchannels. Part I: single microchannel, *Int. J. Heat Mass Transfer*, Vol. 47, pp. 5575–5589.
- Levy S., *1967*, Forced convection subcooled boiling – Prediction of vapor volumetric fraction, *Int. J. Heat Mass Transfer*, Vol. 10, pp. 951-965.
- Li H.Y., Tseng F.G., and Pan C., *2004*, Bubble dynamics in microchannels Part II: two parallel microchannels, *Int. J. Heat Mass Transfer*, Vol. 47, pp. 5591–5601.
- Lie Y.M., and Lin T.F., *2005*, Saturated flow boiling heat transfer and associated bubble characteristics of R-134a in narrow annular duct, *Int. J. Heat Mass Transfer*, Vol. 48, pp. 5602-5615.
- Lin S., Kew P.A., Cornwell K., *2001*. Two-phase heat transfer to a refrigerant in a 1mm diameter tube, *Int. J. of Refrigeration*, Vol. 24, pp. 51-56.
- Liu Z. and Winterton R.H. S., *1991*, A general correlation for saturated and subcooled flow boiling in tubes and annuli, based on a nucleate pool boiling equation, *Int. J. of Heat and Mass Transfer* Vol. 34, No. 11, pp. 2759-2766.
- Lockhart R.W., Martinelli R.C., *1949*. Proposed correlation of data for isothermal two-phase, two-component flow in pipes, *Chemical engineering in process,* Vol. 45*, No.*1, pp. 39-48.
- Mala G.M., Li D., *1999*, Flow characteristics of water in microtubes, *Int. J. Heat and Fluid Flow,* Vol. 20, pp. 142-148.
- McAdams W.H., Woods W.K., Heroman L.C., *1942*, Vaporization inside horizontal tubes-II-Benzene-oil mixtures, *ASME Transaction*, Vol. 64, pp. 193-200.
- Mikic B.B., Rohsenow W.M., and Grifth P., *1970*, On bubble growth rates, *Inl. J. Heat Mass Transfer,* Vol. 13, pp. 657-666.
- Misale M., Bergles A.E., *1997*, The influence of the channel width on natural convection and boiling heat transfer from simulated microelectronic components, *Experimental Thermal and Fluid Science*, Vol. 14, pp. 187-193.
- Mishima K., Hibiki K., *1996*, Some characteristics of air-water two-phase flow in small diameter vertical tubes, *International Journal of Multiphase flow*, Vol. 22, No. 4, pp. 703-712.
- Moffat R.J., *1988*, Describing the uncertainties in experimental results, *Experimental thermal and fluid science,* Vol. 1, p. 3-17.

- Müller-Steinhagen H. and Heck K., *1986*, A simple friction pressure drop correlation for twp-phase flow in pipes, Chem. Eng. Process, Vol. 20, pp. 297-308.
- Owhaib W. and Palm B., *2002*, Experimental investigation of convective single-phase heat transfer and pressure drop in circular microchannels, *Zero Leakage minimum charge conference, August 26-28, Stockholm, Sweden.*
- Owhaib W., Martín-Callizo C., and Palm B., *2004*, Evaporative heat transfer in vertical circular microchannels, *Applied Thermal Engineering*, Vol. 24, pp. 1241-1253.
- Owhaib W., Martín-Callizo C., and Palm B., *2006*, Flow boiling visualization in a vertical circular minichannel at high vapor quality, *Experimental Thermal and Fluid Science*, Vol. 30, pp. 755-763.
- Qu W. and Mudawar I., *2003*, Measurement and prediction of pressure drop in two-phase micro-channel heat sinks, Int. J. of Heat and Mass Transfer, Vol. 46, pp. 2737-2753.
- Qu W. and Mudawar I., *2003*, Flow boiling heat transfer in two-phase micro-channel heat sinks-I, Experimental investigation and assessment of correlation method, Int. J. of Heat and Mass Transfer, Vol. 46, pp. 2755-2771.
- Palm B., *1991*, Enhancement of boiling heat transfer by aid of performed metal foils, *Doctoral Thesis*, Department of Applied thermodynamics and Refrigeration, Royal institute of Technology, Stockholm.
- Palm Björn, Heat Transfer in Microchannels, *International Conference on Heat transfer and Transport Phenomena in Microscale, Banff, Canada,* October 15–20, *2000*, pp. 54-64.
- Petukhov B., Kurgano V., And Gladuntsov A., *1973*, Heat transfer in turbulent pipe flow of gases with variable properties, *Heat Transfer Soviet Research,* Vol. 5, pp. 109-116.
- Pierre B., *1957*, Värmeövergång vid kokande köldmedier I horisontella rör, *kylteknisk tidskrift* , Vol. 16, No 3, pp. 129-137,.
- Pierre B., *1969*, Värmeövergång vid kokande köldmedier I horisontella rör, *kylteknisk tidskritf* , Vol. 28, No 5, pp. 3-12,.
- Plesset M. S., and Zwick S. A., *1954*, The growth of vapor bubbles in superheated fluids, *J. Appl. Phys.,* Vol. 25, pp. 474–478.
- Qu W., Mudawar I., *2004*, Measurement and correlation of critical heat flux in two-phase micro-channel heat sinks, *International Journal of Heat and Mass Transfer,* Vol. 47, pp. 2045-2059.
- Khodabandeh R., Heat Transfer in the evaporator of an advanced two-phase thermosyphon loop, *5th Int. conference on Boiling Heat Transfer*, *May 4-8, 2003, Montego Bay Jamaica.*
- Shah M.M., *1980*, A general correlation for critical heat flux in annuli, Inter. *Journal of Heat and Mass Transfer*, Vol. 23, pp. 225-234.

- Shah M.M., *1982*, Chart correlation for saturated boiling heat transfer: equations and further study, *ASHRAE Trans,* Vol. 88, pp. 185-196.
- Shah M.M., *1979*, A generalized graphical method for predicting CHF in uniformly heated vertical tubes, *Inter. Journal of Heat and Mass Transfer*, Vol. 22, pp. 557-568.
- Shah M.M., *1987*, Improved general correlation for critical heat flux during upflow in uniformly heated vertical tubes, *Heat and Fluid Flow*, Vol. 8, No.4, pp. 326-335.
- Shah M.M., *1976*, A new correlation for heat transfer during boiling flow through pipes, *ASHRAE, Trans* Vol. 82, No. 2, pp. 66-86.
- Sheng C.H., and Palm B., The visualization of boiling in small diameter tubes, in: *Proceedings of the International Conference on Heat Transfer and Transport Phenomena in Microscale, Banff, Canada*, October 15–20, *2000*, pp. 204– 208.
- Sieder E.N., and Tate G.E., *1936*, Heat transfer and pressure drop of liquids in tubes, *Ind. Eng. Chem.*, Vol. 28, pp. 1429-1435.
- Situ R., Hibiki T., Ishii M., and Mori M., *2005*, Bubble lift-off size in forced convective subcooled boiling flow, *Int. J. Heat Mass Transfer*, Vol. 48 (25-26), pp. 5536-5548.
- Situ R., Mi Y., Ishii M., and Mori M., *2004*, Photographic study of bubble behaviors in forced convection subcooled boiling, *Int. J. Heat Mass Transfer*, Vol. 47, pp. 3659-3667.
- Steinke M.E., Kandlikar S., *2006*, Single-phase liquid friction factors in microchannels, *Int. J. of Thermal Sciences*, Vol. 45, pp. 1073-1083.
- Sturgis J.C., Mudawar I., *1999a*, Critical heat flux in a long, rectangular channel subjected to one-sided heating—I. Flow visualization, *Int. J. Heat Mass Transfer* Vol. 42, pp. 1835–1847.
- Sturgis J.C., Mudawar I., *1999b*, Critical heat flux in a long, rectangular channel subjected to one-sided heating—II. Analysis of critical heat flux data, *Int. J. Heat Mass Transfer* Vol. 42, pp. 1849–1862.
- Thorncroft G.E., Klausner J.F., and Mei R., *1998*, An experimental investigation of bubble growth and detachment in vertical up-flow and down-flow boiling, *Int. J. Heat Mass Transfer*, Vol. 41, pp. 3857–3871.
- Tolubinsky V.I., and Ostrovsky J.N., *1966*, On the mechanism of boiling heat transfer (vapor bubbles growth rate in the process of boiling of liquids, solutions, and binary mixtures), *Int. J. Heat Mass Transfer* , Vol. 9, pp. 1463-1470.
- Tong L.S., and Hewitt G.F., *1972*, Overall view point of film boiling CHF mechanisms, *ASME* Paper No. 72-HT-54.
- Tran T.N., Wambsganss M.W., Chyu M.C. and France D.M., *1997*, A correlation for nucleate flow boiling in small channels, *In: Shah, R.K. (Ed), Compact Heat Exchanger for the Process Industries. Begell House, New York*, pp. 353-363.

- Tran T., Wambsganss M., and France D., *1996*. Small circular and rectangular channel boiling with two refrigerants, *Int. J. of Multiphase Flow,* Vol. 22, pp. 485-498.
- Tran T.N., Chyu M.C., Wambsganss M.W., France D.M., *2000*, Two-phase pressure drop of refrigerants during flow boiling in small channels: an experimental investigation and correlation development, *Int. J. of Multiphase Flow,* Vol. 26, pp. 1739-1754.
- Triplett K.A., Ghiaasiaan S.M., Abdel-Khalik S.I. and Sadowski D.L., *1999*, Gas-liquid two-phase flow in microchannels, Part I – two-phase flow patterns, *Int. J. Multiphase Flow*, Vol. 23, pp. 377-394.
- Tuckerman D.B. and Pease R.F.W., *1981*, High-performance heat sinking for VLSI*, IEEE Electron. Device Letters, Vol. EDL-2* pp. 126-129.
- Gnielinski V., *1976*, New equations for heat transfer in turbulent pipe and channel flow, *International Chemical Engineering,* Vol. 16, pp. 359-368.
- Wambsganss M.W., France D.M., Jendrzejczyk J.A., and Tran T.N., *1993*, Boiling heat transfer in a horizontal small-diameter tube, *Journal of heat transfer,* Vol. 115, pp. 963-972.
- Wang C.C., Chiang C.S., Lu D.C., *1997*. Visual observation of two-phase flow pattern of R-22, R-134a, and R-407C in a 6.5-mm smooth tube, *Experimental Thermal and Fluid Sciences*, Vol. 15, pp. 395-405.
- Warrier G.R., Pan T., and Dhir V., Heat transfer and pressure drop in arrow rectangular channels, *Proceedings of 4th international conference on multiphase flow, New Orleans*, May-June *2001*, ASME.
- Warrier G.R., Dhir Vijay K. and Momoda Leslie A., *2002*, Heat transfer and pressure drop in narrow rectangular channels, *Experimental Thermal and Fluid Science,* Vol. 26, No. 1, pp. 53-64.
- Warrier, G. R., Basu N., and Dhir, V. K., *2002*, Interfacial heat transfer during subcooled flow boiling, *Int. J. Heat Mass Transfer*, Vol. 45, pp. 3947-3959.
- Wattelet, J.P., *1995*, Predicting boiling heat transfer in a small-diameter round tube using an asymptotic method. *Proceedings of the Convective Flow Boiling*, pp. 377-382.
- Wattelet J.P., Chato J.C., Souza A.L., Christoffersen B.R., *1994*, Evaporative characteristics of R12, R134a, and a mixture at low mass fluxes, *ASHRAE Tran. Sympos*. Vol. 100, pp. 603-615.
- Wattelet J.P., *1995*, Predicting boiling heat transfer in a small-diameter round tube using an asymptotic method. *Proceedings of the Convective Flow Boiling*, pp. 377-382.
- Webb R.L., Gupte N.S. *1992*, A critical review of correlations for convective vaporization in tubes and tube banks, *Heat Transfer Eng.*, Vol. 13, No. 3.
- Weisman J., Pei B.S., *1983*, Prediction of critical heat flux in low boiling at low qualities, *Int. J. Heat Mass Transfer* Vol. 26, pp. 1463–1477.

- Wen D.S., Kenning D.B.R., *2004*, Two-phase pressure drop of water during flow boiling in a vertical narrow channel, *Experimental Thermal and Fluid Sciences,* Vol. 28, pp. 131-138.
- Wu P.Y. and Little W.A., *1983*, Measuring of friction factor for the flow of gases in very fine channels used for micro miniature Joule Thompson refrigerators, *Cryogenics,* Vol. 23, pp. 273-277.
- Wu P.Y. and Little W. A., *1984*, Measuring of the heat transfer characteristics of gas flow in fine channel heat exchangers for micro miniature refrigerators, *Cryogenics,* Vol. 24, pp. 415-420.
- Yan Y.Y., Lin T.F., *1998,* Evaporation heat transfer and pressure drop of refrigerant R-134a in small pipe, *Int. J. Heat Mass Transfer,* Vol. 41, pp. 4183-4194.
- Yang C.Y., Webb R.L., *1996*, Friction pressure drop of R-12 in small hydraulic diameter extruded aluminum tubes with and without micro-fins, *Int. J. of Heat and Mass Transfer, Vol.* 39, *No.* 4, pp. 801-809.
- Yin C.P., Yan Y.Y., Lin T.F., and Yang B.C., *2000*, Subcooled flow boiling heat transfer of R-134a and associated bubble characteristics in a horizontal annular channel, *Int. J. Heat Mass Transfer,* Vol. 43, pp. 1885–1896.
- Yu W., France D.M., Wambsganss M.W. and Hull J.R., *2002*, Two-phase pressure drop, boiling heat transfer, and critical heat flux to water in a small-diameter horizontal tube, *Int. J. of Multiphase Flow,* Vol. 28, No. 6, pp. 927-941.
- Yu W., France D.M., Wambsganss M.W., Hull J.R., *2002*, Two-phase pressure drop, boiling heat transfer coefficient, and critical heat flux to water in a small-diameter horizontal tube, *Int. J. of Multiphase Flow, Vol.* 28, pp. 927-941.
- Yu D., Warrington R., Barron R. and Ameel T., *1995*, An Experimental and Theoretical Investigation of fluid flow and heat transfer in microtubes, *Proc. ASME/JSME Thermal Eng Conf*, Vol. 1, pp. 523-530.
- Zang M., Webb R.L., *2001*, Correlation of two-phase friction for refrigerants in small-diameter tubes, *Experimental Thermal and Fluid Sciences, Vol.* 25, pp. 131-139.
- Zeng L.Z., Klausner J.F., and Mei R., *1993b*, A unified model for the prediction of bubble detachment diameters in boiling systems. Part II: Flow boiling, *Int. J. Heat Mass Transfer,* Vol. 36, pp. 2271– 2279.
- Zeng L.Z., Klausner J.F., and Mei R., *1993a*, A unified model for the prediction of bubble detachment diameters in boiling systems. Part I: Pool boiling, *Int. J. Heat Mass Transfer*, Vol. 36, pp. 2261– 2270.
- Zivi S. M., *1964*, Estimation of steady-state steam void-fraction by means of the principle of minimum entropy production, *J. Heat Transfer* 86 pp. 247-252.

• Zuber N., *1959*, Hydrodynamic aspects of boiling heat transfer, *Ph.D. thesis*, *Research Laboratory, Los Angeles and Ramo-Wooldrige Corporation, University of California, Los Angeles.*